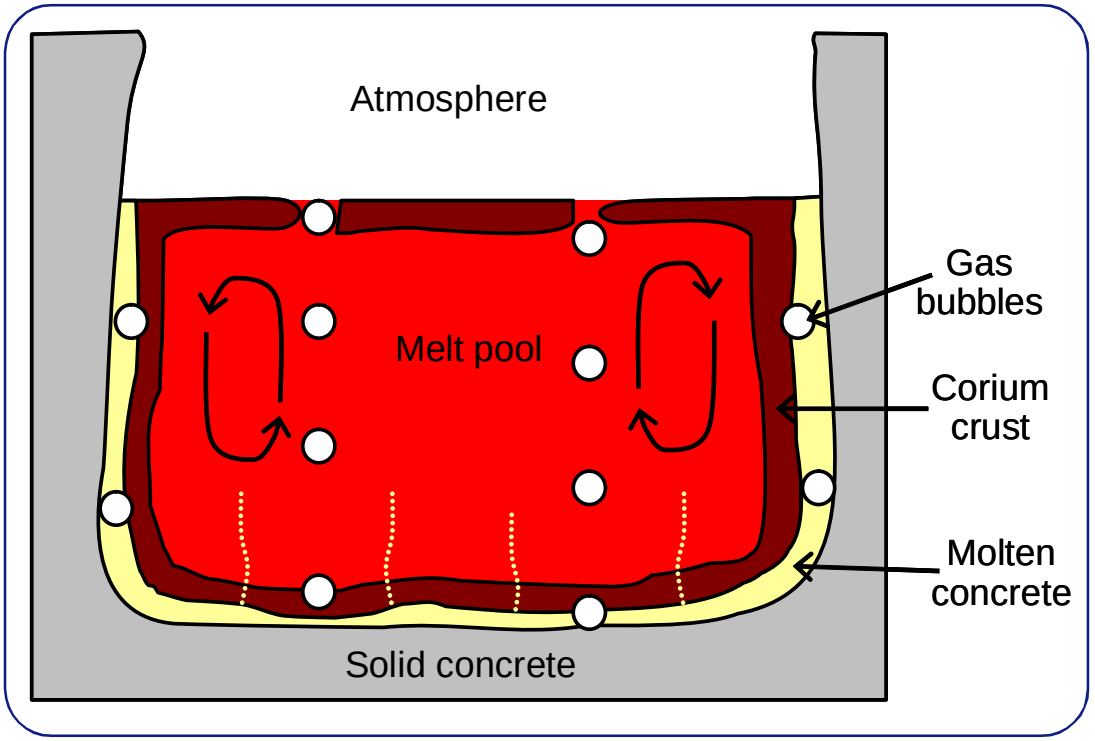

Tuomo Sevón

Molten Core - Concrete Interactions in Nuclear Accidents

I Theory and Design of an Experimental Facility

VTT TIEDOTTEITA – RESEARCH NOTES 2311

Molten Core – Concrete Interactions in Nuclear Accidents

Theory and Design of an Experimental Facility

Tuomo Sevón

VTT Processes

ISBN 951–38–6743–9 (soft back ed.)
ISSN 1235–0605 (soft back ed.)

ISBN 951–38–6744–7 (URL: http://www.vtt.fi/inf/pdf/)
ISSN 1455–0865 (URL: http://www.vtt.fi/inf/pdf/)

JULKAISIJA – UTGIVARE – PUBLISHER

VTT, Vuorimiehentie 5, PL 2000, 02044 VTT
puh. vaihde 020 722 111, faksi 020 722 4374

VTT, Bergsmansvägen 5, PB 2000, 02044 VTT
tel. växel 020 722 111, fax 020 722 4374

VTT Technical Research Centre of Finland, Vuorimiehentie 5, P.O.Box 2000, FI–02044 VTT, Finland
phone internat. +358 20 722 111, fax +358 20 722 4374

VTT Prosessit, Lämpömiehenkuja 3 A, PL 1604, 02044 VTT
puh. vaihde 020 722 111, faksi 020 722 5000

VTT Processer, Värmemansgränden 3 A, PB 1604, 02044 VTT
tel. växel 020 722 111, fax 020 722 5000

VTT Processes, Lämpömiehenkuja 3 A, P.O.Box 1604, FI–02044 VTT, Finland
phone internat. + 358 20 722 111, fax + 358 20 722 5000

Technical editing Anni Kääriäinen

Otamedia Oy, Espoo 2005

Sevón, Tuomo. Molten Core – Concrete Interactions in Nuclear Accidents. Theory and Design of an Experimental Facility [Sydänsulan ja betonin vuorovaikutukset ydinvoimalaonnettomuuksissa: Teoriaa ja koelaitteiston suunnittelu]. Espoo 2005. VTT Tiedotteita – Research Notes 2311. 83 p.

Keywords nuclear power plants, nuclear safety, reactor core, meltdown, concrete structures, containment buildings, spalling, cracking, simulation, MELCOR

Abstract

In a hypothetical severe accident in a nuclear power plant, the molten core of the reactor may flow onto the concrete floor of containment building. This would cause a molten core – concrete interaction (MCCI), in which the heat transfer from the hot melt to the concrete would cause melting of the concrete. In assessing the safety of nuclear reactors, it is important to know the consequences of such an interaction.

As background to the subject, this publication includes a description of the core melt stabilization concept of the European Pressurized water Reactor (EPR), which is being built in Olkiluoto in Finland. The publication includes a description of the basic theory of the interaction and the process of spalling or cracking of concrete when it is heated rapidly. A literature survey and some calculations of the physical properties of concrete and corium–concrete mixtures at high temperatures have been conducted. In addition, an equation is derived for conservative calculation of the maximum possible concrete ablation depth. The publication also includes a literature survey of experimental research on the subject of the MCCI and discussion of the results and deficiencies of the experiments.

The main result of this work is the general design of an experimental facility to examine the interaction of molten metals and concrete. The main objective of the experiments is to assess the probability of spalling, or cracking, of concrete under pouring of molten material. A program of five experiments has been designed, and pre-test calculations of the experiments have been conducted with MELCOR 1.8.5 accident analysis program and conservative analytic calculations.

Sevón, Tuomo. Molten Core – Concrete Interactions in Nuclear Accidents. Theory and Design of an Experimental Facility [Sydänsulan ja betonin vuorovaikutukset ydinvoimalaonnettomuuksissa: Teoriaa ja koelaitteiston suunnittelu]. Espoo 2005. VTT Tiedotteita – Research Notes 2311. 83 s.

Keywords nuclear power plants, nuclear safety, reactor core, meltdown, concrete structures, containment buildings, spalling, cracking, simulation, MELCOR

Tiivistelmä

Vakavassa ydinvoimalaitosonnettomuudessa reaktorin sulanut sydän voi valua suojarakennuksen betonilattialle. Tästä voi seurata sydänsula–betoni-vuorovaikutus, jossa lämpöä siirtyy kuumasta sulasta betoniin, mikä aiheuttaa betonin sulamisen. Arvioitaessa ydinvoimaloiden turvallisuutta on tärkeää tuntea tällaisen vuorovaikutuksen seuraukset.

Tässä tutkimuksessa aiheen taustaksi kuvataan Olkiluotoon rakennettavan EPR-painevesireaktorin sydämen sulamisonnettomuuden hallintakonsepti. Tutkimuksessa kerrotaan sydänsula–betoni-vuorovaikutuksen perusteista sekä betonin nopean lämmittämisen aiheuttamasta spalling-ilmiöstä eli lohkeilusta. Betonin ja corium–betoni-seosten fysikaalisia ominaisuuksia korkeissa lämpötiloissa selvitetään kirjallisuuden ja laskujen avulla. Lisäksi johdetaan yhtälö betonin suurimman mahdollisen sulamissyvyyden laskemiseksi. Julkaisu sisältää myös kirjallisuusselvityksen sydänsula–betoni-vuorovaikutusten kokeellisesta tutkimuksesta sekä pohdintaa kokeiden tuloksista ja puutteista.

Tutkimuksen tärkein tulos on yleissuunnitelma koelaitteistolle, jolla voidaan tutkia sulan metallin ja betonin vuorovaikutusta. Kokeiden tärkein tavoite on selvittää spalling-ilmiön todennäköisyyttä, kun sulaa materiaalia kaadetaan betoniastiaan. Tutkimuksessa suunnitellaan viiden kokeen ohjelma ja kokeista on tehty laskelmia MELCOR 1.8.5 -onnettomuusanalyysiohjelmalla sekä konservatiivisilla käsinlaskuilla.

Preface

This text has been written as a master's thesis for the department of Engineering Physics and Mathematics at Helsinki University of Technology. Part of the funding was obtained from SAFIR, the Finnish research program on nuclear power plant safety. I am grateful to VTT Processes for the opportunity to write my master's thesis on this interesting subject. I want to thank especially my instructor, senior research scientist Ilona Lindholm, and supervisor, professor Rainer Salomaa for advice and comments about the work. Thanks go also to Heikki Sjövall from TVO and Risto Sairanen from STUK for providing information about the sacrificial concrete in the EPR reactor pit and for reviewing this thesis. And finally, thanks to my parents who have supported my studies.

Otaniemi, 13 October 2005

Tuomo Sevón

Contents

1. Introduction

Large amounts of radioactive material are present in a nuclear fission reactor, and the release of these into the environment would be harmful. Therefore, the risk of a severe accident must be reckoned with in the design, construction and operation of a nuclear power plant. To prevent the hazardous emissions, the concept of defense in depth (IAEA 1996) is applied in modern nuclear power plants. The first level of defense in depth is the prevention of failures. However, if failures do occur, the purpose of the second level is to prevent the failures from evolving into accidents. If this does not succeed, the third level of the concept is to control the accidents so that the fuel rods would stay intact. In the very unlikely case that all these three levels of defense fail and the fuel rods are damaged, the fourth level, severe accident management, should prevent emissions to the environment. There is even fifth level in the defense in depth concept: mitigation of the consequences of the emissions, in the case that all the four previous defense levels fail. This publication deals with the fourth level of defense.

Severe accident is defined as an accident involving the melting or breakdown of a substantial portion of the fuel rods in the core of a nuclear reactor. This is the only mechanism that has the potential of a large release of radioactive materials to the environment. In nuclear power plants, there are three barriers to keep the radioactive material inside the plant: the fuel rods, the reactor coolant pressure boundary, which includes the pressure vessel, and the containment building around the reactor. In the case of a severe accident, the first barrier fails. In many reactor types, it is probable that also the reactor pressure vessel would be breached by the hot core melt. So the main objective of severe accident management is to keep the containment building intact.

In the history of commercial nuclear power, a severe accident has occurred twice. In 1979 in Three Mile Island, USA, a part of the fuel rods melted, but the reactor pressure vessel remained intact and prevented large emissions. In 1986 in Chernobyl, an explosion destroyed the fuel rods and the pressure boundary, and there was no proper containment building to prevent radioactive releases to the environment.

Since the Three Mile Island accident, extensive research on severe accidents has been conducted and many improvements to existing and new power plants have been implemented. However, because of the complexity of the physical and chemical phenomena in severe accidents, some uncertainties concerning the coolability of the molten core and the management of hydrogen in the containment remain. This publication contributes to the issue of molten core – concrete interactions (MCCI) in the reactor cavity. This subject is of special interest in the EPR (European Pressurized water Reactor) that is being constructed at Olkiluoto in Finland, because the severe accident management of the EPR involves deliberate interaction of the core melt with sacrificial

concrete. Experimental data about the special concrete type used in the EPR is scarce. The MCCI phenomena are also important in some other plants to prevent the penetration of the concrete basemat by the hot core melt.

Chapter two of this publication provides background to the subject by introducing the core melt stabilization concept of the EPR. In chapter three, the basic phenomena of molten core – concrete interactions are explained. The chapter also includes a literature survey and calculations of the physical properties of concrete and corium at high temperatures, which are important in all accident calculations. In section 3.3 some heat transfer correlations for the MCCI are quoted, and in section 3.4 a simple equation for conservative calculation of the maximum possible concrete ablation depth is derived. Chapter four includes a literature survey of experimental work on the subject and discussion of the results and deficiencies of the experiments. Because the knowledge of the subject of MCCI, especially the spalling of concrete, is scarce, a new experimental facility has been designed. Chapter five includes the general design of the facility and some pre-test calculations.

2. EPR Core Melt Stabilization Concept

A core melt accident could occur if all emergency measures fail to transfer the decay heat power out of the fuel after reactor shutdown. Such a situation could only be developed if the initiating event, for example a large leak of cooling water or a total loss of electricity, is combined with a major loss of plant safety systems. According to the design phase PSA (probabilistic safety analysis), the probability of a core melt accident is estimated to be $1.8 \cdot 10^{-6}$ per year, i.e. once in 560 000 reactor years for the Olkiluoto 3 plant (STUK 2005). However, even this very unlikely situation has been reckoned with.

In the core melt accident, the molten core must be cooled to avoid an attack of the hot melt on load-bearing structures of the containment. In the EPR, core melt accident mitigation strategy is based on spreading of the melt over a large area in a so-called core catcher. Its target is to increase the surface area of the melt, which makes cooling more effective.

There are large uncertainties in the course of the core melting and release of the melt from the reactor pressure vessel (RPV), depending on the accident scenario. The core catcher design must be capable of coping with all the uncertainties and the different accident scenarios. In the EPR, this problem has been solved by placing the core catcher in a lateral spreading compartment, separated from the reactor pit by a melt discharge channel. The aim of this design is to increase the predictability of the melt properties in the spreading area and to protect the core catcher from the mechanical loads resulting from the failure of the RPV. The separation of the core catcher from the reactor also avoids risks resulting from an unintended flooding of the catcher during power operation. (Fischer 2004.)

The core melt stabilization concept of the EPR is illustrated in Figure 1. After the failure of the RPV lower head, the melt is released into the reactor pit. There is no water in the pit, which prevents steam explosions. When the molten core contacts the sacrificial concrete layer, the concrete begins to melt. The concrete is backed up by a protective refractory layer except under the melt plug. The thickness of the sacrificial concrete layer is about 50 cm. After destroying the melt plug, the melt flows to the spreading compartment through the melt discharge channel. This happens about one hour after the failure of the RPV (Eppinger et al. 2000). The melt spreads over a large area (170 m^2) on the floor of the spreading compartment. The arrival of the melt triggers the opening of spring-loaded valves, and cooling water flows by gravity from the In-containment Refueling Water Storage Tank (IRWST). The water fills the cooling channels under the core catcher. Then the water rises to the space behind the spreading area sidewalls and overflows onto the surface of the melt. This fill-up process takes about 5 minutes, and it

is fully passive: no pumps are needed. The decay heat is removed very effectively from the melt because of the large surface area completely surrounded by water. It is estimated that the melt will be completely solidified after a few days. (Fischer 2004.)

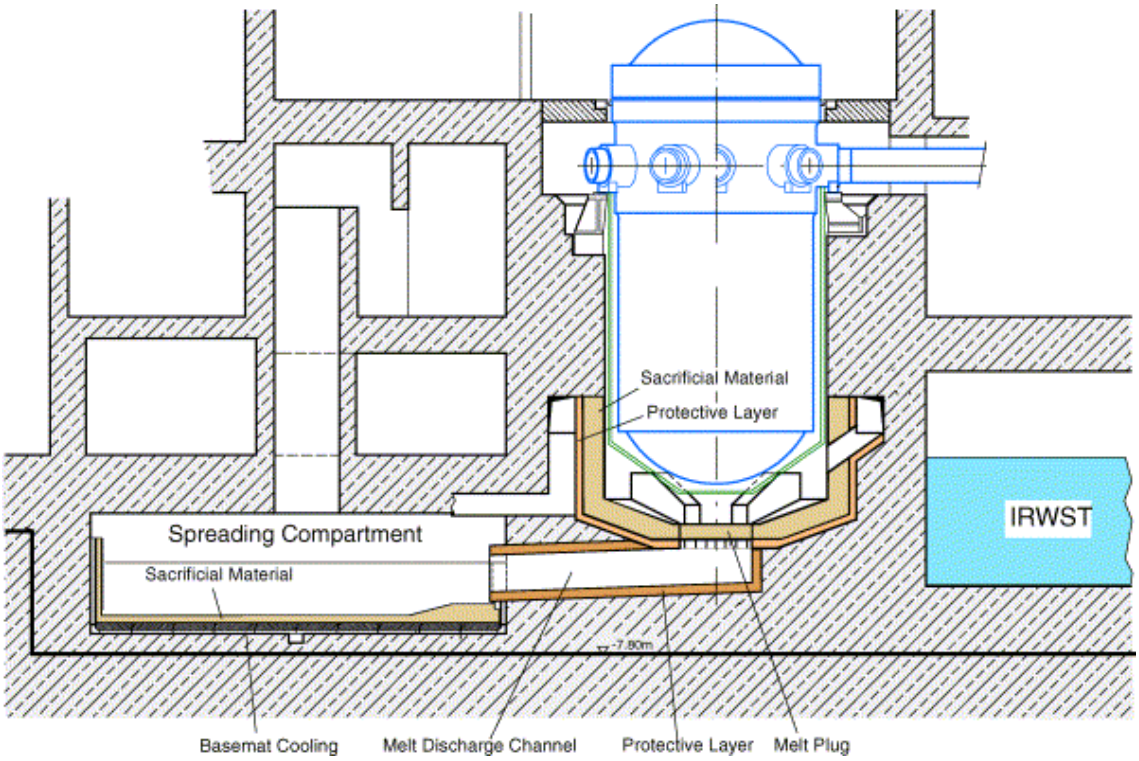

Figure 1. Main components of the EPR core melt stabilization concept (Fischer 2004).

The melt release rate from the RPV and the melt composition depend on the accident scenario. If the core catcher was placed directly under the RPV, then slow gradual melt release would cause the melt to solidify upon contact with the floor and spreading would be prevented. One purpose of the melt retention in the reactor pit is to collect the entire melt before releasing it into the spreading compartment, which ensures efficient spreading of the melt. Another purpose is to lower the solidus and liquidus temperatures of the melt by mixing molten concrete with the core melt. This enhances the spreading of the melt, too. The temporary retention of the melt in the reactor pit increases the predictability of the melt properties in the spreading area because of its self-adjusting characteristic. Ablation through the sacrificial concrete layer requires a certain amount of heat. Slower melt release and smaller melt mass results in a longer retention time, during which more melt can accumulate in the pit.

A possible concern in the EPR concept is a too early failure of the melt plug. In this case the first melt discharge into the spreading area may trigger the flooding valves, and subsequent melt release occurs into a flooded spreading area. Melt spreading in a pool may not be efficient. A small initial melt mass may also solidify in the melt discharge

channel or the core catcher without proper spreading, which would inhibit efficient cooling of the melt. If some melt is released from the RPV after the failure of the melt plug, then this late release will not be mixed with concrete and hence it may not spread efficiently. To ensure the safety of the proposed core melt stabilization concept, one must be able to predict the melt behavior in the reactor pit. This requires knowledge of the heat transfer from the melt to ablating concrete.

3. Theory of Molten Core – Concrete Interactions

3.1 Phenomenology

The core of a nuclear reactor consists of uranium dioxide in the fuel, zirconium in the fuel rod cladding and carbon steel and stainless steel in other structures. At high temperatures zirconium is oxidized by water vapor, so the main constituents of core melt, or corium, are UO_2, ZrO_2, Zr, Fe, Cr and Ni. The melting point of the pure oxides is around 2700 °C, while the metals melt at 1350–1900 °C. Mixtures of different species do not have single melting points. Instead, they change from solid to liquid over a range of temperatures, between so-called solidus and liquidus temperatures. The density of corium is around 6000–7000 kg/m^3.

Molten core – concrete interaction (MCCI) is illustrated in Figure 2. The solid concrete and the molten corium pool may be separated by a thin layer of partly molten concrete. The concrete melt rises upwards as "streamers" because it is less dense than the overlying core melt. Also the gas bubbles, rising from the decomposing concrete, cause mixing of the liquids. A layer of solid corium crust may also exist at the core-concrete interface. The crust is probably porous and permeable to gases from the concrete.

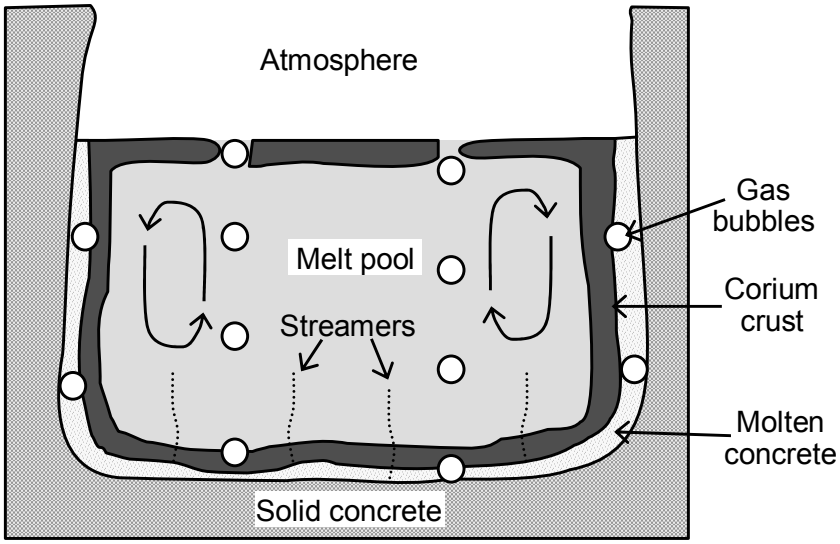

Figure 2. Melt pool and its boundaries.

The oxides in corium and concrete are miscible with each other, but the metallic species are immiscible with the oxides. Because the metals are lighter than the corium oxides, a metallic layer may be formed on the surface of the oxidic pool. When concrete oxides are added to the melt, its density decreases eventually below the density of the metals. After this, the metallic layer may relocate to the bottom of the pool. On the other hand,

intense stirring of the pool by the rising gas bubbles may cause the metals and the oxides to be mixed with each other.

The rate of concrete ablation is controlled by the heat transfer from the melt to concrete. The core melt pool is stirred by the rising gas bubbles, which enhances the heat transfer. On the other hand, the possible corium crust at the interface inhibits heat transfer. Because the heat conductivity of concrete is very poor, almost all of the heat goes to the heat-up and melting of the surface of the concrete wall.

Some concrete erosion may take place in the impingement region when the melt jet flows from the pressure vessel to the concrete floor. This impingement erosion (Swedish et al. 1979) probably lasts only a short time, since the formation of a corium pool or crust prevents the melt jet from directly hitting the concrete floor. However, the rapid initial impingement heat transfer may initiate a sustained concrete spalling. Spalling means that pieces crack off the concrete surface because very rapid evaporation of the water in the concrete increases pressure inside the concrete. Spalling may become self-sustaining since, as pieces of concrete crack off the surface, the hot melt suddenly contacts fresh concrete and vapor pressure inside the concrete rises rapidly.

The viscosity of the melt pool also affects the heat transfer: Higher viscosity means lower heat transfer rate. Between the solidus and liquidus temperatures the viscosity of the mixture increases sharply with decreasing temperature. An additional complication comes from the fact that the melt composition and its physical properties change over time as more concrete is added to the melt. It is unknown whether the oxides with high melting points (UO_2 and ZrO_2) are segregated to the crust at the pool boundaries, or if they are dispersed as solid particles among the melt, which would increase the viscosity of the melt.

Some of the heat is transferred away from the surface of the pool by thermal radiation and convection. Usually there is air above the pool surface, but the surface can also be cooled by water. The surface temperature of the pool is also affected by the presence of a crust cover and the passing of gas bubbles through the surface.

The core melt is continuously heated by the radioactive decay of the fission products in the melt. Another heat source is the chemical reaction heat. The most important chemical reaction in the pool is the oxidation of metals by the concrete decomposition gases:

$$Zr + 2\ H_2O \rightarrow ZrO_2 + 2\ H_2 \ + \ 6.3\ MJ/kg_{Zr}$$

$$Zr + 2\ CO_2 \rightarrow ZrO_2 + 2\ CO \ + \ 5.7\ MJ/kg_{Zr}$$

$$2\ Cr + 3\ H_2O \rightarrow Cr_2O_3 + 3\ H_2 \ + \ 3.6\ MJ/kg_{Cr}$$

$$2\ Cr + 3\ CO_2 \rightarrow Cr_2O_3 + 3\ CO\ +\ 2.8\ MJ/kg_{Cr}$$

$$Fe + H_2O\ +\ 3.0\ kJ/kg_{Fe}\ \rightarrow FeO + H_2$$

$$Fe + CO_2\ +\ 480\ kJ/kg_{Fe}\ \rightarrow FeO + CO$$

Also the reduction of SiO_2 and Fe_2O_3 by zirconium plays an important role:

$$Zr + SiO_2 \rightarrow ZrO_2 + Si\ +\ 1.6\ MJ/kg_{Zr}\ (T < 1870\ °C)$$

$$Zr + 2\ SiO_2 + 4.7\ MJ/kg_{Zr} \rightarrow ZrO_2 + 2\ SiO(g)\ (T > 1870\ °C)$$

$$3\ Zr + 2\ Fe_2O_3 \rightarrow 3\ ZrO_2 + 4\ Fe + 5.8\ MJ/kg_{Zr}$$

$$Si + 2\ H_2O \rightarrow SiO_2 + 2\ H_2 + 15\ MJ/kg_{Si}$$

$$Si + 2\ CO_2 \rightarrow SiO_2 + 2\ CO + 14\ MJ/kg_{Si}$$

If the further oxidation of metallic Si is taken into account, the oxidation of 1 kg of Zr by any material produces about 6 MJ of heat at temperatures <1870 °C. Equilibrium constants for the reactions tell that Zr is oxidized first, and Si, Cr, and Fe follow in this order. The amounts of Fe_2O_3, Fe_3O_4 and NiO generated in oxidation reactions are so small that they can be ignored. The reaction enthalpies and equilibrium constants were obtained from the reference (Outokumpu Research Oy 2002) at the temperature of 2000 K, except the SiO(g) producing reaction at 2000 °C.

3.2 Behavior of Concrete at High Temperatures

3.2.1 Composition and Physical Structure of Concrete

Concrete is a composite material that consists of mineral aggregate bound by a matrix of hardened cement paste. Aggregates generally occupy 65–80 % of the total volume (75–90 % of weight) of concrete (Bažant & Kaplan 1996). Concrete types are defined by the type of the aggregates used in the concrete. A common aggregate in Finland is siliceous, which contains mainly quartz (SiO_2). Calcareous aggregates contain mainly limestone (calcium carbonate, $CaCO_3$). In the sacrificial concrete used in the EPR reactor pit, hematite (Fe_2O_3) is also used as an aggregate (Nie 2004). Basaltic concrete, which is used in some nuclear power plants, is similar to siliceous concrete but with more impurities like MgO, Al_2O_3, Fe_2O_3, K_2O and CaO.

The density of the most common cement type, Portland cement, is about 3150 kg/m^3 in its initial, anhydrous state. A typical composition of dry Portland cement is: CaO 60–67 %, SiO_2 17–25 %, Al_2O_3 3–8 %, Fe_2O_3 0.5–6 %. Small amounts of other materials such as $CaSO_4$, MgO, K_2O and Na_2O may also be present. When manufacturing

concrete, aggregates, cement and water are mixed. The cement reacts chemically with water, and the product is hardened cement paste, which binds the aggregate particles in concrete. Knowledge of the cement–water reaction, i.e. hydration, is incomplete. However, it seems that the most important products of the various hydration reactions are $Ca(OH)_2$ (calcium hydroxide), $3CaO{\cdot}2SiO_2{\cdot}3H_2O$ (calcium silicate hydrate or "tobermorite gel"), $3CaO{\cdot}Al_2O_3{\cdot}6H_2O$ (calcium aluminate hydrate), $3CaO{\cdot}Fe_2O_3{\cdot}6H_2O$ (calcium ferrite hydrate) and $CaSO_4{\cdot}2H_2O$ (gypsum). The amount of water which combines chemically with Portland cement is about 23–28 % of the weight of the dry cement. (Bažant & Kaplan 1996.)

Hardened cement paste consists of the porous hydrated cement (called also "gel") and capillary pores. The porosity of the gel is about 28 % of the total volume of the gel. The gel pores have an average width of 1.5–2 nm. For complete hydration of the cement, a water–cement ratio of at least 0.36 by weight is necessary. If the amount of water in the mix is larger than this, then the excess water forms capillary pores. The size of the capillary pores is 10–200 nm. Water in the gel pores and capillary pores is called evaporable or "physically bound" water, in contrast to the chemically bound water in the hydrates and hydroxides. If the concrete is kept in dry conditions, some of the physically bound water slowly evaporates from the pores. (Bažant & Kaplan 1996.)

3.2.2 Temperature Effects on the Composition of Concrete

In the following, the most important reactions that take place when concrete is heated are listed. The exact reaction temperatures depend on the heating rate and pressure.

- 100 °C: Loss of evaporable water.
  $H_2O(l) + 2258\ kJ/kg_{H2O} \rightarrow H_2O(g)$

- 100–850 °C: Dehydration of hydrates (Bažant & Kaplan 1996).
  $3CaO{\cdot}2SiO_2{\cdot}3H_2O \rightarrow 2CaO{\cdot}SiO_2 + CaO{\cdot}SiO_2 + 3\ H_2O(g)$
  (Similar reactions for other hydrates; the reaction heats of these endothermic reactions are about 250–500 $kJ/kg_{hydrate}$)

- 400–600 °C: Dehydration of calcium hydroxide (Bažant & Kaplan 1996; Peehs et al. 1979).
  $Ca(OH)_2 + 1340\ kJ/kg_{Ca(OH)2} \rightarrow CaO + H_2O(g)$

- 574 °C: Crystalline transformation from α- to β-quartz (Chase 1998).
  $SiO_2(\alpha) + 12\ kJ/kg_{SiO2} \rightarrow SiO_2(\beta)$

- 600–900 °C: Decomposition of calcium carbonate (Bažant & Kaplan 1996).
  $CaCO_3 + 1637\ kJ/kg_{CaCO3} \rightarrow CaO + CO_2(g)$

- 1200–1500 °C: Melting of Portland cement (Bažant & Kaplan 1996).

- 1423 ± 50 °C: Melting of quartz (Chase 1998).
  $SiO_2(s) + 130\ kJ/kg_{SiO2} \rightarrow SiO_2(l)$

- 1462 °C: Decomposition of hematite into magnetite (Chase 1998).
  $6\ Fe_2O_3 + 480\ kJ/kg_{Fe2O3} \rightarrow 4\ Fe_3O_4 + O_2(g)$

- 1597 °C: Melting of magnetite (Chase 1998).
  $Fe_3O_4(s) + 600\ kJ/kg_{Fe3O4} \rightarrow Fe_3O_4(l)$

In addition, CaO and SiO_2 may form some compounds, like $CaSiO_3$, but the phase diagram of these is very complex.

From the reactions, it can be seen that water vapor and carbon dioxide are released from concrete when it is heated from 100 to 900 °C. Siliceous concrete releases mainly water vapor, while calcareous concrete releases also substantial amounts of carbon dioxide.

3.2.3 Spalling of Concrete

In fire tests of concrete, spalling has been observed. This means that pieces crack off the concrete surface when it is heated rapidly. Spalling of concrete can occur by two processes. In the thermo-mechanical process, temperature gradients and non-uniform thermal expansion induce stresses in the concrete. In the thermo-hydraulic process, evaporation of water increases pressure in the concrete pores, which generates stresses in the concrete (Kalifa et al. 2000). The thermo-hydraulic process is generally considered more important (Bažant & Kaplan 1996).

The thermo-hydraulic spalling process is illustrated in Figure 3. As temperature gets higher, water in the concrete pores evaporates, which increases pressure in the pores. Under the pressure gradient, water vapor is transported both outwards and inwards in the concrete element. If the stress induced by the pressure gradient is higher than the strength of the concrete, spalling occurs.

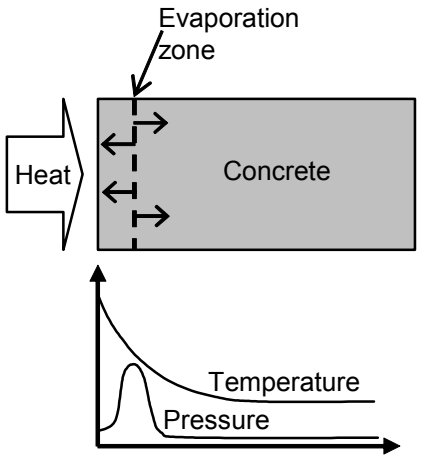

Figure 3. The process for the build-up of pressure in heated concrete.

The flow rate $\boldsymbol{J}$ (kg/m^{2}s) of water, water vapor and air in the porous concrete is driven by the gradient of the pressure p, and it can be modeled by the Darcy's law:

$$\boldsymbol{J} = -\rho \frac{K}{\mu} \nabla p \,. \tag{1}$$

Here ρ is the density and μ is the dynamic viscosity of the fluid, and K is the intrinsic permeability of the concrete (m^2). The permeability is different for gas and liquid flows (Chung & Consolazio 2005). The permeability of concrete varies many orders of magnitude, depending on the porosity, temperature and water content. Especially the temperature dependence of permeability is not known accurately enough to make reliable predictions of concrete spalling by computer simulations.

Experiments on concrete spalling have been reported for example by Kalifa et al. (2000) and Sullivan (2004). According to the experiments, the most important factor that affects spalling is the heating rate: The probability of spalling increases with faster heating. Another important factor is the permeability of concrete. In very porous, high permeability concrete the vapor flows easily and the pressure gradients remain small enough not to induce spalling. On the contrary, high strength concretes, which are made with low water-to-cement-ratio, have low porosity and permeability. According to equation (1), this means that heating high strength concrete induces larger pressure gradients, and these are not completely compensated by the higher strength. Hence, spalling may be more probable for high strength concretes. Third factor that affects spalling is the amount of evaporable water in the concrete: Spalling occurs more easily in moist concrete.

3.2.4 Thermal Properties of Concrete at High Temperatures

In this section, the enthalpy, specific heat, thermal conductivity and density of concrete from the room temperature to melting are discussed. Since the physical and chemical changes in concrete occur at a certain rate, the thermal properties also depend on the heating rate and the experimental techniques. Because of this and the non-homogeneity of concrete, the dependence of concrete properties on temperature cannot be defined by unique relations. However, some "apparent" thermal properties to be used in heat transfer calculations can be determined from experiments and theoretical considerations. The zero point of enthalpy is set to 25 °C.

The specific heat of idealized Portland cement paste with water–cement weight ratio 0.5 is presented in Figure 4. The curves are based on both theoretical considerations and experimental data. The dashed line represents the sensible heat, and the solid line includes also the latent heat from the dehydration of hydrates and calcium hydroxide. The figure does not include any evaporable water, which has a large effect on the specific heat at temperatures ≤ 100 °C.

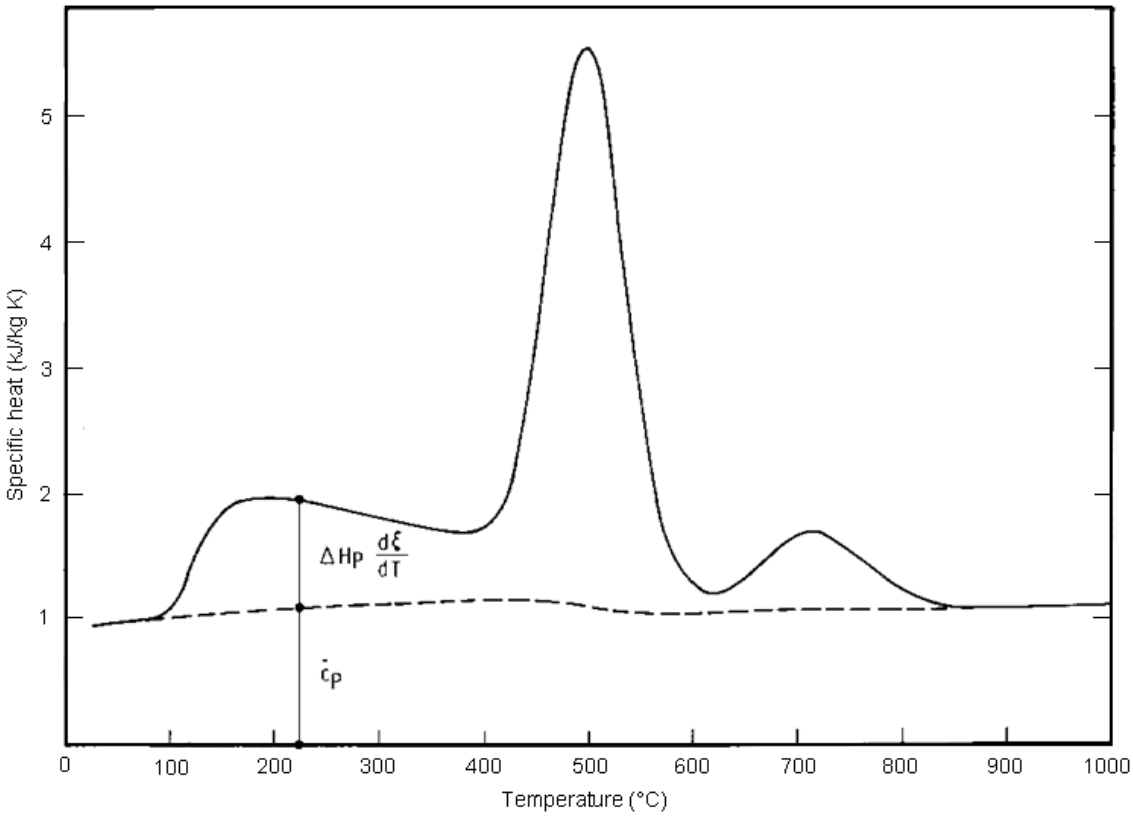

Figure 4. Specific heat of idealized Portland cement paste with water–cement ratio 0.5 and without evaporable water. The dashed line represents the sensible heat and the solid line the latent heat from dehydration reactions. (Harmathy & Allen 1973.)

The enthalpy of cement paste as a function of temperature can be estimated by integration of the specific heat. The heat of melting of cement is unknown, but as a rough estimate the heat of melting of quartz (130 kJ/kg) can be used. In Figure 5, the enthalpy of the idealized Portland cement paste with water–cement ratio 0.5 and without evaporable water is presented. The enthalpy has been integrated from the specific heat data of Figure 4. The constant specific heat of 1.1 kJ/kg·K above 1000 °C has been used, and the heat of melting has been divided uniformly to the interval 1200–1500 °C. In calculations, the content of evaporable water has to be estimated and the heating and evaporation of the water at ≤ 100 °C has to be taken into account.

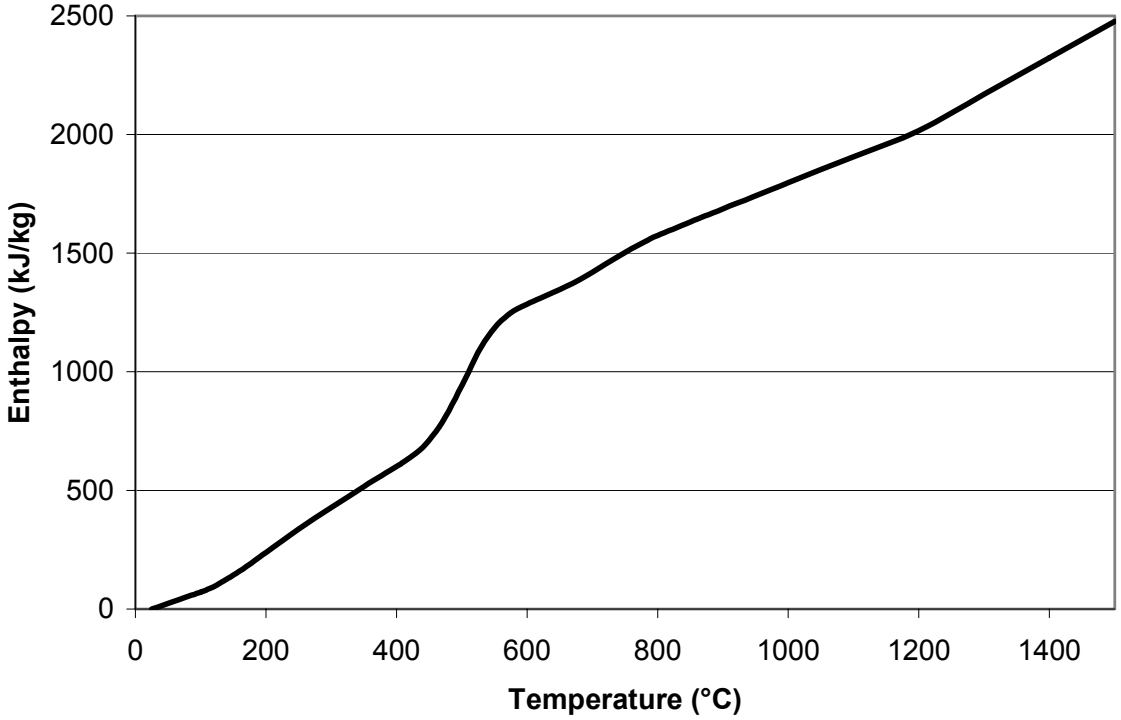

Figure 5. Enthalpy of Portland cement paste without evaporable water.

The specific heat and enthalpy of siliceous aggregate (quartz) is presented in Figure 6, calcareous aggregate (calcium carbonate) in Figure 7, and hematite (Fe_2O_3), which is used as an aggregate in the EPR sacrificial concrete, in Figure 8.

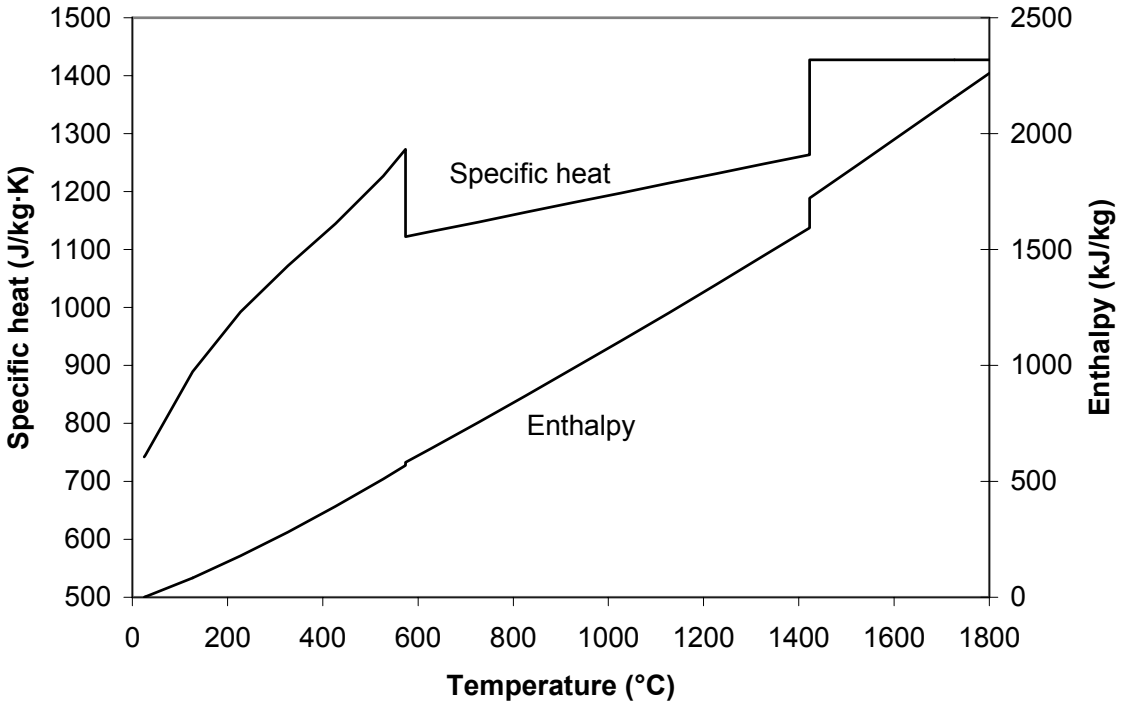

Figure 6. Specific heat and enthalpy of quartz (SiO_2) (Chase 1998).

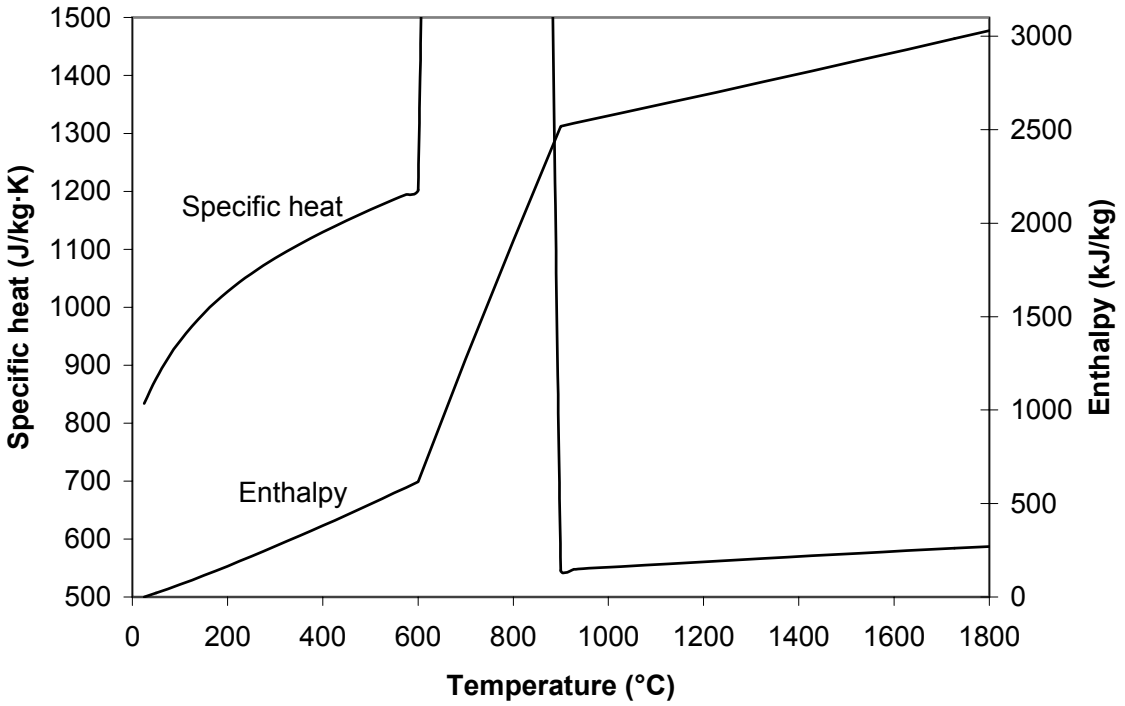

Figure 7. Specific heat and enthalpy of calcium carbonate (Outokumpu Research Oy 2002; Chase 1998). Calcium carbonate decomposes into calcium oxide and carbon dioxide at 600–900 °C, and above that, the values correspond to one kilogram of the original carbonate. The specific heat between 600 and 900 °C is about 6400 J/kg·K.

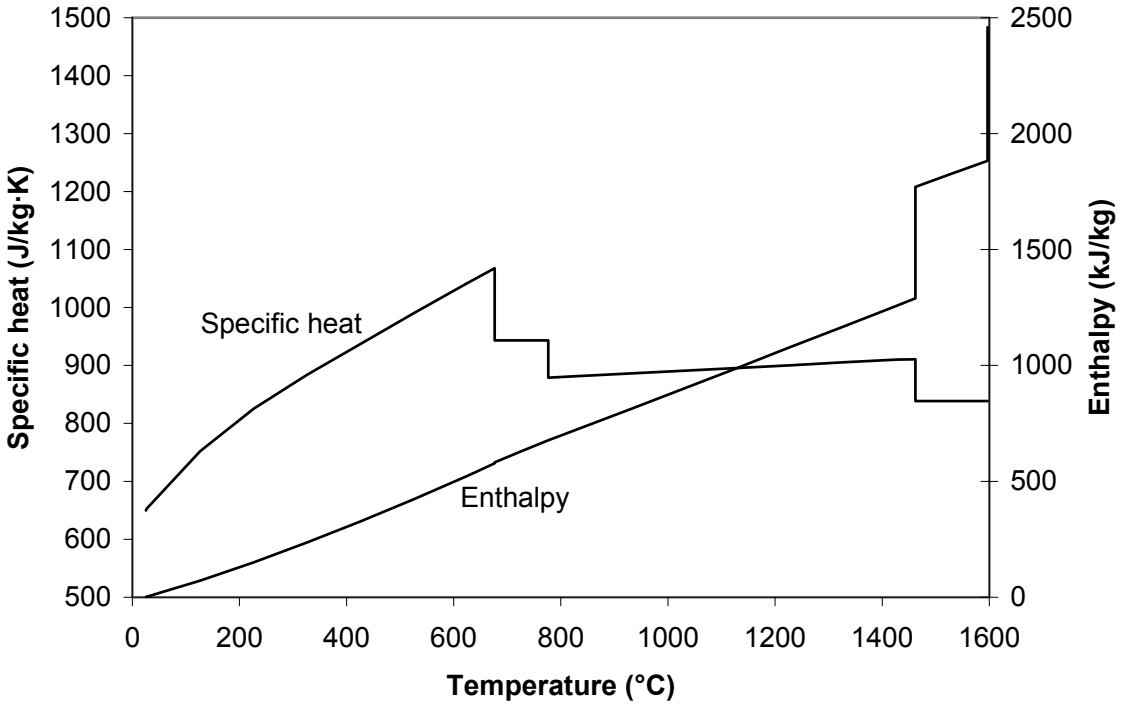

Figure 8. Specific heat and enthalpy of hematite (Fe_2O_3) (Chase 1998). Hematite decomposes into magnetite (Fe_3O_4) and oxygen at 1462 °C, and above that, the values correspond to one kilogram of the original hematite.

Based on the specific heat and enthalpy data presented above, the specific heats and enthalpies of hypothetical concretes with 20 % Portland cement and 80 % aggregates by weight have been calculated. The presence of evaporable water has been ignored. The data for siliceous concrete, a common structural concrete in Finland, is presented in Figure 9 and for calcareous concrete in Figure 10.

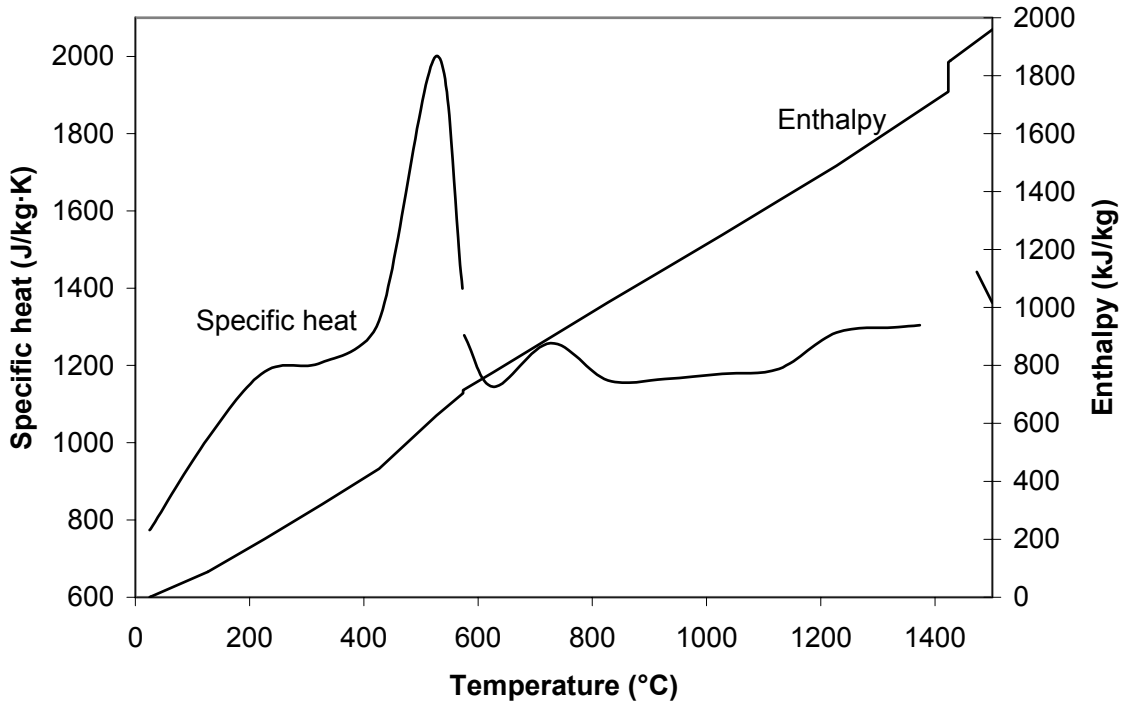

Figure 9. Calculated specific heat and enthalpy of siliceous concrete with 20 % cement paste and 80 % quartz aggregate and no evaporable water.

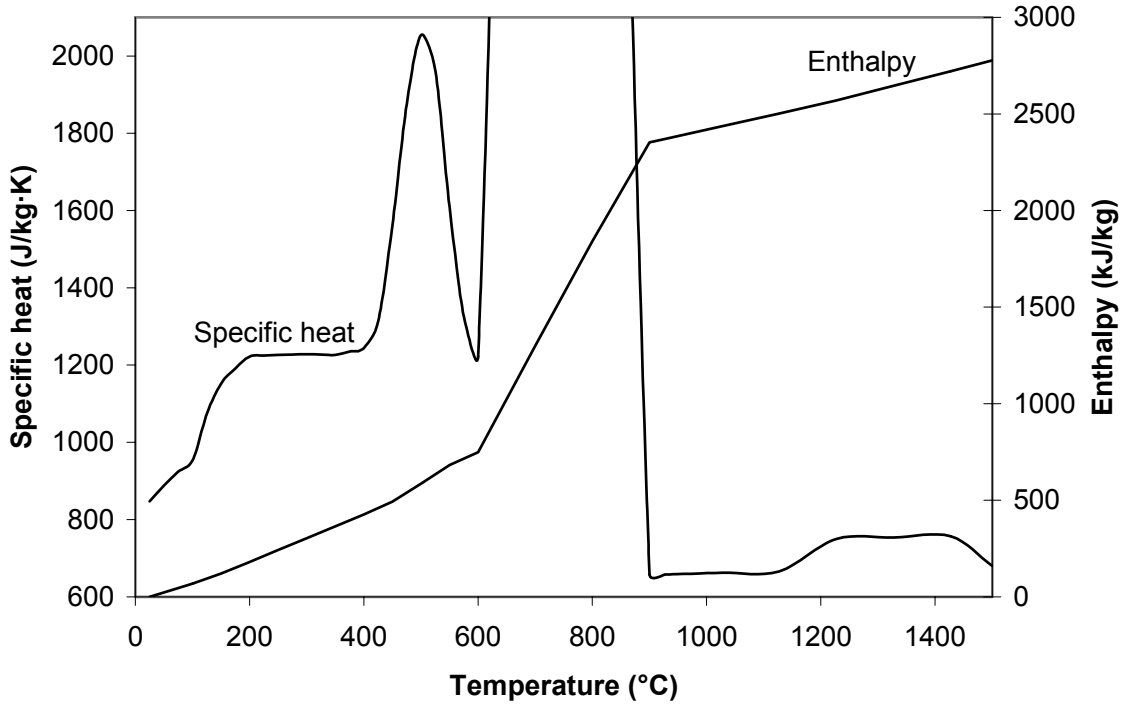

Figure 10. Calculated specific heat and enthalpy of calcareous concrete with 20 % cement paste and 80 % limestone aggregate and no evaporable water. The specific heat between 600 and 900 °C is about 5400 J/kg·K

The preliminary composition of the sacrificial concrete to be used in the EPR reactor pit is given in Table 1. The concrete type FeSi/PZ15/8 means that it is made from 15 % dry Portland cement and siliceous and iron-oxide-rich aggregates mixed in the proportion 1:1. The maximum grain size of the aggregates is 8 mm. After hydration reactions, the mass fraction of Portland cement paste is about 20 %. Ignoring the impurities in the aggregates, the fractions of siliceous and hematite aggregates can be estimated as about 40 %. Based on this assumption, the calculated specific heat and enthalpy of the sacrificial concrete is presented in Figure 11. The evaporable water has been ignored to maintain comparability with the siliceous and calcareous concrete properties.

Table 1. Preliminary composition of the EPR sacrificial concrete FeSi/PZ15/8 (Nie 2004).

Component	Fraction (weight-%)
SiO_2	42.9
Fe_2O_3	35.3
$Ca(OH)_2$	12.2
$CaCO_3$	3.32
$Al_2O_3 \cdot 3H_2O$	2.4
Al_2O_3	2.24
H_2O (free)	1.2
$MgCO_3$	0.44

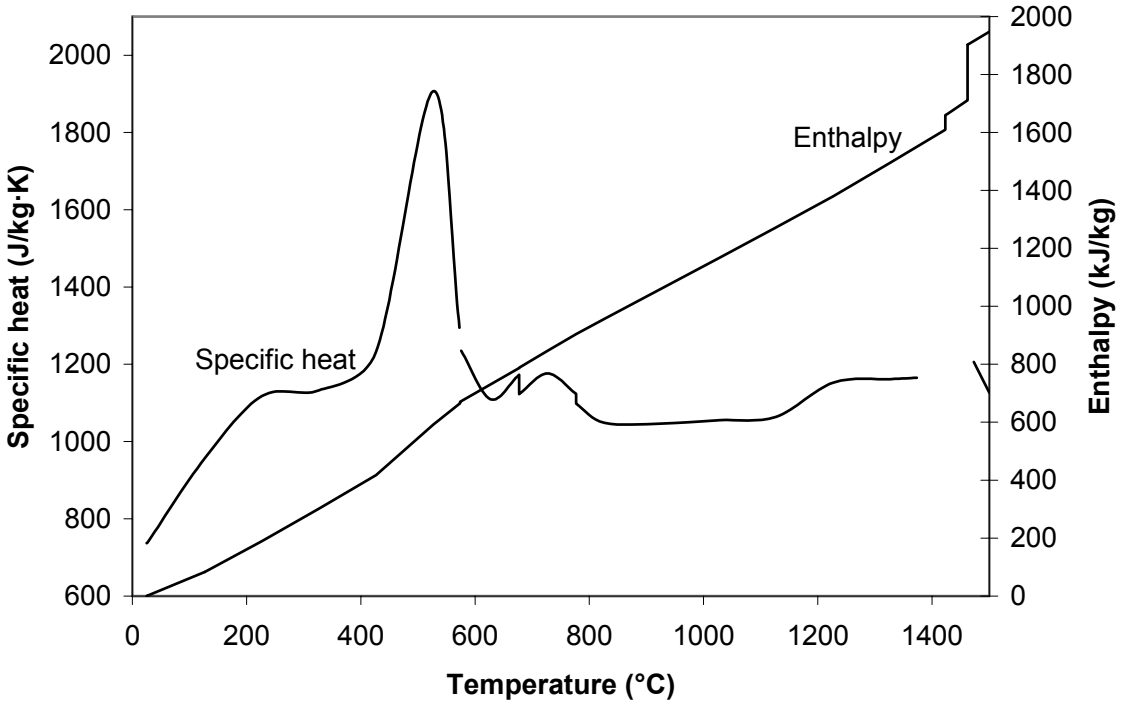

Figure 11. Calculated specific heat and enthalpy of EPR sacrificial concrete with 20 % cement paste, 40 % quartz aggregate, 40 % hematite aggregate and no evaporable water.

The specific heat of the three concrete types at room temperature is about 800 J/kg·K. This agrees with the experimental data in Figure 12. At elevated temperatures, the specific heat increases to about 1200 J/kg·K. This increase is similar in the experiments, but the exact numbers differ somewhat because of the large variation in different experiments. In the calculated specific heat curves, there is a peak at 400–600 °C because of the endothermic dehydration of calcium hydroxide. This peak is not clearly visible in the experimental curves. At 600–900 °C the specific heat of calcareous concrete is significantly higher than the other concrete types due to the endothermic decomposition of calcium carbonate. At temperatures ≥ 900 °C the specific heat of calcareous concrete is lower than siliceous and sacrificial concretes. This is because the specific heat has been calculated per kilogram of concrete at room temperature, and after the decomposition of $CaCO_3$, the mass of calcareous concrete has decreased significantly.

The enthalpy needed to heat one kilogram of dry concrete from the room temperature to 1500 °C is about 2000 kJ for both siliceous and sacrificial concretes. However, the density of the sacrificial concrete is higher than siliceous concrete. Because of this, the specific heat and enthalpy per cubic meter is higher for sacrificial than for siliceous concrete. The corresponding enthalpy for calcareous concrete is about 2800 kJ/kg, which is significantly higher than for siliceous and sacrificial concretes. This is due to the endothermic decomposition of calcium carbonate.

Nie (2004) reports decomposition temperature of 1080 °C for the sacrificial concrete, compared with 1295 °C for siliceous concrete. The latter number is in line with the melting temperatures of Portland cement, but there seems to be no explanation for the lower decomposition temperature for the sacrificial concrete. Calculations with GEMINI2 thermochemical software and NUCLEA03-1 database (Kekki 2005) give the solidus temperature of 1127 °C and liquidus temperature 1727 °C for the EPR sacrificial concrete. The ablation temperature can be estimated to be 1207 °C, where the GEMINI2 code gives solid fraction of 50 % for the concrete. The decomposition enthalpies 1950 kJ/kg for siliceous and 1730 kJ/kg for sacrificial concrete (Nie 2004) are on the same order of magnitude as the ones calculated in this paper.

The results calculated above do not contain evaporable water in concrete. For example, 2 % of evaporable water would increase the specific heat at ≤ 100 °C by about 10 % and the enthalpy above 100 °C by about 50 kJ/kg. This is a significant increase at low temperatures, but has only a small effect on the total decomposition enthalpy of concrete.

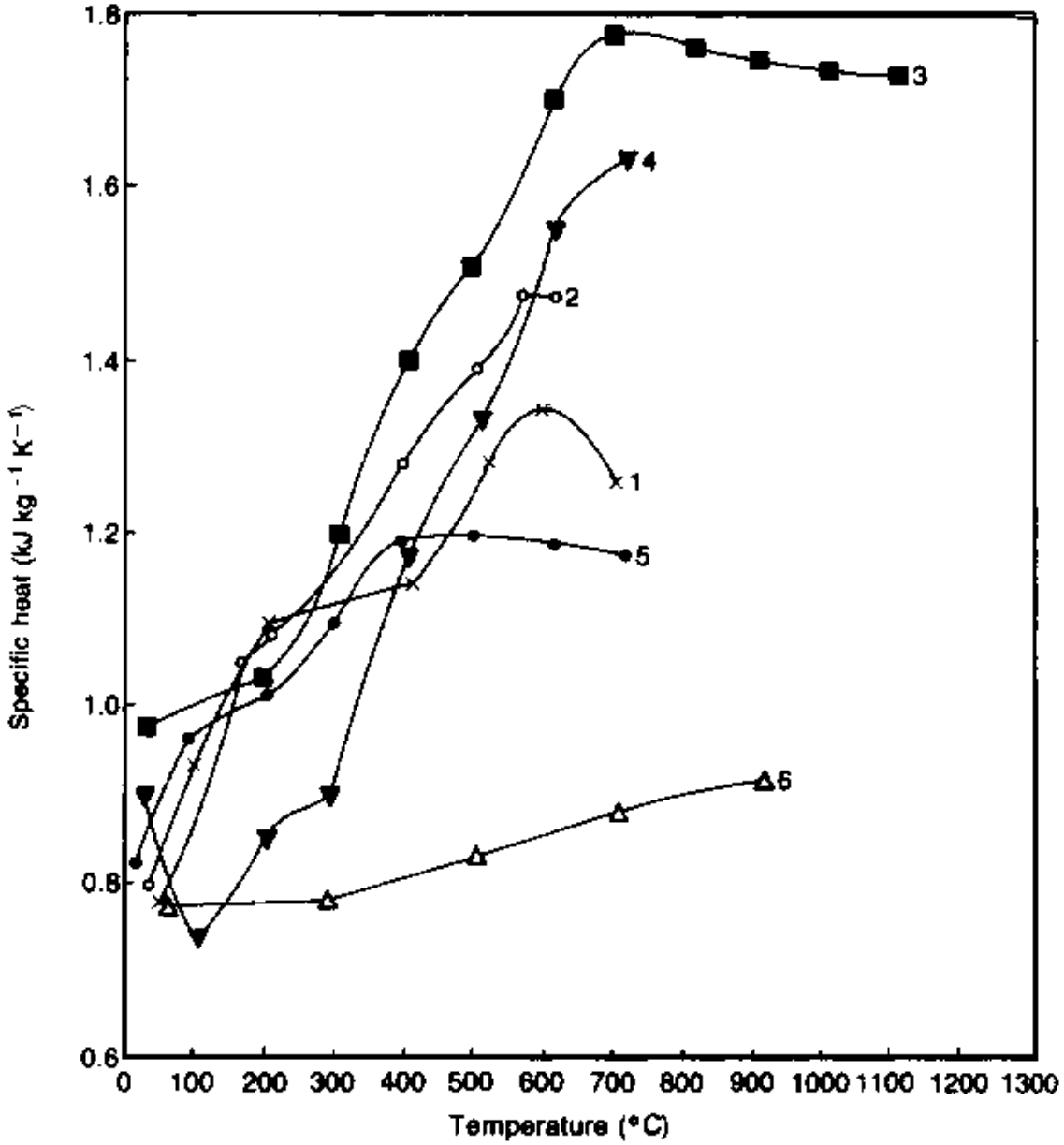

Figure 12. Measured specific heats of siliceous (curves 2 and 3), limestone (1, 4 and 5) and granite (6) aggregate concretes (Bažant & Kaplan 1996).

The thermal conductivity of Portland cement paste at normal temperatures depends strongly on the water content of the paste: The conductivity of saturated cement paste is 1.1–1.6 W/m·K, while the conductivity of oven-dried cement paste is only about 0.4 W/m·K. At temperatures over 100 °C, the conductivity of cement paste is approximately constant at 0.4 W/m·K. (Bažant & Kaplan 1996.)

According to Harmathy (1970), the thermal conductivity of quartz aggregate is about 6 W/m·K at room temperature and decreases to 3 W/m·K at 300 °C. The conductivity of limestone is about 4 W/m·K at room temperature and it decreases only a little at higher

temperatures (Bažant & Kaplan 1996). For hematite (Fe_2O_3), Mølgaard & Smeltzer (1971) report a linear decrease of conductivity from 6.1 W/m·K at 67 °C to 3.9 W/m·K at 402 °C.

The thermal conductivity of siliceous concrete decreases from about 2.5 W/m·K at room temperature to about 1.3 W/m·K at 800 °C and is approximately constant until melting. The conductivity of limestone concrete is about 2 W/m·K at room temperature and approximately equal to siliceous concrete above 100 °C. Because the conductivity of hematite is better than that of the common rock aggregates, it is expected that the conductivity of the EPR sacrificial concrete is a little better than that of normal structural concretes. Increasing the moisture content of concrete should increase its thermal conductivity, but because of large variation in experimental data, this has not been quantified experimentally. The conductivity of molten concrete is 1.0–1.2 W/m·K. (Bažant & Kaplan 1996.)

The density of Portland cement paste at room temperature without evaporable water is about 1400 kg/m^3. The density of the most common rock aggregates is about 2650 kg/m^3 (Harmathy 1970) and the density of hematite is 5300 kg/m^3 (Barthelmy 2004). The density of siliceous concrete at room temperature is around 2300 kg/m^3, and it decreases to about 2100 kg/m^3 at 800 °C. For calcareous (limestone) concrete, the density decreases from about 2300 kg/m^3 at room temperature to 2200 kg/m^3 at 600 °C. When calcium carbonate in calcareous concrete decomposes at 600–900 °C, the density of the concrete decreases significantly, to about 1400 kg/m^3. In the molten state, the density of both siliceous and calcareous concrete is about 2200 kg/m^3. (Bažant & Kaplan 1996.) According to Nie (2004), the density of the EPR sacrificial concrete is 2540 kg/m^3.

3.3 Heat Transfer from Molten Material to Concrete

The free convection heat transfer from hot liquid to horizontal or vertical surfaces has been studied extensively. The heat transfer correlations are generally presented as functions of the dimensionless Nusselt number

$$Nu = \frac{h L}{k} \tag{2}$$

and the dimensionless Rayleigh number

$$Ra = \frac{g\beta(T_{\text{melt}} - T_{\text{surface}})L^3\rho^2 c_p}{\mu k}, \tag{3}$$

where h is the heat transfer coefficient (W/m^{2}K), L is the characteristic length of the geometry, k is the heat conductivity, β is the coefficient of thermal expansion, ρ is the density, c_p is the heat capacity and μ is the dynamic viscosity of the melt, g is the acceleration of gravity, and T is the temperature. The melt properties are evaluated at the temperature $(T_{melt} + T_{surface})/2$.

In the case of molten core – concrete interactions, the heat transfer is substantially enhanced by the gas bubbles emerging from the concrete surface. However, correlations for the free convection heat transfer are quoted here, because they provide the lower limits for heat transfer in the limit of very low gas bubbling. According to Incropera & DeWitt (2002), the free convection heat transfer coefficient to a vertical wall can be calculated from

$$Nu = \left(0.825 + \frac{0.387\, Ra^{1/6}}{\left[1 + \left(0.492 / \mathrm{Pr}\right)^{9/16}\right]^{8/27}} \right)^2 , \tag{4}$$

where $\mathrm{Pr} = c_p\, \mu / k$ is the dimensionless Prandtl number of the melt. This correlation is valid for all Rayleigh numbers, i.e. for both laminar and turbulent convection. For free convection from hot fluid to a cooler horizontal bottom plate, Incropera & DeWitt (2002) recommend the correlation

$$Nu = 0.27\, Ra^{1/4} , \tag{5}$$

which is valid for the range $10^5 \le Ra \le 10^{10}$. The characteristic length is defined as L = area / perimeter of the plate.

The bubble-enhanced heat transfer from a melt pool to the boundaries, which is the dominant heat transfer mode for the MCCI, has not been the subject of extensive research. Based on his own and other published experiments, Greene (1991) recommends the following equation for the bubbling heat transfer coefficient h (W/m^{2}K):

$$h = 0.28\, k\, j_g^{0.22}\, \mathrm{Pr}^{1/3}\, g^{1/3}\, \nu^{-2/3} , \tag{6}$$

where j_g = volumetric gas flux / area = superficial gas velocity, and ν is the kinematic viscosity. The variables have to be presented in the SI units, and all properties are evaluated at the pool temperature. The same correlation can be applied for both the horizontal and the vertical surfaces.

Another correlation for bubble-enhanced heat transfer is the Bradley-CORCON model, which was originally implemented in the CORCON-Mod3 computer code (Bradley et al. 1993). The same model is also part of the Cavity package in the MELCOR 1.8.5

severe accident analysis program. The model uses a modified version of the Kutateladze correlation for bubbling heat transfer coefficient h:

$$h = \frac{1.6 \cdot 10^{-7} \sigma^2 \, h_1 + j_g^2 \mu^2 \, h_2}{1.6 \cdot 10^{-7} \sigma^2 + j_g^2 \mu^2} \tag{7}$$

$$h_1 = 1.5 \cdot 10^{-3} \frac{k^{1/3}}{g^{1/6}} \left(c_p \, p\right)^{2/3} \left(\frac{\rho - \rho_g}{\sigma} \right)^{1/2} j_g^{2/3} \tag{8}$$

$$h_2 = 3 \cdot 10^{-5} \frac{k^{1/3}}{g^{1/6}} \left(c_p \, p\right)^{2/3} \left(\rho - \rho_g\right)^{1/2} j_g^{1/6} \mu^{-1/2}, \tag{9}$$

where p is the pressure, ρ_g is the density of the gas in the bubbles and σ is the surface tension. Equation (7) is used for downwards heat transfer. Because of the high viscosities of the oxidic corium melts, h_2 usually has more weight in the weighted average of equation (7). For radial heat transfer, CORCON and MELCOR use equation (9).

The correlations presented above are based on low-temperature experiments with simulant materials. When applied to the molten core – concrete interactions, additional heat transfer resistances must be added to take account of the crusts and the possible layer of molten concrete at the boundaries of the pool. Enough experimental data does not exist to allow validation of these or any other heat transfer correlations for MCCI with real reactor materials (see section 4.9). In addition, the various material properties, which are necessary to apply the heat transfer models, are not known with satisfactory accuracy for the high temperatures and mixtures of materials that are encountered in MCCI.

3.4 Conservative Estimation of the Ablation Depth

Because of the complexity of the heat transfer problems associated with MCCI, the difficulties in conducting experiments with real reactor materials, and the lack of accurate material properties, it is not expected that an accurate heat transfer model for the MCCI could be developed in the near future. However, as regards nuclear accidents, it is often enough to be able to calculate the worst possible situation. For the MCCI, a conservative estimate can be made by assuming that all the heat from the molten corium goes into melting of the concrete. This assumption gives the fastest possible concrete erosion, as long as the interaction involves only melting of the concrete and not spalling.

The energy balance for the molten core – concrete interaction can be expressed as

$$Q_{\text{conc}} = m_{\text{melt}}(h_{\text{init}} - h_{\text{end}}) + Q_{\text{dh}} + Q_{\text{chem}} - Q_{\text{surf}}, \tag{10}$$

where Q_{conc} is the heat transferred from melt to concrete, m_{melt} is the melt mass, h_{init} is the initial and h_{end} is the final enthalpy of the melt per unit mass, Q_{dh} is the decay heat, Q_{chem} is the heat from chemical reactions and Q_{surf} is the heat transferred from the melt surface to the environment. As far as concrete ablation is considered, the smallest possible h_{end} equals the enthalpy of the melt at the ablation temperature of concrete, i.e. $h_{end} = h_{ablT}$. To find the largest possible value of Q_{conc}, the heat transferred through the melt surface can be ignored, so that

$$Q_{conc,\,max} = m_{melt}(h_{init} - h_{ablT}) + Q_{dh} + Q_{chem} \,. \tag{11}$$

If we assume constant decay heat power P_{dh} per unit mass of melt, then, at time t,

$$Q_{dh} = m_{melt}\, P_{dh}\, t \,. \tag{12}$$

The maximum ablation depth is achieved when the concrete-area-to-melt-volume ratio is at its minimum, i.e. when the pool is hemispherical. Assuming uniform concrete ablation gives

$$Q_{conc} = \rho_{conc}\, V_{conc}\, \Delta H = \rho_{conc}\, \Delta H \cdot 2/3\, \pi\, (r_{end}^3 - r_{init}^3) \,, \tag{13}$$

where ρ_{conc} is the density of concrete, V_{conc} is the volume of the molten concrete and ΔH is the decomposition enthalpy, i.e. the heat needed to convert a unit mass of concrete at the initial temperature to the concrete decomposition products at the ablation temperature. r_{init} is the initial and r_{end} the final cavity radius. If the melt includes metals, the chemical reaction heat of oxidation of the metals can be accounted for by reducing ΔH:

$$\Delta H = \Delta H_{actual} - \sum_i x_i\, Q_{react,\,i} \,. \tag{14}$$

Here x_i is the mass fraction of the decomposition product i from the concrete, and $Q_{react,\,i}$ is the heat that is released when unit mass of substance i reacts with the metals in the melt.

Inserting equations (12) and (13) into equation (11) (with Q_{chem} already included in ΔH) gives

$$r_{end}^3 - r_{init}^3 = \frac{3}{2\pi} \cdot \frac{m_{melt}\left(h_{init} - h_{ablT} + P_{dh} t\right)}{\rho_{conc}\, \Delta H} \,. \tag{15}$$

r_{init} can be solved from

$$V_{init} = \frac{2}{3}\pi\, r_{init}^3 = \frac{m_{melt}}{\rho_{melt}} \,. \tag{16}$$

The ablation depth d_{abl} is given by

$$d_{\mathrm{abl}} = r_{\mathrm{end}} - r_{\mathrm{init}} \ . \tag{17}$$

From these three equations, the maximum ablation depth as a function of time and melt mass can be expressed as:

$$d_{\mathrm{abl,\,max}} = \left(\frac{3\,m_{melt}}{2\,\pi} \right)^{1/3} \cdot \left[\left(\frac{h_{\mathrm{init}} - h_{\mathrm{ablT}} + P_{\mathrm{dh}}\,t}{\rho_{\mathrm{conc}}\,\Delta H} + \frac{1}{\rho_{\mathrm{melt}}} \right)^{1/3} - \left(\frac{1}{\rho_{\mathrm{melt}}} \right)^{1/3} \right]. \tag{18}$$

This equation allows a quick and conservative estimate of the ablation depth without complicated computer simulations. The only material properties that are needed are the densities of the concrete and the melt, the decomposition enthalpy of the concrete, and the enthalpy loss of the melt when cooling from the initial to the ablation temperature. This result could be refined by deriving an expression for the minimum heat transfer from the surface of the pool. Equation (18) assumes uniform ablation. If ablation is non-uniform, then ablation depth can be larger in some direction. Ablation can also be faster than calculated if pieces crack off the concrete surface.

If decay heat power or melt mass are not constants, then the decay heat term in equation (18) can be integrated:

$$d_{\mathrm{abl,\,max}} = \left(\frac{3\,m_{\mathrm{melt,tot}}}{2\,\pi} \right)^{1/3} \cdot \left[\left(\frac{h_{\mathrm{init}} - h_{\mathrm{ablT}} + \int_0^t \frac{m_{\mathrm{melt}}(t)}{m_{\mathrm{melt,tot}}} P_{\mathrm{dh}}(t)\,dt}{\rho_{\mathrm{conc}}\,\Delta H} + \frac{1}{\rho_{\mathrm{melt}}} \right)^{1/3} - \left(\frac{1}{\rho_{\mathrm{melt}}} \right)^{1/3} \right]. \tag{19}$$

3.5 Physical Properties of the Melt

Application of heat transfer correlations to molten core – concrete interactions requires values for various physical properties of the corium–concrete mixture. Due to the difficulties in measurements at very high temperatures and the complexity of the multi-component mixtures encountered in hypothetical nuclear accidents, the available data on the physical properties is scarce and uncertain. However, some values for the solidus and liquidus temperatures, viscosity, density, specific heat, thermal conductivity and surface tension can be found in literature.

The solidus and liquidus temperatures for corium–concrete mixtures with UO_2-to-ZrO_2 mole ratio of 1.6:1 (mass ratio 3.55:1) are summarized in the reference International Nuclear Safety Center (1998). The recommended values are presented in Figure 13. The

data is based on experiments with differential thermal analysis and rotational viscometry. Uncertainties in the solidus temperatures are estimated as ±10 %. Errors in the liquidus temperatures for mixtures with limestone and limestone/common-sand concretes are considerably larger. As can be seen from the figure, the differences between the solidus and liquidus temperatures are over 1000 degrees for corium–concrete mixtures. This corresponds to the "mushy" zone, in which both liquid and solid phases are present. To the author's knowledge, similar data for the EPR sacrificial concrete has not been reported in the public literature.

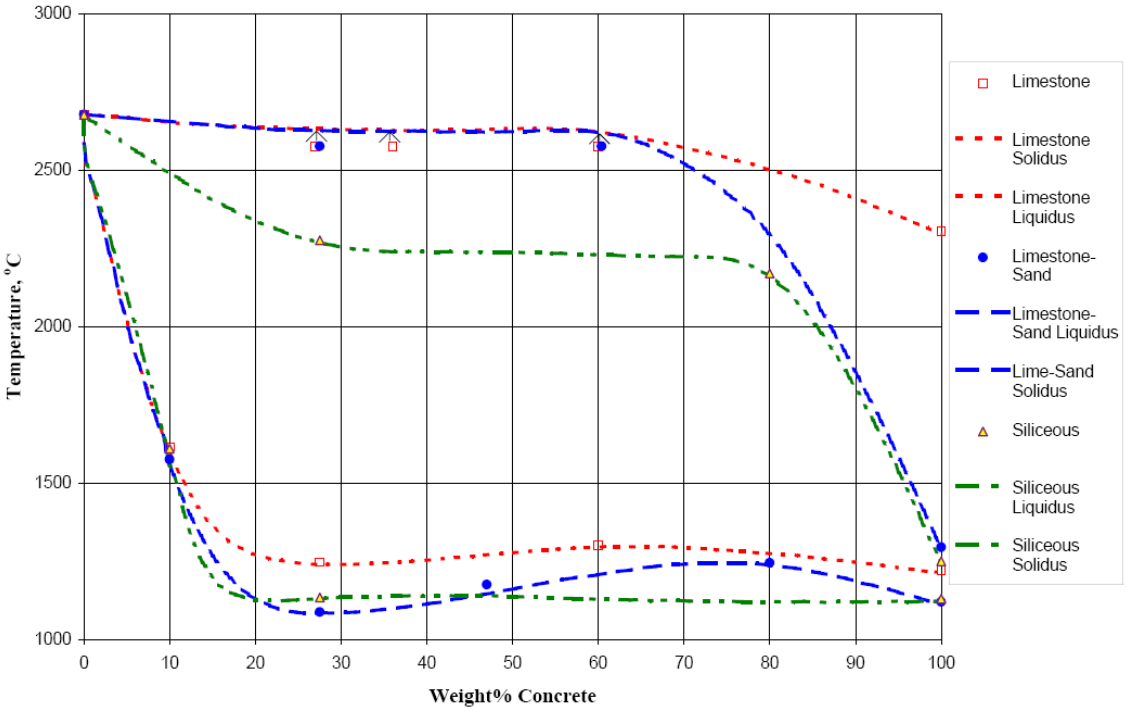

Figure 13. Solidus and liquidus temperatures of UO_2-ZrO_2-concrete mixtures (International Nuclear Safety Center 1998).

Epstein (1998) has presented an analysis of the viscosities of corium–concrete mixtures measured by Roche et al. in Argonne National Laboratories. The UO_2-to-ZrO_2 mole ratio was 1.6:1 (mass ratio 3.55:1). The measured viscosities were dependent on the rotation speed of the rotational viscometer, with very high apparent viscosities measured at small rotation speeds. Epstein interpreted this as viscoplastic behavior, where a certain yield stress τ_0 must be exceeded before the fluid will start flowing. Epstein applied the two-parameter Bingham model, where the shear stress τ is

$$\tau = \mu_0 \frac{du}{dy} + \tau_0 \quad \text{if } \tau > \tau_0 \tag{20}$$

and

$$\frac{du}{dy} = 0 \qquad \text{if } \tau < \tau_0 \,. \tag{21}$$

Here y is a direction normal to the flow, and $u(y)$ is the flow velocity as a function of the y-coordinate. When the shear stress exceeds τ_0, the fluid flows much like normal Newtonian fluid with Bingham viscosity μ_0. Epstein demonstrated that the flow during an MCCI is near-Newtonian, and the viscosity to be used in the heat transfer correlations for MCCI is the Bingham viscosity parameter μ_0.

The most reliable viscosity measurement was conducted with 27.5 weight-% siliceous concrete, and the viscosity of this mixture, analyzed by Epstein (1998), is presented in Figure 14. The data can be correlated by the equation

$$\mu_0 = \begin{cases} 5.187 \cdot 10^{-17}\, \mathrm{e}^{82\,230/T} \,, & 2000\,\mathrm{K} < T < 2284\,\mathrm{K} \\ 1.275 \cdot 10^{-5}\, \mathrm{e}^{22\,200/T} \,, & 2284\,\mathrm{K} \le T < 2600\,\mathrm{K} \end{cases} . \tag{22}$$

The data shows the strong temperature dependence of viscosity in the "mushy" zone between solidus and liquidus temperatures: The viscosity varied by a factor of over 500 at a temperature interval of 600 degrees. The scatter in the other measurements was so large that the dependence of viscosity on the concrete fraction cannot be analyzed. For mixtures with limestone/common-sand concrete, Epstein recommends a constant viscosity of 0.3 ± 0.2 kg/m·s and for limestone concrete 1.5 ± 1 kg/m·s. However, these values are not credible because they include no temperature dependence. Seiler and Ganzhorn (1997) have developed a method to calculate viscosities of corium–concrete mixtures, but this is beyond the scope of this paper.

The density of mixtures can be approximated by volume-averages of the individual components. According to Asmolov et al. (2003), the density of liquid UO_2 at its melting point is 8860 kg/m^3 and ZrO_2 5150 kg/m^3. The density of molten concrete is about 2200 kg/m^3 (Bažant & Kaplan 1996).

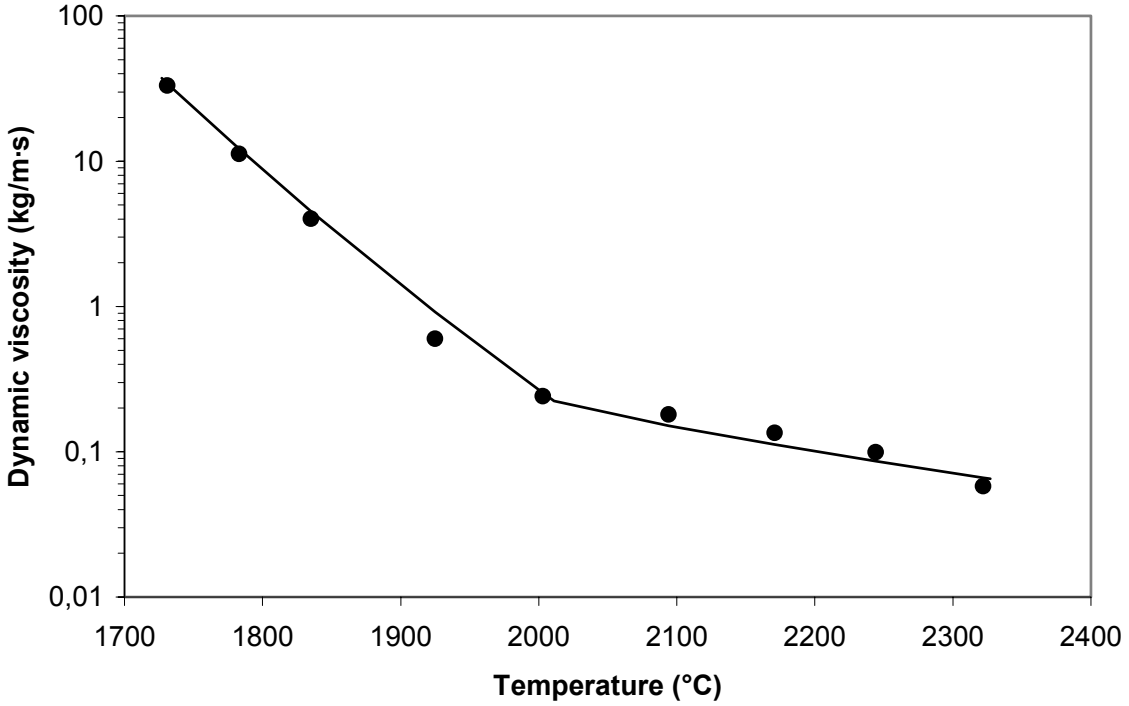

Figure 14. Viscosity of corium–concrete mixture with 27.5 weight-% siliceous concrete.

The specific heat of corium–concrete mixtures can be approximated as weight-averages of the individual components, although this is not exactly valid between the solidus and liquidus temperatures, because the mixtures melt over a temperature interval rather than at a single melting point. The data for three different concrete types are calculated in section 3.2.4. According to International Nuclear Safety Center (1999a & 1999b), the enthalpy H (kJ/kg) and heat capacity C_p (J/kg·K) of UO_2 can be calculated from the equations

$$H = -78.4217 + 193.217\,\tau + 162.853\,\tau^2 - 103.99\,\tau^3 + 29.2024\,\tau^4 - 1.9504\,\tau^5 + 2.6438\,\tau^{-1}, \quad 298\ \text{K} \le T \le 3120\ \text{K} \qquad (23)$$

$$H = 2976.8 + 9.3087 \cdot 10^{-4}\,T - \frac{4.9211 \cdot 10^6}{T}, \quad 3120\ \text{K} \le T \le 4500\ \text{K} \qquad (24)$$

$$C_p = 193.217 + 325.71\,\tau - 311.969\,\tau^2 + 116.81\,\tau^3 - 9.7522\,\tau^4 - 2.6438\,\tau^{-2}, \quad 298\ \text{K} \le T \le 3120\ \text{K} \qquad (25)$$

$$C_p = 0.93087 + \frac{4.9211 \cdot 10^9}{T^2}, \quad 3120\ \text{K} \le T \le 4500\ \text{K}. \qquad (26)$$

Here T is the temperature in kelvins and $\tau = T / 1000$. For ZrO_2 Gauntt et al. (2000a) give constant specific heat of 544.3 J/kg·K, heat of fusion 707 kJ/kg and melting temperature 2717 °C. The constant specific heat of ZrO_2 is not credible, but, however,

these values can be used for example in calculating the maximum ablation depth by equation (18).

The thermal conductivity of molten corium–concrete mixtures can be calculated as molar averages of the individual components. According to International Nuclear Safety Center (1996a), the thermal conductivity of liquid UO_2 is in the range of 2.5 to 3.6 W/m·K. Gauntt et al. (2000a) give the thermal conductivity of 2.49 W/m·K at $\geq$ 1727 °C for ZrO_2. The conductivity of molten concrete is about 1.1 W/m·K (Bažant & Kaplan 1996).

The surface tension of the melt is needed in the Kutateladze correlation, equations (7) and (8). International Nuclear Safety Center (1996b) recommends that the surface tension of liquid UO_2 is calculated from

$$\sigma\ (\mathrm{N/m}) = 0.513 - 1.9 \cdot 10^{-4} \cdot (T - 3120\ \mathrm{K}). \tag{27}$$

Values for the surface tension of ZrO_2 and concrete have not been found in literature.

4. Experiments on Molten Core – Concrete Interactions

This chapter includes a literature survey of experiments on molten core – concrete interactions. This text does not include the detailed results of the experiments, but it is intended to describe what kinds of experiments have been conducted and what kind of data is missing from the experimental data base. References to the detailed reports are given.

Basic information of past experiments is presented in Table 2. The table does not include the experiments where concrete has been replaced by a simulant material to measure the heat transfer rates in low temperatures. In the experiments involving concrete ablation, molten material has been poured into a concrete crucible, or the material has been melted in the crucible (in situ). Some of the tests are transient tests with no decay heat simulation, while in others the interaction has been prolonged by heating the melt with electricity or chemical reactions. Concrete ablation has been measured by thermocouples embedded in the concrete. When the temperature reading increases above the melting temperature of concrete, it can be concluded that the melt front has reached the thermocouple. In most experiments, only axial (downwards) ablation has been investigated, and the sidewalls have been constructed of a refractory material. In some experiments, also the radial erosion of the concrete sidewalls has been investigated. In the following, the experiments are briefly discussed.

Table 2. Basic information of experiments on molten core – concrete interactions. Abbreviations: LCS=Limestone/Common-Sand; BSG=BoroSilicate Glass; FeSi=Iron-oxide/silicate; Ax=axial; Rad=radial; SS=Stainless Steel; DEH=Direct Electrical Heating.

Experiment	Concrete type	Ablation direction	Melt composition	Melt delivery	Decay heat simulation
ACE L1 & L7	LCS	Ax	UO_2, ZrO_2, Zr, SiO_2, CaO	In situ	DEH
ACE L2	Siliceous	Ax	UO_2, ZrO_2, SiO_2, Zr	In situ	DEH
ACE L4	Serpentine/ Siliceous	Ax	UO_2, ZrO_2, Zr, SiO_2	In situ	DEH
ACE L5	LCS	Ax	UO_2, Fe_2O_3, ZrO_2, Cr_2O_3	In situ	DEH
ACE L6	Siliceous	Ax	UO_2, Zr, ZrO_2, SiO_2, SS	In situ	DEH
ACE L8	Limestone	Ax	UO_2, ZrO_2, CaO, Zr	In situ	DEH
BETA V0.1	Siliceous	Ax & Rad	Fe	Pour	None
BETA V0.2	Siliceous	Ax & Rad	Fe	Pour	Induction
BETA V0.3 & V1.2	Siliceous	Ax & Rad	Fe, Al_2O_3	Pour	Induction
BETA V1.3	Siliceous	Ax & Rad	SS, Al_2O_3	Pour	Induction
BETA V1.4	Siliceous	Ax & Rad	SS	Pour	None
BETA V1.5	Siliceous	Ax & Rad	SS	Pour	Induction
BETA V1.6–V1.9 & V2.1–V2.3	Siliceous	Ax & Rad	SS, Al_2O_3, CaO, SiO_2	Pour	Induction
BETA V3.1 & V3.3	LCS	Ax & Rad	SS, Al_2O_3, CaO, SiO_2	Pour	Induction
BETA V3.2	Limestone	Ax & Rad	SS, Al_2O_3, CaO, SiO_2	Pour	Induction
BETA V4.1 & V5.1–V5.3	Siliceous	Ax & Rad	SS, Zr, Al_2O_3, CaO, SiO_2	Pour	Induction
BETA V6.1	Siliceous	Ax & Rad	SS, Al_2O_3, ZrO_2	Pour	Induction
CCI 1	Siliceous	Ax & Rad	UO_2, ZrO_2, SiO_2, Cr	In situ	DEH
CCI 2	LCS	Ax & Rad	UO_2, ZrO_2, SiO_2, Cr	In situ	DEH
KAJET KJ02 & KJ08	Siliceous	Ax	Fe, Al_2O_3	Pour	None
KAJET KJ04	Siliceous	Ax	Al_2O_3	Pour	None
KAJET KJ05–KJ07	BSG	Ax	Fe, Al_2O_3	Pour	None
KAPOOL 1 & 5	BSG	Ax	Fe, Al_2O_3	In situ	None
KAPOOL 2 & 3	BSG	Ax	Fe, Al_2O_3	In situ	Addition of thermite powder
KAPOOL 6	FeSi	Ax	Fe, Al_2O_3	In situ	None
KAPOOL 7 & 8	FeSi	Ax	Fe, Zr, Al_2O_3	In situ	None
SURC 1	Limestone	Ax	UO_2, ZrO_2, Zr	In situ	Induction
SURC 2	Basaltic	Ax	UO_2, ZrO_2, Zr	In situ	Induction
SURC 4	Basaltic	Ax	SS, Zr	In situ	Induction
TURC 2	LCS	Ax	UO_2, ZrO_2	Pour	None
TURC 3	LCS	Ax	UO_2, ZrO_2, Zr	Pour	None
WETCOR 1	LCS	Ax	Al_2O_3, CaO, SiO_2	In situ	Induction

4.1 ACE Experiments

Seven experiments have been conducted in the ACE (Advanced Containment Experiments) program in Argonne National Laboratories in 1988–1991. They involved melting of about 300 kg of oxidic corium and zirconium on 50 by 50 cm concrete basemat. The electrical heating power was 35–100 kW. The temperature of the melt was measured by several thermocouples, and in four experiments the temperature data seems consistent and quite reliable. The melt was thoroughly mixed by the gases from the decomposing concrete, and no stratification of the oxidic and metallic melts was observed. In tests L1 and L7, a large amount of porous foam filled the test apparatus. The results are summarized and discussed in section 4.9. (Thompson et al. 1997.)

4.2 BETA Experiments

The BETA (Beton-Schmelz-Anlage) test series I (Alsmeyer 1987; Corradini & Reineke 1989) was conducted in 1984–1986 in Kernforschungszentrum Karlsruhe and it included the experiments V0.1–V4.1. The test series II (Alsmeyer et al. 1992; Firnhaber & Alsmeyer 1992; Alsmeyer et al. 1995), conducted in 1990–1992, included the experiments V5.1–V6.1. 300–880 kg of 1800–2300 °C melt was generated by the thermite reaction and poured into a cylindrical concrete crucible with diameter 38 cm (except 60 cm in test V4.1). After the pour, the underlying metallic portion of the melt was heated inductively with power up to 2 MW. The melt temperatures were measured with dip-in thermocouples, and in series II also with thermocouples embedded in the concrete. The V1 series studied the MCCI of siliceous concrete and very high heating power, while the V2 series used lower heating power. In the V3 series, calcareous concrete was used. The V4.1 test studied the effect of a larger crucible and zirconium addition. In V5 series, zirconium was added to the melt, and in V6.1 there was a water pool behind the concrete sidewall.

For the high-power experiments, axial erosion was much greater than the radial. With lower heating power and longer erosion times, the behavior was quite similar for the axial and radial directions. The data display a strong linear coupling between axial erosion rates and power input. The results of the test V4.1 were similar to the other experiments, and it can be concluded that the 38 cm crucible was large enough not to introduce unwanted scaling effects.

In all the experiments, the measured metal temperatures fell near to the metal solidification temperature in a couple of minutes. This may be due to very efficient heat transfer to concrete. Another explanation to the rapid decrease of temperature may be the splashing of the melt to the crucible walls in the beginning of the interaction.

However, this did not happen in all experiments, but the temperature drop was measured in every test. Also the accuracy of the temperature measurements has been questioned. However, in test series II, several different temperature measurements gave values within ±25 °C, which would imply that the dip-in measurement technique was reliable.

4.3 CCI Experiments

In the MCCI (Melt Coolability and Concrete Interaction) program in Argonne National Laboratories, two CCI experiments have been conducted. The experiments used a chemical reaction to melt 400 kg of mostly UO_2, ZrO_2, SiO_2 and Cr over a 50 by 50 cm concrete basemat. Two opposing sidewalls were made of concrete and the other two of refractory MgO. Siliceous concrete and electrical heating power of 150 kW was used in CCI 1 (Farmer et al. 2004), while limestone/common-sand concrete and heating power of 120 kW was used in CCI 2 (Farmer et al. 2005). After some ablation, the cavity was flooded with water to obtain data on the coolability of a core melt. The results indicate that radial ablation is an important element of the cavity erosion process. The detailed result data is protected by a proprietary agreement.

4.4 KAJET Experiments

The KAJET experiments were conducted in Forschungszentrum Karlsruhe in 1999–2002 to study the interaction of a compact melt jet with concrete. 40–160 kg of molten Al_2O_3 and Fe was released from a nozzle under driving pressures of 3–8 bar. The jet was directed onto a concrete surface. The concrete samples were attached to a revolving mechanism to allow separate studies of metallic and oxidic melts. The experiments lasted only a few seconds. The velocity of the melt jets were calculated to be 7.7–18 m/s. The measured erosion rates were 8.9–11.2 mm/s (iron) and 4.5–10 mm/s (oxide) for siliceous concrete, and 5.2–8 mm/s (iron) and 2.8–5.1 mm/s (oxide) for borosilicate glass concrete. The conclusion was that the erosion is mainly due to the impingement heat transfer from the jet, and mechanical and chemical processes have a minor influence. (Albrecht et al. 2005.)

4.5 KAPOOL Experiments

In KAPOOL experiments, conducted in Forschungszentrum Karlsruhe, 100–150 kg of melt was generated by the strongly exothermic thermite reaction $8\ Al + 3\ Fe_3O_4 \rightarrow 4\ Al_2O_3 + 9\ Fe$. In KAPOOL 7 and 8, some zirconium was added to the melt. Due to the

different densities of Al_2O_3 and Fe, the materials stratify so that alumina is on the surface and only the metal is in contact with the concrete basemat. In KAPOOL 1–5 (Fellmoser et al. 1999), the basemat was made of borosilicate glass concrete, in which the main constituents of the aggregate were 60 % SiO_2 and 17.6 % B_2O_3. KAPOOL 6–8 (Eppinger et al. 2000) used hematite/silicate concrete similar to the EPR sacrificial concrete, except that only 8 % of the dry materials was cement, compared to 15 % in the preliminary EPR concrete (Nie 2004). This probably made the concrete porous, and the density of the KAPOOL 6–8 concrete is reported to be only 2200–2300 kg/m^3, compared to 2540 kg/m^3 reported by Nie (2004). In all tests, the concrete was oven-dried to remove all the evaporable water. The tests were transient, i.e. there was no decay heat simulation (except the addition of some thermite powder in KAPOOL 2 and 3).

The temperature measurements were consistent and can be considered quite reliable. The erosion rates versus iron melt temperatures are plotted in Figure 15. According to (Fellmoser et al. 1999), the temperature measurement for KAPOOL 3 was uncertain by 47 °C, and in the following calculations, its temperature value has been decreased by 47 °C to give a better fit to the other results. For the sacrificial concrete, the erosion stops when the temperature decreases to about 1450 °C. If a linear function is fitted into the borosilicate glass concrete data, the corresponding temperature is about 1550 °C. Probably these are the solidification temperatures of the iron–concrete mixtures.

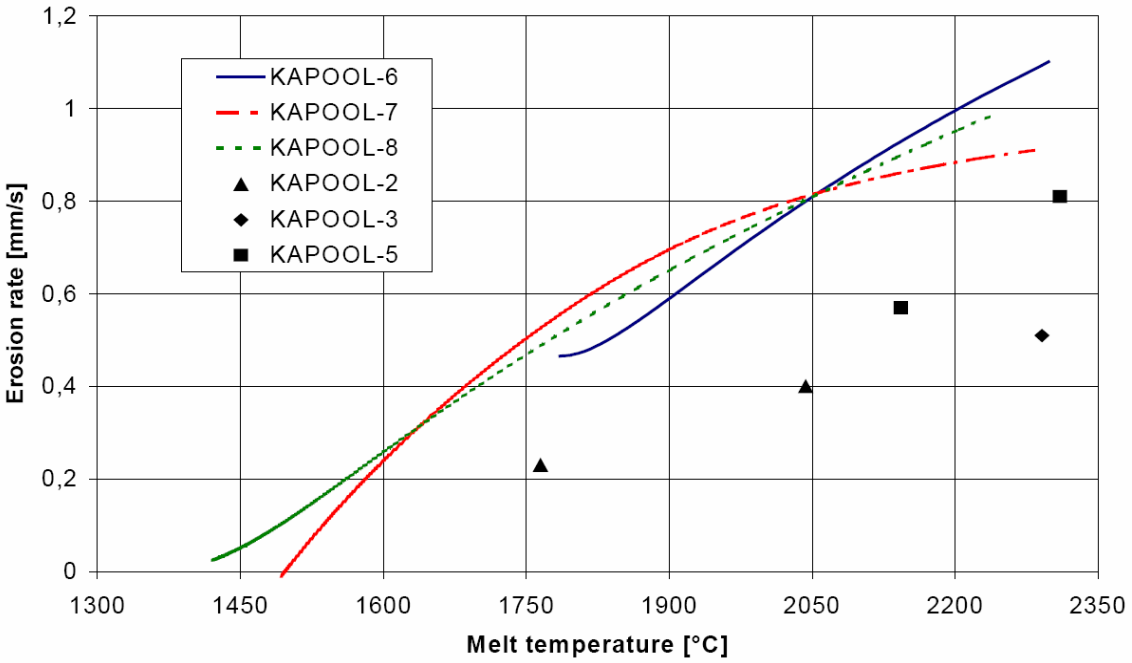

Figure 15. Erosion rates for borosilicate glass concrete (KAPOOL 2, 3 and 5) and sacrificial concrete (KAPOOL 6, 7 and 8) as a function of the iron melt temperature (Eppinger et al. 2000).

The heat transfer coefficient from the melt to concrete can be estimated from

$$\alpha = \frac{\rho \Delta H v}{T_{\text{melt}} - T_{\text{surface}}} \tag{28}$$

where ρ is the density of the concrete (assumed 2300 kg/m^3) ΔH is the decomposition enthalpy of the concrete (assumed 2 MJ/kg), v is the velocity of the erosion front, and T_{melt} and T_{surface} are the temperatures of the melt and the concrete surface. With the assumption that the decomposing concrete surface is at the temperature of 1300 °C, the heat transfer coefficients in the KAPOOL experiments have been calculated and are presented in Figure 16. For sacrificial concrete, the coefficient is approximately constant at 4900 W/m^2·K at temperatures >1700 °C and decreases to zero at 1450 °C. This decrease is probably due to solidification and increase of viscosity of the melt. For borosilicate glass concrete, the heat transfer coefficient is approximately half of the sacrificial concrete.

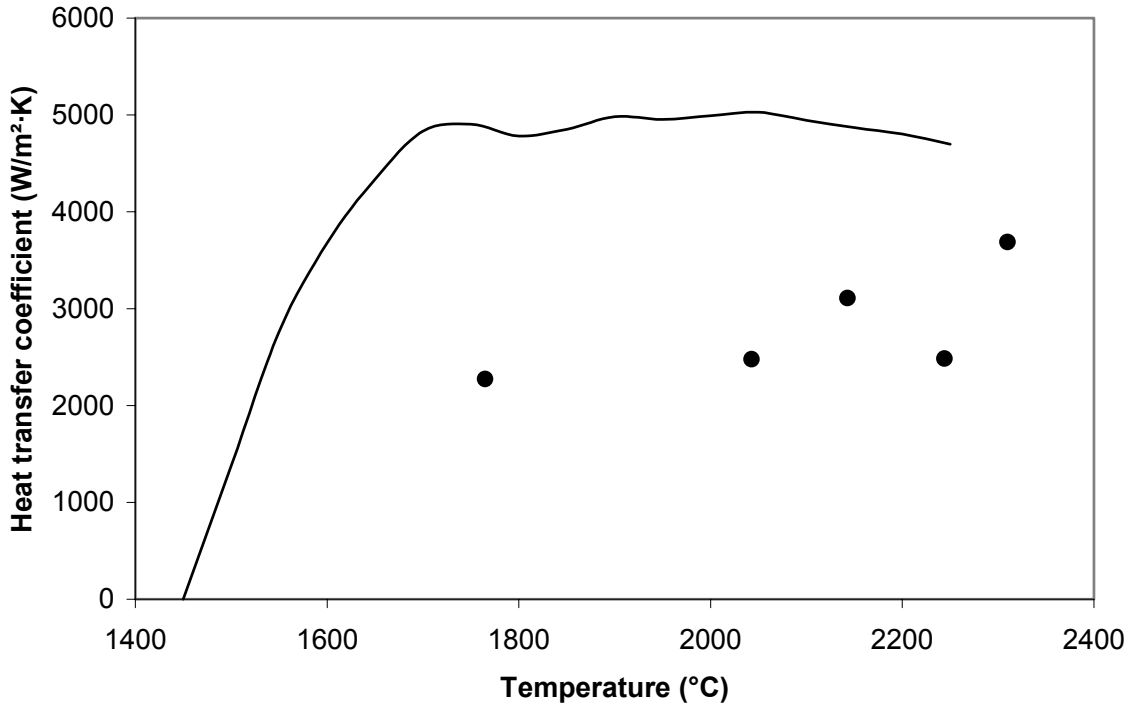

Figure 16. Calculated heat transfer coefficients in KAPOOL experiments for sacrificial concrete (line) and borosilicate glass concrete (points) as a function of the iron melt temperature.

4.6 SURC Experiments

The SURC (Sustained Urania–Concrete) experiments were conducted in Sandia National Laboratories. In the experiments, oxidic and/or metallic material was melted

and heated by induction heating in a crucible with diameter 40 cm, which had MgO refractory sidewalls and concrete basemat.

In SURC 1 (Copus et al. 1992a) and 2 (Copus et al. 1992b) experiments, 204 kg of UO_2, ZrO_2 and Zr was melted over limestone (SURC 1) or basaltic (SURC 2) concrete. The experiment reports contain contradictory values for the net heating power, but it seems that, during concrete ablation, the heating power was 60–100 kW in both experiments. The power histories were nearly identical in both tests. In 150 minutes, the limestone concrete ablated 27 cm and the basaltic concrete 35 cm. The melt temperature was measured with several thermocouples and optic pyrometers. In both experiments, the measurements gave values which differed hundreds of degrees from each other. So the melt temperature is not known with satisfactory accuracy.

In SURC 4 experiment (Copus et al. 1989), 200 kg of stainless steel was melted over basaltic concrete basemat. 20 kg of zirconium metal was added after ablation of about 5 cm of concrete, which took about 15 minutes. The heating power was 63 ± 6 kW, except for a power outage of about 8 minutes. In 60 minutes, the concrete ablated about 25 cm. The melt temperature was about 1500 °C in the beginning of the interaction, peaked at 1650 °C after zirconium addition, and then decreased back to 1500 °C. In this experiment, the temperature measurements are consistent with each other and therefore can be considered quite reliable. Remarkable in this experiment was the production of about 100 kg of very porous oxide "foam" with density of 700–1200 kg/m^3. The foam might accelerate concrete erosion by acting as thermal insulation at the surface of the pool. On the other hand, the report of the ACE experiments (Thompson et al. 1997) concludes that foaming reduces the heat transfer to concrete.

4.7 TURC Experiments

TURC 2 and 3 (Transient Urania–Concrete Test) experiments were conducted in Sandia National Laboratories. They consisted of pouring corium melt onto limestone/common-sand concrete. In TURC 2 the melt was 147.2 kg of UO_2 and ZrO_2, and in TURC 3 the 46.45 kg melt included also Zr. The tests were transient, i.e. no decay heat simulation was included. The temperature of the melt was only little above the melting temperature, so it solidified upon contact with concrete and less than 5 mm concrete ablated. Transient heat conduction into the concrete was observed, resulting in the decomposition of the concrete and release of H_2O and CO_2. (Gronager et al. 1986.)

4.8 WETCOR Experiment

WETCOR 1 experiment was conducted in Sandia National Laboratories in 1991. It involved melting of 34.1 kg of Al_2O_3, CaO and SiO_2 over limestone/common-sand concrete basemat with diameter of 40 cm. The average heating power during concrete ablation was 20 kW. After 63 minutes and 0–3 cm of ablation, water was added onto the pool surface to demonstrate corium quenching by water. The water addition was unable to stop the concrete ablation, and after 90 minutes a total of 5–6 cm of concrete had ablated. (Blose et al. 1993.)

4.9 Discussion

Reports of a total of 50 MCCI experiments were found in the open literature. 37 of these were measurements of metallic melt penetration into concrete, and in 13 experiments oxidic melt was used. The most reliable data is the concrete erosion velocity v, which was measured by thermocouples embedded in concrete. The heat flux to concrete can be calculated by

$$\dot{Q} = \rho \, \Delta H \, A \, v, \tag{29}$$

where ρ is the concrete density, ΔH is the decomposition enthalpy per unit mass of concrete, and A is the area of the eroding concrete. In this equation, the heat conduction deeper into concrete is ignored because of the very poor heat conductivity of concrete. To obtain heat transfer correlations, the temperatures of the melt pool and the concrete surface should be known. The concrete surface can be assumed to be at the concrete melting temperature, which is around 1300 °C for most commonly used concrete types. Measuring the melt temperature is difficult because of the high temperatures (especially for oxidic melts) and the chemically aggressive environment. The melt temperature should be measured by several methods, and if the different measurements agree with each other, then the data can be considered reliable.

In Figure 17, the average heat flux to concrete basemat per unit area as a function of measured steady-state temperature has been plotted for nine experiments with metallic melts. Included are the eight BETA experiments for which the necessary data has been reported in obtainable literature, and the SURC 4 experiment. The heat flux has been calculated by equation (29). The density has been assumed to be 2300 kg/m^3 and the decomposition enthalpy 2 MJ/kg for siliceous and basaltic and 2.4 MJ/kg for limestone/common-sand concrete. As can be seen from the figure, the scatter of the data points is so large that no heat transfer correlation can be obtained from the data. In Figure 18, the average axial heat flux in the same experiments has been plotted as a function of the average heating power to the melt. Approximations of the chemical

heating power from zirconium oxidation have been added to the electric heating powers. A linear function has been fitted to the data points, and the match is reasonably good.

It would be expected that the heat transfer rate from melt to concrete basemat would be a function of the melt temperature. However, Figure 17 shows that this is not the case for metallic melts. On the contrary, the coupling between the heating power and heat transfer rate in Figure 18 is remarkably good. The easy explanation would be that the temperature measurements were inaccurate. However, in BETA test series II, the dip-in thermocouple technique was validated against different thermocouples protruding from the walls to the melt, and the agreement was very good. Based on comparisons between BETA and SURC experiments, Epstein (1998) hypothesized that a spalling process was initiated in BETA experiments because of the pouring of the melt onto the concrete, and this would explain the discrepancy between temperatures and erosion rates. However, the calculated heat fluxes to concrete in the experiments are substantially smaller than the heating powers, which would suggest that the ablation can be due to heat transfer and melting, not necessarily spalling.

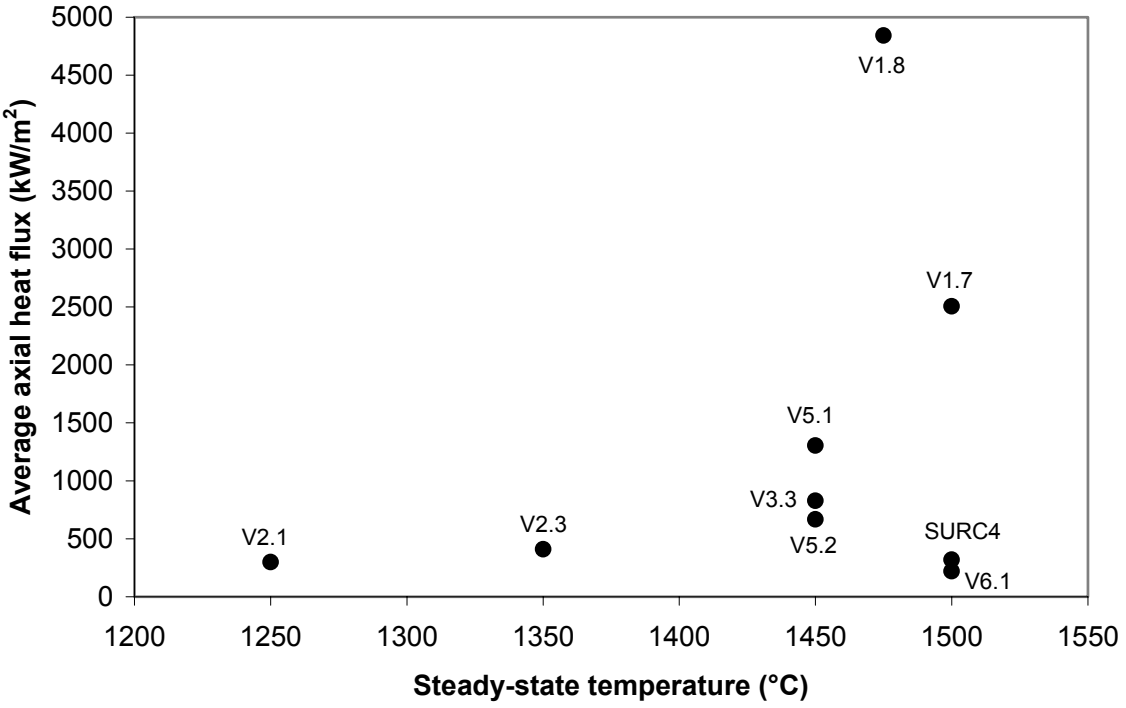

Figure 17. Average heat flux to concrete basemat as a function of metallic melt steady-state temperature from eight BETA experiments and SURC 4 experiment.

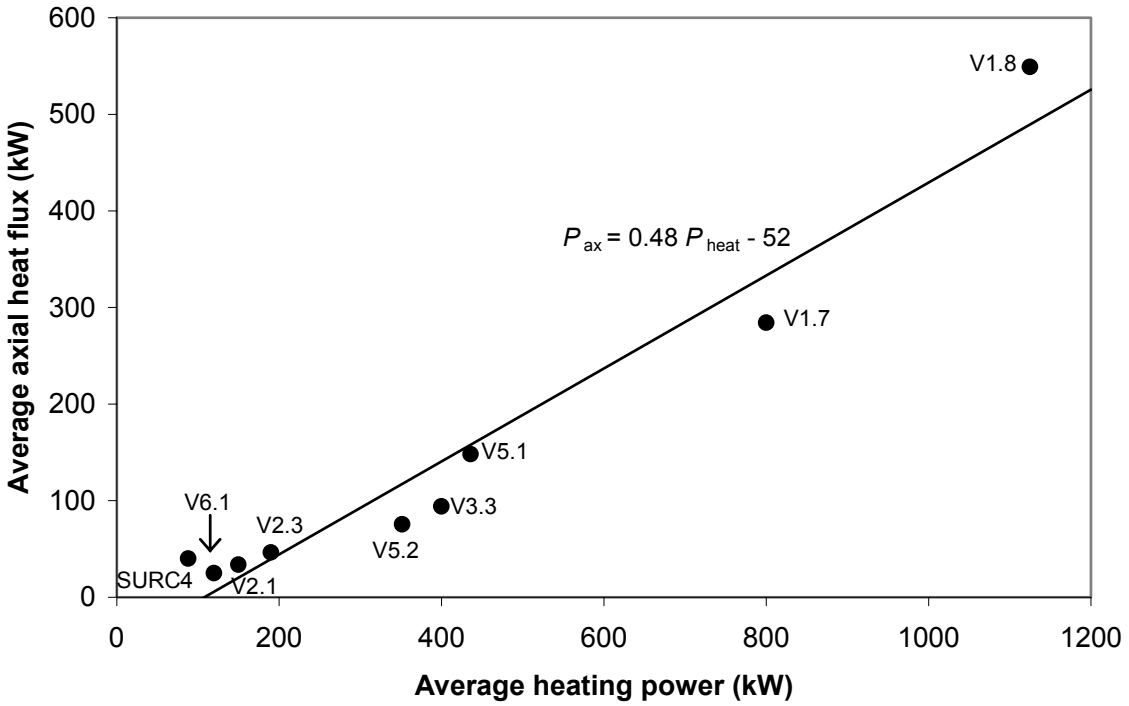

Figure 18. Average heat flux from metallic melts to concrete basemat as a function of the average heating power from eight BETA experiments and SURC 4 experiment. A linear function has been fitted to the data points.

In all BETA experiments, the melt rapidly cooled from the high initial temperatures to near the solidification temperature. This would suggest a very efficient heat transfer induced by the gas bubbles from the decomposing concrete, as long as the pool is in the liquid state. The coupling between heat transfer rate and the heating power can be explained by the crust thickness: With lower heating power, a thicker crust is present between the melt and the concrete surface. The crust thickness

$$d_{\text{crust}} = \frac{\lambda_{\text{crust}} \left(T_{\text{melt,solidus}} - T_{\text{concrete,melting}} \right)}{\dot{Q}_{\text{conduction}} / A} \tag{30}$$

is such that the heating power can be transferred through the crust, with the inner surface at the melt solidification temperature and the outer surface at the concrete melting temperature. λ_{crust} is the heat conductivity of the crust. Because of the very efficient heat transfer in the liquid phase, the metallic melt would always be near to the solidification temperature. If this hypothesis is correct, all attempts to correlate temperatures and steady-state heat transfer rates from metallic melts to decomposing concrete would be doomed to fail, as the melt steady-state temperature would depend only on the solidification temperature of the melt.

The situation is different for the transient case, like the KAPOOL experiments (section 4.5). There a sensible correlation between the melt temperature and the heat transfer

coefficient can be obtained (Figure 16). The surprising feature is that the heat transfer coefficient saturates at a constant level above 1700 °C, while it would be expected to keep rising with increasing gas flux through the melt at rising temperatures and erosion rates.

In Figure 19, the average heat flux to concrete basemat per unit area as a function of measured average temperature has been plotted for four ACE experiments with oxidic melts. Included are the oxidic melt experiments for which the temperature data seems consistent and reliable. The experiment L8 provides two data points, as the heating power was reduced during the experiment. The heat flux has been calculated by equation (29). The concrete density has been assumed to be 2300 kg/m^3 and the decomposition enthalpy 2 MJ/kg for siliceous, 2.4 MJ/kg for limestone/common-sand and 2.8 MJ/kg for limestone concrete. The heat flux seems to increase with increasing temperature, as is expected.

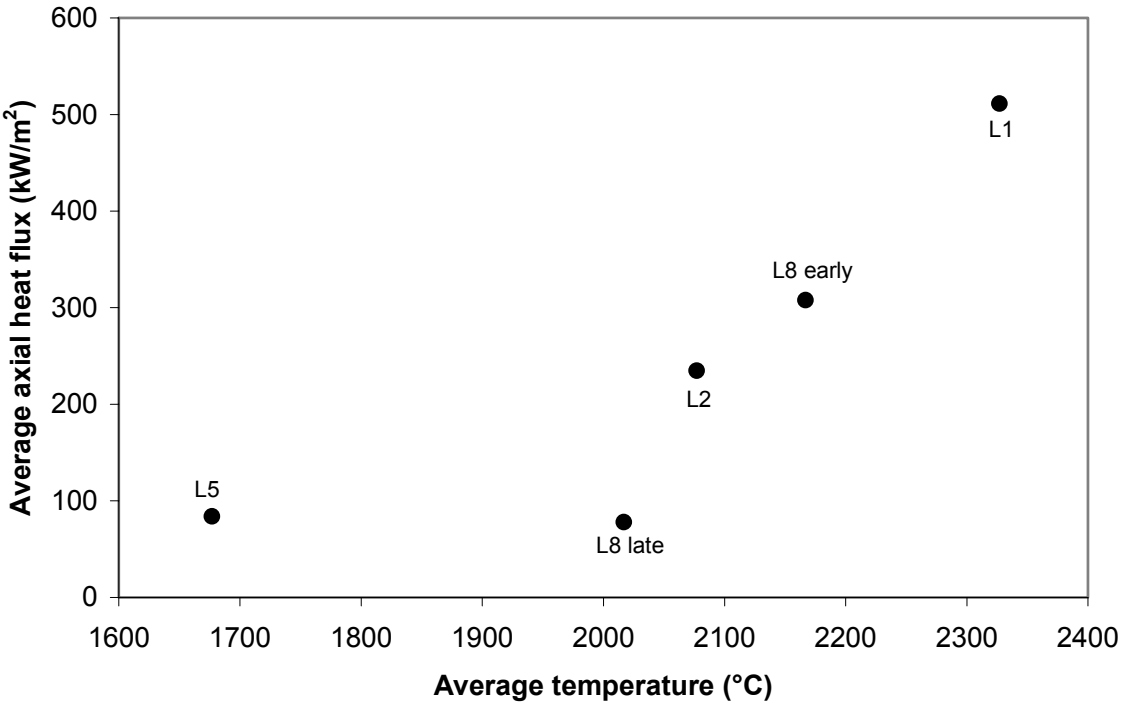

Figure 19. Average heat flux to concrete basemat as a function of oxidic melt average temperature from four ACE experiments.

In Figure 20, the average axial heat flux in six ACE experiments has been plotted as a function of the average heating power to the melt. Approximations of the chemical heating power from zirconium oxidation have been added to the electric heating powers. The L1 experiment has been ignored, since during the experiment the heating power fluctuated so that no reliable average value can be estimated. The experiment L8 provides two data points, as the heating power was reduced during the experiment. The reported

electric heating powers in the ACE experiments do not include the portion of the power that was transferred out through the sides of the crucible. Because of this, the powers of the ACE and SURC experiments are not comparable. A linear function has been fitted to the data points, and the match is not as good as for the metallic melts (Figure 18).

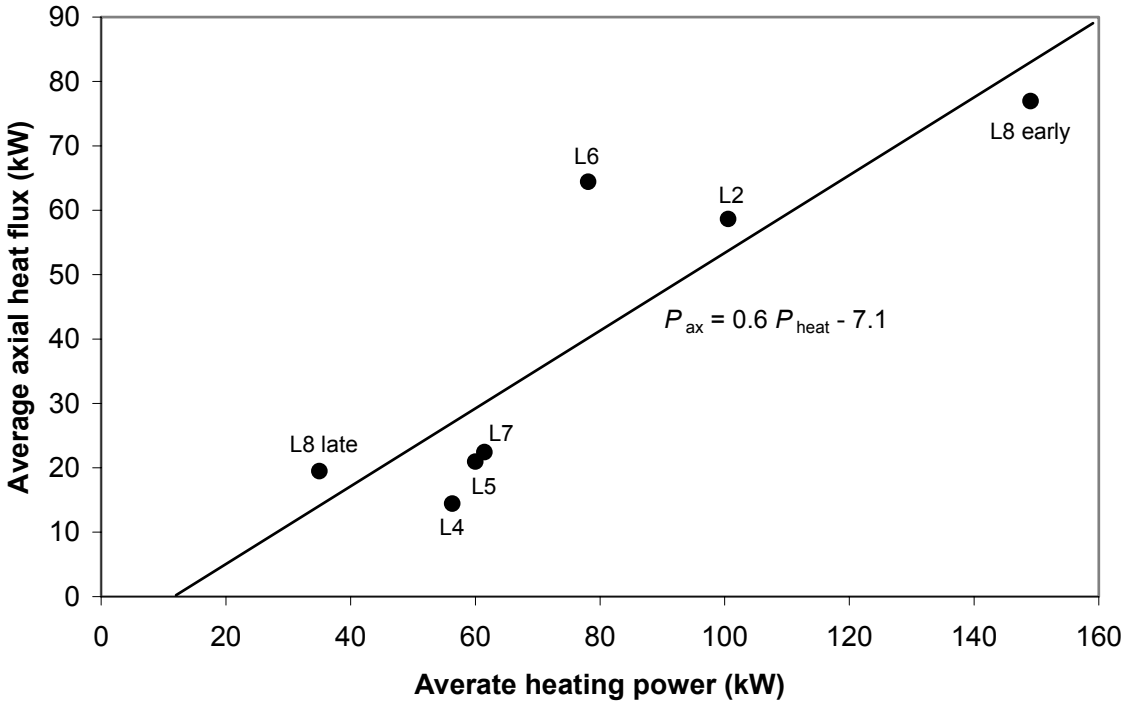

Figure 20. Average heat flux from oxidic melts to concrete basemat as a function of the average heating power from six ACE experiments. A linear function has been fitted to the data points.

Contrary to the metallic experiments, the oxidic experiments show quite clear temperature dependence. Probably this is due to the fact that the oxidic melts do not solidify at a single temperature, but instead between solidus and liquidus temperatures, which are quite far apart. The measured temperatures in ACE experiments were between the solidus and liquidus temperatures of the corium–concrete mixtures. The available experimental data of only five points with reliably measured temperatures is not enough to justify any heat transfer correlation, since there are differences in the concrete types and their gas contents. In addition, the viscosities of the melts are not known sufficiently well.

The BETA experiments concentrated more on the axial erosion, but also radial erosion rates comparable to the axial rates were measured in the low power experiments. Considering also the (unpublished) results of the CCI experiments, it can be recommended that the same erosion rate for radial and axial directions would be used in calculations.

There are only a few experiments with real oxidic corium materials, where the temperature has been measured reliably. This is understandable, since handling of radioactive uranium and achieving and measuring the necessary high temperatures are very difficult and expensive tasks. To obtain reliable heat transfer correlations, more experimental data is needed. However, such correlations may not be absolutely necessary to analyze the safety of nuclear power plants. As long as the concrete erosion involves only melting and not spalling, the maximum possible erosion depth can be calculated by the conservation of energy (see section 3.4). More important is the possible spalling of concrete: If pieces crack off the concrete surface, erosion can be much faster than predicted by energy balances.

5. Design of an Experimental Facility

5.1 Objectives of the Experiments

The main goal of this work is to design an experimental facility to obtain more information on the interactions of molten core with concrete. This information is important in verifying the functioning of the core melt stabilization concept of the EPR, and also in severe accident analysis of many other nuclear power plants. The design of the EPR is so robust that even large uncertainties in heat transfer correlations and physical properties of the core melt do not threaten the safety of the environment even in the extreme case of a core melt accident. However, rapid spalling of the sacrificial concrete in the reactor pit is a phenomenon that might have an impact on the proper functioning of the core catcher and the stabilization of the corium melt. No systematic experimental program for testing the spalling of concrete under pouring of molten material has been conducted.

The main objective of the experimental program under design is to assess the probability of concrete spalling under pouring of molten material and the factors that affect the phenomenon. In addition, more data on heat transfer from melt to concrete can be obtained from the experiments if the temperature of the melt can be measured accurately. An interesting factor is the initial impingement heat transfer from the melt jet, which has not been studied extensively, since in most previous experiments the melt has been generated in the concrete crucible, not poured as would be the case in an accident. Another interesting factor is the ratio of the erosion of the horizontal bottom plate to the erosion of the vertical sidewalls. To keep the costs at a reasonable level, the aerosol and gas release from the melt will not be measured in these experiments.

5.2 General Design of the Facility and the Experiments

This section covers the main aspects of the experimental facility and the experimental program. The details of the construction will be designed by experts of scientific apparatus building, taking into account the available resources. The main components of the facility are illustrated in Figure 21.

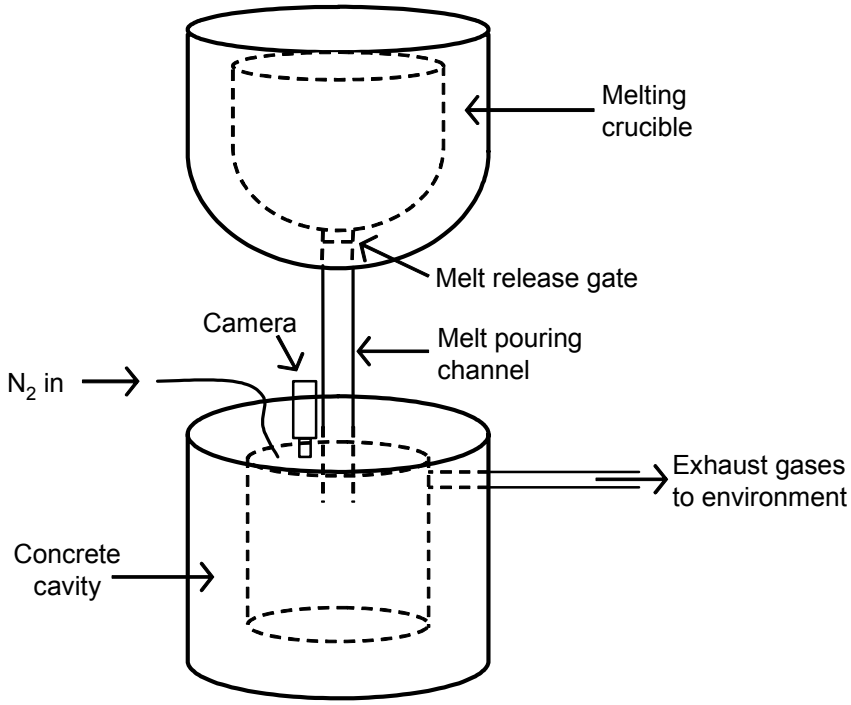

Figure 21. Main components of the experimental facility.

5.2.1 Concrete Cavity

The shape of the reactor pit in most nuclear power plants, including the EPR, is cylindrical. Because of this, most accident analysis programs have been designed to work with cylindrical cavities only. To allow analysis of the experiments by these programs, the shape of the concrete cavity in these experiments has been decided to be cylindrical, even though it may be more difficult to construct than a rectangular cavity.

The majority of MCCI experiments have concentrated on measuring the axial ablation, i.e. the melting of the basemat of the cavity. However, the radial sidewall erosion is equally important in accident analysis of nuclear power plants. Because of this, it has been decided to construct both the bottom and the sidewall of the cavity from the same kind of concrete and to insert proper instrumentation also into the sidewall to measure the radial ablation rate. This also eliminates the difficulties in ensuring the leak-tightness of the joint between the bottom and the sidewall materials.

In order to save costs and decrease the safety risks of the experiments, the concrete cavity shall be as small as possible, as long as all the necessary measuring instruments and the pouring channel for the melt fit in to the cavity area. As a preliminary plan, a diameter of 30 cm for the cylindrical cavity is used. In small-scale models of power plants, ratio of surface area to volume is always larger than in the plant scale, and hence

the melt will cool down much faster than in the reactor accident. To minimize the area-to-volume ratio, the depth of the melt pool should equal the diameter of the pool. However, in practice the diameter must be large enough to fit all the instrumentation, but for the depth there is no such limitation. To limit the size of the experiments, it has been decided to keep the depth of the melt pool somewhat smaller than the diameter. As a preliminary plan, a melt mass of 70 kg is used. With melt density of about 7000 kg/m^3, this produces a depth of about 14 cm.

5.2.2 Melt Generation, Pouring and Heating

During the hypothetical core melt accident, the molten UO_2 fuel, Zr fuel rod cladding and stainless steel support structures would relocate to the bottom of the reactor pressure vessel. Because the metals and oxides are immiscible with each other, it is expected that the melt separates into two layers: the heavier UO_2 and ZrO_2 at the bottom of the vessel, and the lighter metals on the surface (Figure 22). Because of the high solidification temperature of the oxides, a thick solid crust would be formed between the oxidic melt and the pressure vessel. As the thermal conductivity of the oxides is very poor, the crust would decrease the heat transfer rate from the oxides to the pressure vessel. On the contrary, the thermal conductivity of the metals is very good. The metal layer may be heated a couple of hundred degrees above the melting point of steel due to the upward heat transfer from the oxide pool, and convection heat transfer from the molten metal to the pressure vessel takes place. Because of this, it is expected that the thermal load to the pressure vessel would be highest at the location of the overlying metal layer. This focusing effect is illustrated in the calculated heat flux distribution to the Loviisa RPV wall in Figure 23. As a consequence, the vessel may be breached first at the height of the metallic melt. So the metallic melt would be poured first in to the reactor pit, followed later by the oxidic melt.

To simulate the beginning of the melt release, it has been decided to conduct the experiments with molten stainless steel and zirconium. This decision is supported by the fact that the facilities to handle large amounts of molten radioactive uranium are not readily available, and the high temperatures needed to melt UO_2 and ZrO_2 would be very difficult to achieve and measure.

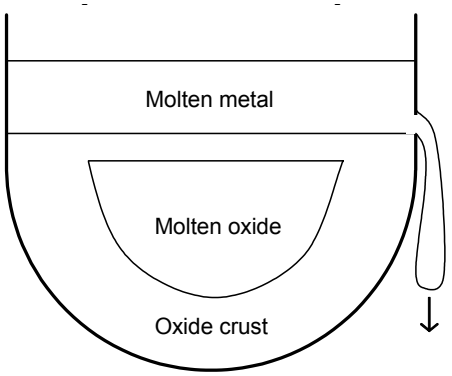

Figure 22. Expected melt configuration in the reactor pressure vessel and breach of the vessel wall.

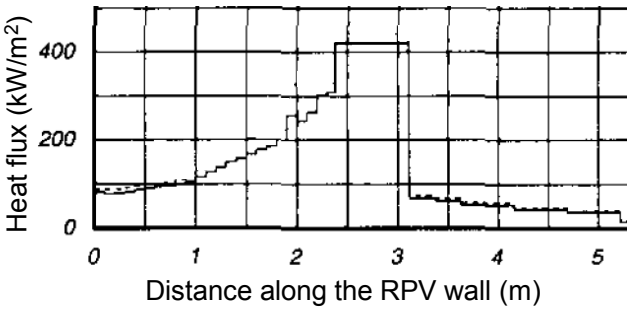

Figure 23. Calculated heat flux to the Loviisa RPV wall (Kymäläinen et al. 1997). The maximum heat flux occurs at the elevation of the metallic pool.

The melting temperature of stainless steel is slightly over 1400 °C, while pure Zr melts at 1852 °C and mixtures of steel and zirconium at about 1500 °C. To prevent the melt from solidifying upon contact with concrete, the initial temperature should be substantially above the melting temperature. Some accident analyses by VTT suggest that the temperature of the metallic melt at the time of release from the EPR pressure vessel is less than about 1800 °C. Based on these values, 1900 °C is considered to be a good target temperature for the experiments under design.

The easiest technique to melt the steel before pouring is induction heating. The steel will be placed into a crucible made of refractory material with water-cooled copper induction coil outside the crucible. When alternating current is generated in the coil, the varying magnetic field induces eddy currents to the metal inside the crucible, and the currents cause an increase of the temperature of the metal. For ferromagnetic materials, such as iron below 770 °C and nickel below 358 °C, induction heating is especially efficient because of hysteresis losses: The alternating magnetic field causes the magnetic dipoles to oscillate, which generates heat due to friction.

According to Gauntt et al. (2000a), the enthalpy change of stainless steel from 25 to 1900 °C is 1.46 MJ/kg. If the mass of the steel is about 70 kg, about 100 MJ of energy would be needed for the heating and melting. Neglecting the heat losses to the environment, a power of 14 kW would be needed to reach the target temperature in two hours, which is a reasonable time. In practice the time would be somewhat longer because of the heat losses.

Another method to generate the melt would be the strongly exothermic chemical thermite reaction

$$8\ Al + 3\ Fe_3O_4 \rightarrow 4\ Al_2O_3 + 9\ Fe + 15.7\ MJ/kg_{Al},$$

which can reach temperatures up to 2300 °C (Albrecht et al. 2005). Based on the material property data from Gauntt et al. (2000a), cooling of the mixture (55 w-% Fe, 45 w-% Al_2O_3) from 2300 °C to the target temperature of 1900 °C releases about 900 kJ/kg thermal energy. This energy can be used to melt some additional metals, e.g. Cr, Ni and Zr. The melting point of Al_2O_3 is 2054 °C (Gauntt et al. 2000a), so the alumina would solidify during the cooling. Because aluminum oxide is lighter than iron, the melt would stratify so that alumina would be on the surface and iron at the bottom. Then the iron melt should be poured from a hole at the bottom of the crucible. The problem with this method would be to stop the pouring when the flow changes from iron to alumina, if pure metallic melts are wanted.

The decision between induction heating and thermite reaction has been postponed until more data about the costs of the techniques is available. Calculations for both pure metallic melts and metal-alumina-mixtures are presented in section 5.3.

After the melt has reached the target temperature, it must be poured into the concrete crucible. One way to do the pouring is simply to tilt the melting crucible by a crane or some other tilting mechanism. Another possibility is to make a hole to the bottom of the melting crucible and let the melt flow out through the hole. This technique was used in the TURC experiments, where the bottom of the melting crucible was breached by firing an explosive projectile to the base of the crucible. The hole could be also generated by some kind of remotely controlled hatch or slide-valve.

The melt pour could also be initiated by placing a sacrificial plug to the base of the melt crucible. The plug would be constructed from a material that melts at the target temperature and thereby releases the steel from the crucible. If using induction heating, it is very difficult to predict the time in which the plug would fail after the steel has reached the melting temperature of the sacrificial material. Also the chemical reactions and eutectic formation between the steel melt and the plug material are difficult to assess. If using the thermite reaction to generate the melt, a thin steel plate could be used to release the melt. The plate would fail when the reaction front has reached the plate.

To simulate the accident situation as closely as possible, the melt should include zirconium in addition to stainless steel. Molten zirconium is difficult to handle because it reacts violently with oxygen. If the melt generation and pouring can be protected by an inert cover gas, then zirconium can be mixed and melted together with the steel. It the melt is in contact with air in some stage of melt generation and release, then solid zirconium must be placed into the concrete crucible and the steel melt shall be poured onto the zirconium. In this case the zirconium must be placed to the sides of the concrete crucible, leaving bare concrete to the floor area where the melt jet will hit. This

way the zirconium will not interfere with the impingement heat transfer and the possible spalling of the concrete floor. However, heating and melting of the solid zirconium would consume thermal energy from the steel melt, which would lower the temperature of the melt and reduce the interaction time available to gather measurement data. This would also limit the amount of Zr significantly below the level that is expected in the reactor accident.

Heating after the pouring of the melt is not necessary to examine concrete spalling. However, to prolong the interaction and to get data on steady state heat transfer from the melt, some kind of decay heat simulation could be beneficial. In previous MCCI experiments, the melt has been heated by direct electrical heating or induction heating. Direct electrical heating means that electric current is conducted through the melt. The difficult thing about this method is that the conducting electrodes are directly exposed to the melt, and common cheap electrodes cannot withstand the high temperatures and the mechanical stresses. Induction heating, on the other hand, is a non-contact heating method. However, the penetration depth of induction heating currents is relatively small, and the heating power tends to concentrate on the outer surfaces of the melt. This can prevent crust formation next to the sidewalls and hence distort the ratio of radial and axial ablation rates. Induction heating also generates electromagnetic noise, which may disturb the temperature measurements by thermocouples.

In the reactor accident situation, most of the fission products that generate decay heat are located in the oxidic portion of the melt, and there is not much decay heat in the metallic melt. If the metallic part of the melt flows from the pressure vessel to the reactor cavity before the oxidic part, it is heated mainly by thermal radiation from the hot reactor pressure vessel, and only in minor part by internal decay heat generation. A rough estimate for the thermal radiation from the pressure vessel bottom at a temperature of 1000 °C and emissivity of 0.2 is

$$\frac{\dot{Q}}{A} = \varepsilon \sigma T^4 = 0.2 \cdot 5.67 \cdot 10^{-8}\ \mathrm{W/m^2K^4} \cdot (1273\ \mathrm{K})^4 \approx 30\ \mathrm{kW/m^2}\,. \tag{31}$$

In the experiment, the thermal radiation from the bottom of the reactor pressure vessel could be simulated by infrared heating of the surface of the melt. For melt pool diameter of 30 cm, radiation power on the order of 2 kW should be used to mimic the accident situation. High power tungsten filament lamps are available that can generate short wavelength thermal radiation with a temperature of 2200 °C. These lamps are made in the form of quartz tubes, and their price is less than 100 dollars. The lamp should be installed in a reflector, which directs the radiation from the lamp downwards. The challenge with these lamps is to protect them from melt splatters and too high temperatures.

Because the emissivity of the metallic melt surface is quite small, a large part of the radiation is reflected away from the surface. Also aerosols and water vapor in the atmosphere absorb some of the radiation. According to MELCOR calculations (see section 5.3.1.4), a thermal power of 2 kW absorbed to the melt would have very little effect on the concrete ablation. Because of this and to keep the facility simple, it has been decided to conduct the experiments without any decay heat simulation.

5.2.3 Measurements

The most important thing to be measured is the erosion rate of the concrete. In previous experiments, it has been measured with thermocouples embedded in the concrete. The arrival of the melt front destroys the thermocouple, and the erosion rate can be determined from the destruction times of the thermocouples at different depths in the concrete. In addition, this method allows measuring the temperature profile inside the concrete. Since the thermocouples do not have to withstand the high temperature of the melt, normal inexpensive thermocouples can be used.

Thermocouple is a simple thermoelectric device, which is based on the Seebeck effect. When two different metals are in contact, a small voltage is produced between the metals. The voltage depends on the temperature of the contact point. To measure the voltage, the thermocouple wires have to be connected to a voltmeter. This connection (so called cold-junction) creates two additional Seebeck voltages between the thermocouple wires and the voltmeter wires. However, these unwanted parasitic voltages can be compensated by keeping both cold-junctions at the same temperature, measuring this reference temperature, and calculating the voltage that is caused by the cold-junctions. The voltage produced by thermocouples is some millivolts.

Several types of thermocouples with different metals are available. The different types have different temperature and voltage ranges and different abilities to resist chemicals. Thermocouple types are designated by capital letters. The most common thermocouple applied in MCCI experiments is K-type, in which the positive conductor is made of 90 % Ni and 10 % Cr, and the negative conductor is 95 % Ni and 5 % Al-Si. It has a temperature range from about –200 to +1250 °C. The price of K-type thermocouples is around 20 $, so they can be used in large numbers to measure the concrete ablation rate in many places in the bottom and the sidewalls.

To calculate the energy balance of the melt pool and to find the heat transfer coefficient from the melt to concrete, the temperature of the melt must be measured. The energy balance can be used to observe the possible spalling of the concrete: If the ablation rate at some time interval is larger than the energy released from the melt would allow, it

can be concluded that spalling has taken place. Measuring the high temperatures, about 1900 °C, is very difficult, since conventional thermocouples can not resist such high temperatures. Also the oxidizing environment with water vapor and carbon dioxide emerging from the decomposing concrete sets very high demands for the corrosion resistance of the temperature probe.

In steel industry, molten steel temperature is usually measured by immersing a high-temperature thermocouple in to the steel and measuring its temperature during the short period until the melt destroys the thermocouple. This method was also applied in the BETA and KAPOOL experiments. By this dip-in method the temperature can of course be measured only at certain times, and continuous measurement is not possible. In addition, it is difficult to be sure whether the thermocouple reading has reached the temperature of the melt before it fails. The remote mechanism to immerse the thermocouples to the melt pool increases costs, takes space, and is prone to malfunction. If there is a crust on the surface of the pool, the thermocouple may not be able to penetrate it. For these reasons, the dip-in method is not considered to be a good technique for measuring the melt temperature.

In the ACE and CCI experiments, good temperature measurements were conducted by inserting thermocouples in protection tubes, or thermowells, made of tungsten, to protect the thermocouple from chemical and mechanical damage. They used type C thermocouples, which are made of 95 % W and 5 % Re in the positive side, and 74 % W and 26 % Re in the negative side. These can resist temperatures up to 2300 °C, but their price is over 200 $. Because type C thermocouples are susceptible to oxidation in high temperatures, they should be protected by an inert cover gas. Since the temperatures in our metallic melt experiments will be somewhat lower than in the oxidic melts in ACE and CCI experiments, also alumina (Al_2O_3) protection tubes might be used instead of tungsten. Zirconium reacts chemically with alumina, so with Zr melts Al_2O_3 tubes will not work. Alumina thermocouple protection tubes are being sold for the price of less than a hundred dollars.

Problems with oxidation of the temperature sensor can be avoided by using non-contact temperature measurement with a pyrometer, which measures the thermal radiation from a surface. The inside temperature of a melt pool can be measured by inserting a closed-end pipe in to the melt and installing a pyrometer to measure the temperature of the pipe bottom. Because of multiple reflections, the pipe behaves like a black body with emissivity of about one. This technique was used in the SURC experiments, and it worked fine in the beginning, until the pyrometer became detached from the pipe. High temperature pyrometers are available at the price of around a thousand dollars. A pyrometer is less susceptible to electromagnetic noise than a thermocouple. An interesting feature would be the measurement of the melt surface temperature by a

pyrometer. This was attempted in the ACE experiments, but the results were not good because the aerosols that were released from the melt prevented the pyrometer from seeing the melt surface.

If enough resources are available, it would be preferred to measure the melt temperature by both the C type thermocouples in protection tubes and a pyrometer. This would provide diversity in the case that one of these methods fails. The reliability of the temperature data could be assessed by comparing the results from the both devices. A pyrometer with a pipe could be installed above the melt surface, and perhaps two high temperature thermocouples embedded in the concrete near the surface of the concrete, which would protect the protection tubes from the mechanical loads arising from the pouring of the melt.

The predicted ablation depths in the experiments range from 3 to 9 cm (see section 5.3.1.3), so most of the thermocouples in the concrete will be installed less than 10 cm from the concrete surface. Some thermocouples will be embedded deeper in to the concrete, to reckon with the possibility of faster than predicted concrete erosion. The minimum distance between adjacent type K thermocouples is about 2 cm, so that the large "thermocouple concentration" in the concrete would not affect the erosion velocity.

A preliminary plan for the thermocouples is presented in Figure 24, Table 3 and Table 4. There are 24 type K thermocouples and one type C thermocouple in both basemat and sidewall. The first letter in the code is the thermocouple type and the second letter tells the position (B = basemat, S = sidewall). The cost of the thermocouple instrumentation is estimated to be between 1000 and 2000 €. In the experiments without zirconium, the deepest thermocouples in each array can be omitted, because the expected ablation depths are only about 5 cm.

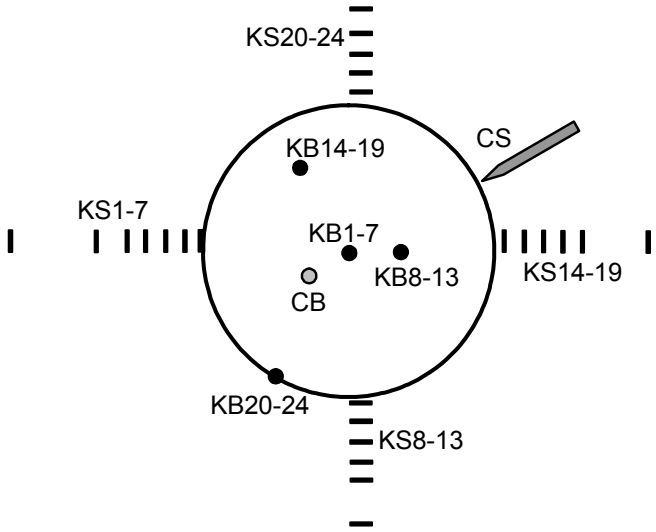

Figure 24. Thermocouple positions and codes, pictured from above the concrete cavity. The black circles are type K thermocouple arrays in the basemat, bars are type K thermocouples in the sidewalls, the gray circle is type C thermocouple in the basemat, and the gray pipe is type C thermocouple in the sidewall.

Table 3. Basemat thermocouple positions.

Thermocouple code	Distance from cavity centerline (cm)	Angular position (degrees)	Depth below cavity bottom (cm)
KB1	0		0
KB2	0		2
KB3	0		4
KB4	0		6
KB5	0		8
KB6	0		11
KB7	0		20
KB8	5	0	1
KB9	5	0	3
KB10	5	0	5
KB11	5	0	7
KB12	5	0	9
KB13	5	0	16
KB14	10	120	0.5
KB15	10	120	2.5
KB16	10	120	4.5
KB17	10	120	6.5
KB18	10	120	8.5
KB19	10	120	13
KB20	15	240	1.5
KB21	15	240	3.5
KB22	15	240	5.5
KB23	15	240	7.5
KB24	15	240	10
CB	5	210	0.1

Table 4. Sidewall thermocouple positions.

Thermocouple code	Height from cavity bottom (cm)	Angular position (degrees)	Depth from cavity sidewall (cm)
KS1	5	180	0
KS2	5	180	2
KS3	5	180	4
KS4	5	180	6
KS5	5	180	8
KS6	5	180	11
KS7	5	180	20
KS8	15	270	0.5
KS9	15	270	2.5
KS10	15	270	4.5
KS11	15	270	6.5
KS12	15	270	8.5
KS13	15	270	13
KS14	10	0	1
KS15	10	0	3
KS16	10	0	5
KS17	10	0	7
KS18	10	0	9
KS19	10	0	16
KS20	0	90	1.5
KS21	0	90	3.5
KS22	0	90	5.5
KS23	0	90	7.5
KS24	0	90	10
CS	5	30	0.1

The melt surface should be monitored by a video camera. During the experiment, it would give information about the state of the melt and the concrete crucible. The video record could also be used to assess the presence of crust on the melt surface. The hot melt surface glows white or red, and this probably gives enough light for the camera even without external lighting. Problems with the video recording include the aerosols coming from the melt, which can dim the sight to the surface, and the splashing of the melt during pouring, which can damage the viewing window of the camera.

As regards other instrumentation, measuring the temperature of the gas coming out of the experiment vessel could be beneficial. Pressure measurements are not necessary, since the facility will be connected to the atmosphere by a pipe and operates at the atmospheric pressure.

After the experiment, the facility will be disassembled and cut into pieces, and the interaction zone will be examined to determine the exact ablation depths and the possible non-uniformity of the ablation profile. The post test examination will also include examination of the possible voids in the solidified melt. Material samples will

be taken at a few places and sent to a chemical analysis to examine the chemical form of the solidified melt and the possible segregation of different materials in the pool.

5.2.4 Safety

The largest safety risk in the experiments is the hydrogen, which is generated when water vapor from the decomposing concrete reacts with the metals in the melt. Hydrogen is flammable in air at concentrations of 4.1–74 volume-percent and explosive at concentrations of 18.3–59 volume-percent (Cadwallader & Herring 1999). Because hydrogen and high temperature surfaces will be present in the test facility, the only way to prevent hydrogen burns is to eliminate oxygen from the cavity. This can be done by feeding inert cover gas into the cavity. The cheapest inert gas is nitrogen. At temperatures over 1200 °C nitrogen and oxygen react and produce toxic nitrogen oxides, but so high gas temperatures are not expected at the outlet of the gas flow to the environment. The cover gas flow shall be directed to the viewing window of the camera to provide cooling for the camera and keep the window clean.

The cover gas feed to the cavity shall be started sufficiently long time before the beginning of the experiment, so that practically all oxygen has been removed from the cavity before the pouring of the melt. The nitrogen–hydrogen mixture will flow to the environment, and the hydrogen must be diluted to less than 4.1 volume-percent before the discharge, so that no hydrogen burn can take place at the outlet of the gas pipe. The necessary nitrogen flow rate will be calculated in section 5.3.

Another safety risk is that the concrete cavity may be breached due to spalling, non-uniform erosion or some other mechanism, and the molten steel may flow out of the cavity. This could damage the property and people around the experiment facility, or initiate a fire. To prevent the outflow of the melt, the concrete cavity shall be surrounded by refractory material, which can stop the melt from flowing out of the facility. In addition, people and flammable material should be evacuated from the immediate vicinity of the facility for the time of the experiment. Pressurization of the cavity is not expected, because it is connected to the atmosphere by a large pipe.

5.2.5 Experiment Program

When examining spalling of concrete, the most important factors to be varied in the experiments are the composition of the melt and the humidity and porosity of the concrete. It is considered sensible to conduct the first experiment with “basic” parameters and, if no spalling was observed, to vary the experimental conditions so that

the probability of spalling is expected to increase. The preliminary experiment matrix contains five experiments, and their parameters are presented in Table 5 for the option of induction heating, and in Table 6 if the thermite reaction is used to generate the melt. The stainless steel composition in the EPR is 72.3 w-% Fe, 16.8 w-% Cr and 10.9 w-% Ni, and the same composition will be used in the experiments. The target temperature in all the experiments is 1900 °C, and the thermite mixtures have been designed so that the final temperature would be about 1900 °C. However, if it seems that the facility can withstand higher temperatures, then it can be attempted to conduct some experiments with a higher temperature melt.

Table 5. Preliminary experiment matrix for induction heating. SS means stainless steel.

Case	Melt composition	Concrete
IND1	70 kg Fe	EPR sacrificial
IND2	70 kg SS	EPR sacrificial
IND3	55 kg SS + 15 kg Zr	EPR sacrificial
IND4	38 kg SS + 32 kg Zr	EPR, low porosity, high H_2O
IND5	38 kg SS + 32 kg Zr	Siliceous

Table 6. Preliminary experiment matrix, if thermite reaction is used for melt generation. SS means stainless steel and TH is thermite powder (76.3 w-% Fe3O4 and 23.7 w-% Al).

Case	Charge composition (kg)	Melt composition (kg)	Concrete
TH1	45 TH + 25 Fe	50 Fe + 20 Al_2O_3	EPR sacrificial
TH2	44 TH + 12 Fe + 8.6 Cr + 5.4 Ni	50 SS + 20 Al_2O_3	EPR sacrificial
TH3	41 TH + 6.5 Fe + 6.7 Cr + 4.3 Ni + 11.5 Zr	40 SS + 11.5 Zr + 18.5 Al_2O_3	EPR sacrificial
TH4	37 TH + 5 Cr + 3 Ni + 25 Zr	28 SS + 25 Zr + 17 Al_2O_3	EPR, low porosity, high H_2O
TH5	37 TH + 5 Cr + 3 Ni + 25 Zr	28 SS + 25 Zr + 17 Al_2O_3	Siliceous

In the first experiment the melt will be pure iron without chromium or zirconium. This eliminates the difficulties with safe handling of molten zirconium. The chemical reactions of the concrete decomposition products with zirconium and chromium are strongly exothermic, which constitutes a safety risk. After confirming the proper functioning of the test facility in the first experiment, stainless steel and zirconium can be added in the subsequent experiments. This will make the experiments more prototypical to the accident situation, and the chemical reaction heat will prolong the interactions to allow more measurement data to be collected. The stainless steel-zirconium-ratio in the last two experiments is taken from MELCOR calculations conducted at VTT, and it corresponds to 34 % in-vessel oxidation fraction of Zr.

The concrete in the first three experiments will be as close to the EPR sacrificial concrete as possible, i.e. Portland cement concrete with siliceous and hematite aggregates. If concrete spalling is not observed, it will be attempted to make the concrete less porous and more saturated with water to increase the probability of spalling. The fifth experiment is designed to be conducted with ordinary siliceous construction concrete, in order to get information on the differences in ablation of the sacrificial and ordinary concrete.

5.3 Pre-test Calculations

5.3.1 MELCOR Simulations

In the following, a short description of the MELCOR model for core–concrete interactions is presented. The details can be found in Gauntt et al. (2000b) and Bradley et al. (1993). The IND2 case (stainless steel without zirconium) has been chosen as the reference case of the designed experiments, and detailed MELCOR 1.8.5 results are presented for it. For the other cases, the main results and differences to the reference case are given. Finally, some sensitivity analysis of the MELCOR parameters is presented.

5.3.1.1 The MELCOR Cavity Package

MELCOR is a computer code for analyzing severe accidents in nuclear power plants. It has been developed at Sandia National Laboratories, Albuquerque, New Mexico. The MELCOR Cavity (CAV) package models core–concrete interactions. It uses models taken from the CORCON-Mod3 code (Bradley et al. 1993).

The program models a cylindrical concrete cavity with a flat bottom and optionally rounded corners. The shape of the cavity is tracked by the positions of "body points" on the concrete surface. The melt pool consists of several oxidic, metallic and mixture layers. Alternatively, the user can choose to treat the whole pool as one homogeneous layer (enforced mixing). The boundary conditions are provided by the concrete cavity walls and the atmosphere or water above the melt pool. In MELCOR, the atmosphere and the water are modeled by the Control Volume Hydrodynamics (CVH) package.

The model reduces the heat transfer problem into two independent one-dimensional problems, one axial and one radial. The heat transfer from the melt to concrete is modeled as a series of heat transfer resistances: from the bulk of the melt to its boundaries, through the possible corium crust layer, and finally through the film of

molten concrete at the interface. Alternatively, the user can choose to replace the molten concrete film ("slag film") by a gas film. However, a stable gas film can only exist at extremely high gas generation rates, which are not realistic in most accident conditions. The program uses iteration to find such interface temperatures that the heat flux is continuous at all interfaces between layers. The surface of the solid concrete is supposed to be at the concrete ablation temperature.

The heat transfer equations from the bulk of the melt pool are quoted in section 3.3 (equations (7)–(9)). In addition to the bubbling heat transfer correlation, the program calculates the pool heat transfer coefficient h_{pool} also by natural convection and by conduction. The largest of these three coefficients is used. Natural convection dominates at low gas velocities, while conduction heat transfer is used for very thin or very viscous layers. It has been found that, for a wide range of material properties, the heat transfer coefficient h_{film} through the film of molten concrete is related to h_{pool} approximately by

$$h_{\text{film}} = 0.41\ h_{\text{pool}}\ . \tag{32}$$

In addition to this relation, the code provides a lower limit of 1000 W/(m^2·K) for the film heat transfer coefficient. This value describes conduction heat transfer across a thin film of molten concrete. The lower limit comes into play with oxidic melts at relatively low temperatures, when the viscosity is high and heat conductivity is poor, so that h_{pool} is less than 2440 W/(m^2·K). The impingement heat transfer from the poured melt jet to the concrete cannot be calculated by MELCOR.

If the calculated pool boundary temperature falls below the solidus temperature, then crust is supposed to form. Heat transfer through the crust is calculated by steady-state conduction with constant volumetric heat source. The inner boundary of the crust is supposed to be at the solidus temperature. The crust thickness and the other interface temperatures are solved so that the heat flux is continuous.

The heat loss from the pool surface includes radiative heat transfer and convection to the atmosphere. The convection heat transfer coefficient is assumed to be constant at 10 W/(m^2·K). When calculating the radiation heat transfer, MELCOR assumes that the temperature of the surrounding walls is the same as the temperature of the gas in the atmosphere. All the radiated heat is absorbed to the atmosphere, and no direct heat radiation to walls above the cavity surface can be calculated.

Chemical equilibrium is assumed to be achieved in the pool during each timestep. The equilibrium composition is solved by minimizing the Gibbs free energy. Chemical reaction heats are implicitly contained in the enthalpies of the different species. After calculating the heat generation and heat loss during the timestep, the enthalpies of the

melt layers are updated so that energy is conserved. The average layer temperature is calculated from the enthalpy.

Various material properties are needed in calculating the heat transfer coefficients. MELCOR Cavity package includes an internal library for the properties of different species as a function of temperature. Most mixture properties, except viscosity and solidus and liquidus temperatures, are calculated as molar or mass averages. Viscosities are calculated using several empirical correlations. The solidus and liquidus temperatures of mixtures are estimated from two- and three-component phase diagrams. The enthalpy between solidus and liquidus is linearly interpolated.

5.3.1.2 MELCOR Simulation of the IND2 Case

The main parameters for the MELCOR 1.8.5 reference calculation (IND2 case) are presented in Table 7. The concrete density was taken from Nie (2004) and the solidus, liquidus and ablation temperatures from a GEMINI2 thermochemical calculation (Kekki 2005). The mixing of the metals and oxides was enforced, because the intense gas bubbling is expected to mix the phases completely, and because there are some numerical problems with MELCOR stratified melt calculations. Another control volume was created for the environment, with time-independent properties of normal air. A flow path from the cavity gas space to the environment was defined to simulate the exhaust pipe from the experimental facility to the environment. The length of the flow path was 10 m and diameter 10 cm.

Table 7. Main parameters for the MELCOR calculation of the IND2 case.

Melt composition	50.61 kg Fe, 11.76 kg Cr, 7.63 kg Ni
Initial temperature	1900 °C
Concrete type	EPR sacrificial (Table 1)
Concrete density	2540 kg/m^3
Concrete solidus	1127 °C
Concrete liquidus	1727 °C
Concrete ablation	1207 °C
Melt/concrete interface	Slag film model
All emissivities	0.6
Melt mixing	Enforce mixing
Initial gas temperature	25 °C
Pressure	1 bar
Initial gas composition	100 % N_2
Gas space volume	0.05 m^3

The predicted axial and radial ablation depths in IND2 case are presented in Figure 25. The interaction lasts for 44 minutes, and the basemat melts to the depth of 4.5 cm and

the sidewall to the depth of 4.1 cm. The initial and final cavity profile is illustrated in Figure 26. About 30 kg of concrete has molten, and about 30 % of the mass of the solidified melt in the cavity is concrete decomposition products. The MELCOR results for the average melt temperature are presented in Figure 27. The plateau at 2–7 min is due to the solidification of the metallic melt at about 1470 °C. The heat losses to concrete and surface and heat generated by chemical reactions during the first 30 minutes are presented in Figure 28, and the corresponding cumulative thermal energies in Figure 29. The chemical reaction heat comes mainly from the oxidation of 3.2 kg of chromium by the concrete decomposition gases. From the gas release rates during the first ten minutes (Figure 30), it can be seen that almost all H_2O and CO_2 that are released from the concrete react with the metals in the melt and produce H_2 and CO. Because of the larger density of CO, its mass flux is larger then that of H_2, even though the volumetric flux of H_2 is much larger.

The nitrogen cover gas flow to the cavity was adjusted so that the hydrogen concentration of the outgas remains below the flammability limit of 4.1 volume-%. As can be seen from Figure 31, the initial nitrogen flow must be high, but it can be substantially decreased after a few minutes, when the interaction has calmed down. About 210 kg of nitrogen is needed during the experiment. The resulting hydrogen volume fraction in the outgas during the first 30 minutes is presented in Figure 32. The three sharp jumps are due to the decreases of the cover gas flow. MELCOR calculates the upward heat transfer based on the temperatures of the melt surface and the gas above the melt (Figure 33). However, the gas temperature results are not reliable because of MELCOR's inability to calculate direct thermal radiation to the surrounding walls. The three sharp jumps in the temperature are again due to the decreases of the cover gas flow.

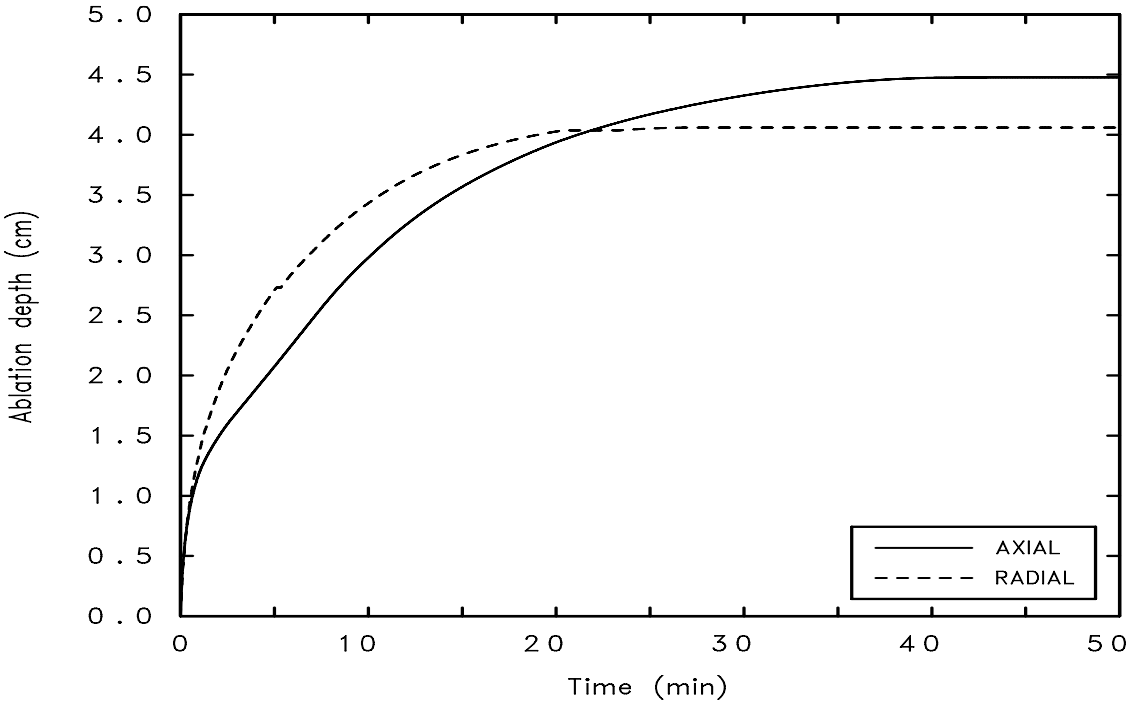

Figure 25. Axial and radial ablation depths in the IND2 case. Calculated with MELCOR.

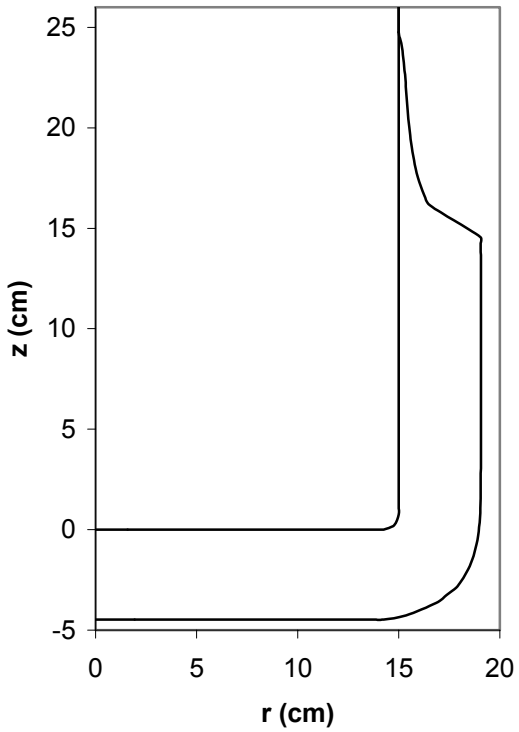

Figure 26. The initial cavity profile and MELCOR prediction of the final ablation profile in the IND2 case.

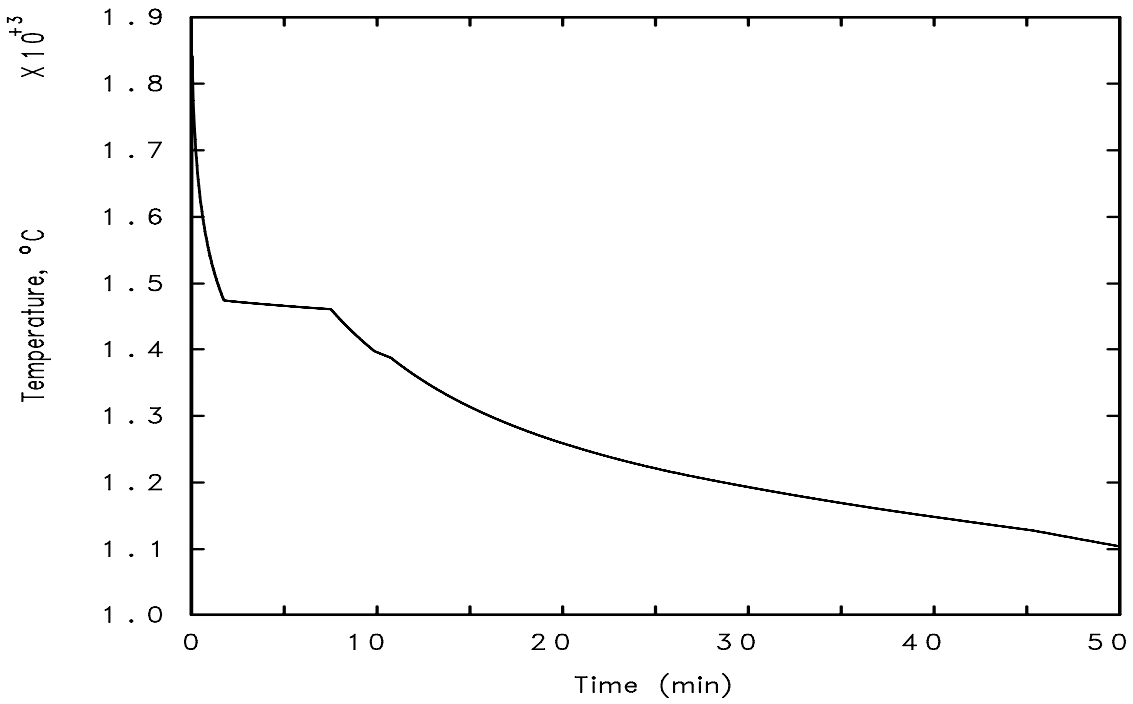

Figure 27. MELCOR calculation of the average melt temperature in IND2 case.

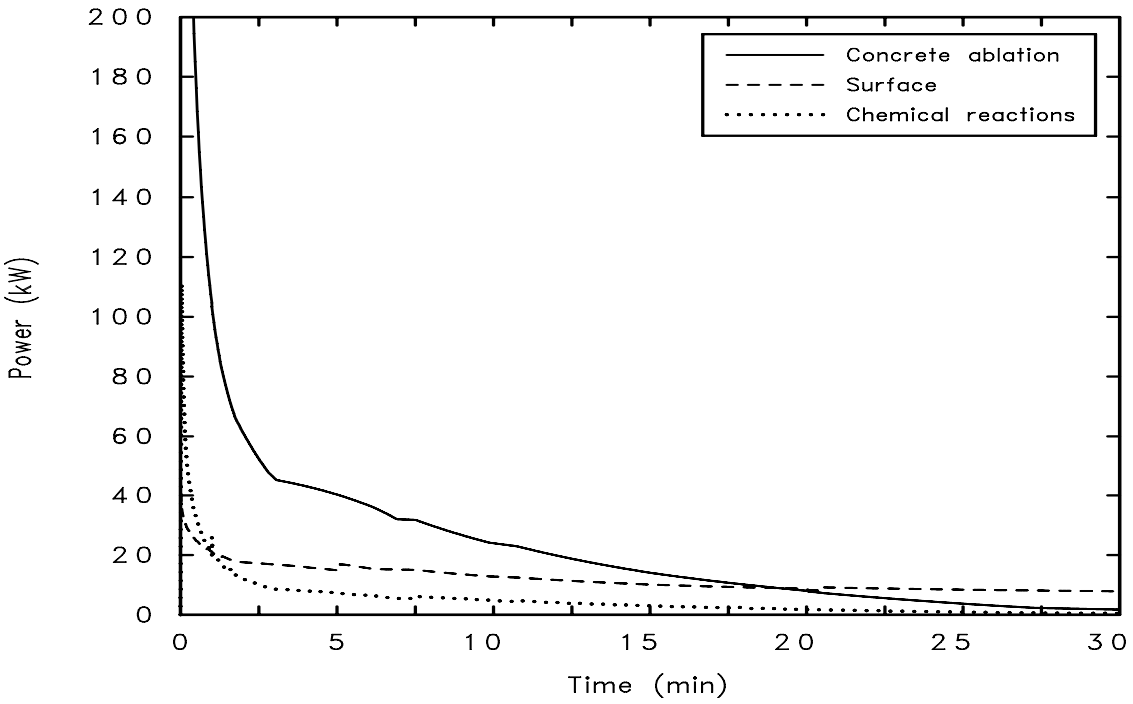

Figure 28. Heat losses to concrete and from the surface, and heat generated by chemical reactions in IND2 case. Calculated with MELCOR.

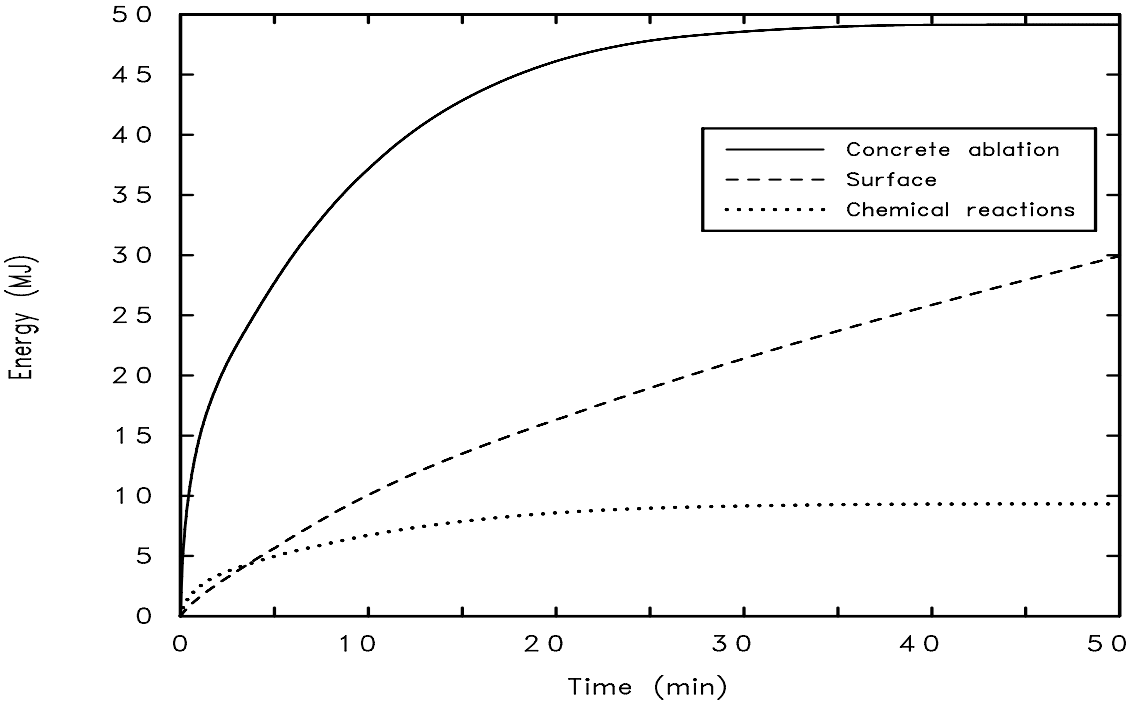

Figure 29. Cumulative heat losses to concrete and from the surface, and heat generated by chemical reactions in IND2 case. Calculated with MELCOR.

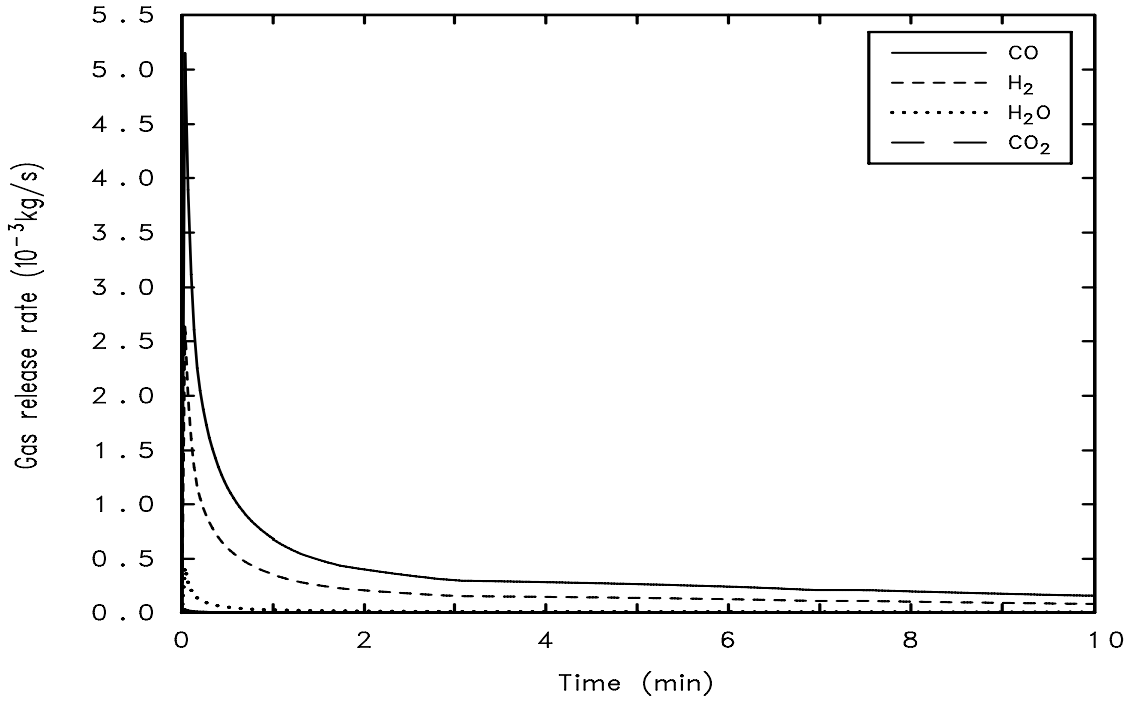

Figure 30. MELCOR calculation of the gas release rates from the melt pool in the IND2 case.

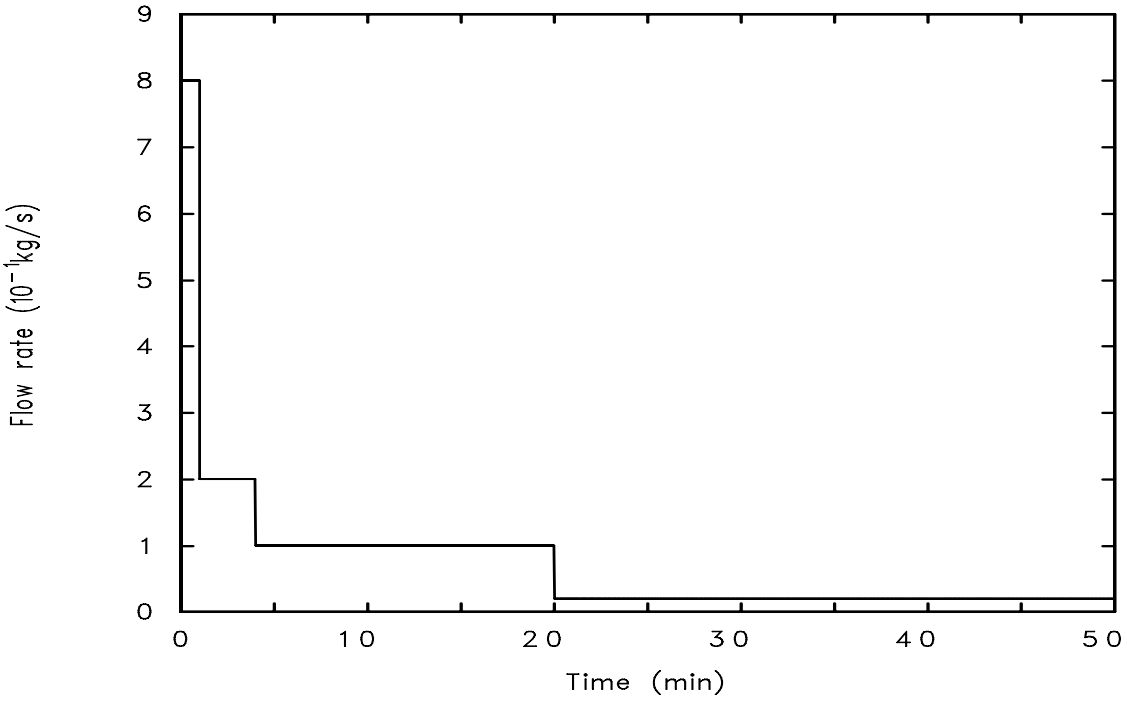

Figure 31. Nitrogen cover gas flow used in the IND2 case MELCOR calculations.

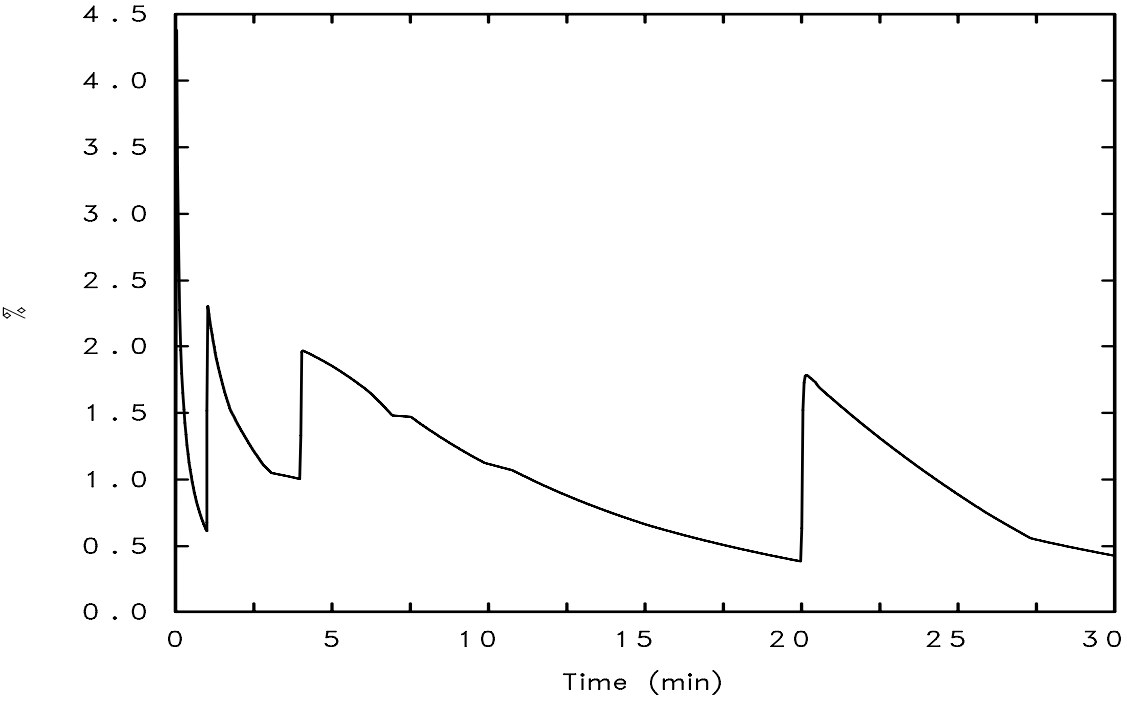

Figure 32. MELCOR results for hydrogen volume fraction in the outgas of IND2 case.

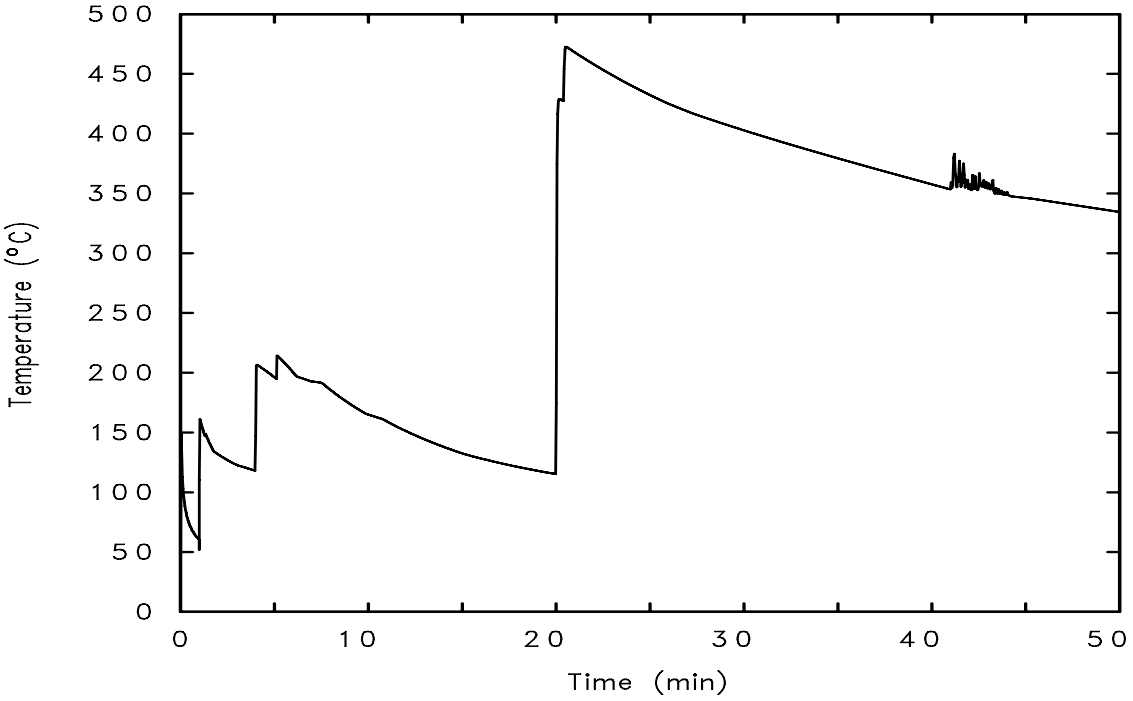

Figure 33. MELCOR prediction of the temperature of the gas above the melt in IND2 case.

5.3.1.3 MELCOR Simulations of the Other Cases

MELCOR simulations of the other cases in the experiment matrix (Table 5 and Table 6) have been conducted using similar parameters as described in the previous section. The nitrogen cover gas flow rate was chanced so that the hydrogen volume-fraction remained below 4.1 % in all the calculated cases. The composition and solidus and liquidus temperatures of the ordinary siliceous concrete for the cases IND5 and TH5 were taken from Kekki et al. (2005) and are presented in Table 8. At the ablation temperature the liquid fraction of the concrete is 50 weight-%. The density of the siliceous concrete is about 2300 kg/m^3. The lower porosity concrete in the IND4 and TH4 cases could be modeled by increasing the density of the concrete. However, the change in density is difficult to quantify without exact knowledge of concrete manufacturing, and so the concrete in these cases was the same as in the cases 1–3.

The main results of the MELCOR simulations of all the cases are summarized in Table 9. Generally MELCOR predicts the radial ablation depth as slightly smaller than the axial, except in cases TH4 and TH5. The trend is that the ablation depths and interaction durations increase significantly as the amount of zirconium in the melt is increased, because the oxidation of Zr generates heat.

Table 8. Composition and properties of siliceous concrete used in the MELCOR calculations (Kekki et al. 2005).

Chemical composition	Weight-%
SiO_2	69.99
CaO	13.5
Al_2O_3	4
K_2O	1.4
Fe_2O_3	1
TiO_2	0.8
MgO	0.7
Na_2O	0.7
CO_2	4.23
H_2O (bind)	1.84
H_2O (free)	1.84
Temperatures	**°C**
Solidus	1127
Ablation	1327
Liquidus	1827

Table 9. Main results of MELCOR simulations of all the cases in the experiment matrix.

Case	Axial ablation depth (cm)	Radial ablation depth (cm)	Interaction time (min)
IND1	3.9	3.5	39
IND2	4.5	4.1	44
IND3	6.7	6.4	59
IND4	8.2	7.8	76
IND5	7.0	6.9	64
TH1	4.9	3.7	82
TH2	5.4	4.3	91
TH3	6.8	6.1	102
TH4	7.0	7.7	109
TH5	6.2	6.6	91

The ablation depths of siliceous concrete in IND5 and TH5 cases is 10–15 % smaller than IND4 and TH4 with the same melt composition but EPR sacrificial concrete. The main reason for this is the 120 degrees higher ablation temperature of the siliceous concrete. However, the ablation temperatures are only based on thermochemical calculations, and they must be treated as crude approximations as long as no measurement data of the correct ablation temperatures is available.

A clear difference between the induction and thermite cases is that the duration of the interaction is by a factor of 1.4–2.1 longer in the thermite cases. The reason for this is the higher solidification temperature and poorer thermal conductivity of Al_2O_3

compared to the metals, which causes larger viscosity, thicker crusts and slower heat transfer than with purely metallic melts.

The ablation depths in the cases without zirconium (1 and 2) are slightly larger for the thermite than for the induction melts, because the specific heat and hence the thermal energy content of Al_2O_3 is higher than that of the metals. This difference is enough to compensate for the larger concrete area exposed to the melt in the TH cases, which follows from the lower density of Al_2O_3. In the cases where Zr is included, the larger mass of Zr in the IND cases causes larger ablation depths.

5.3.1.4 Sensitivity Analysis

To examine the sensitivity of the MELCOR results to changes in the initial parameters, some additional calculations have been conducted. The IND2 case was taken as the reference case, and the parameters were varied one at a time. To maintain exact comparability, the nitrogen cover gas flow was not changed, even though the hydrogen concentration may in some calculations exceed the flammability limit. The changes in the axial ablation depth, induced by changes in the initial parameters, are presented in Table 10.

Table 10. Results of MELCOR sensitivity analysis of the IND2 case.

Variation	Change in axial ablation depth (%)
Initial temperature 1800 °C	– 6.6
Initial temperature 2000 °C	+ 8.3
Decay heat 2 kW	+ 7.1
Melt mass 50 kg	– 14
Melt mass 90 kg	+ 13
Concrete ablation temperature 1327 °C	– 30
Emissivities 0.8	– 2.1
Gas film model	+ 11
Stratified melt	+ 32

The change of ±100 °C in the initial temperature of the melt or applying 2 kW of decay heat to the melt caused relatively small changes to the ablation. Changing the melt mass by 29 % changed the axial ablation depth by 13–14 %, because a deep melt pool cools down slower than a shallow one. Increase of the concrete ablation temperature by 120 °C, to the same value that was used for the siliceous concrete, decreased the ablation depth by as much as 30 %. Hence, the ablation temperature seems to be an important but highly uncertain parameter, which is very difficult to measure in experiments. Increasing the emissivity of the melt and the surroundings from 0.6 to 0.8 increased the heat loss from the surface and slightly decreased the ablation depth. Using

the unrealistic option of a stable gas film between the concrete and the melt, an 11 % larger ablation depth was obtained.

The largest change in the ablation depth, +32 %, was obtained by using the enforced melt stratification option of MELCOR. With this option, the program assumes that the melt is separated into two distinct layers, one metallic and the other oxidic. In this case, the oxidic layer consisted mainly of concrete ablation products, which are lighter than the metals. So the metallic layer was under the oxidic layer, and the poorly heat conducting oxides worked as a "thermal insulation" over the metallic layer and decreased the heat loss from the surface of the pool. However, the validity of the calculation can be questioned because of the numerical problems with the MELCOR stratified melt model. These can be seen from the temperature curve in Figure 34, in which the metal temperature oscillates after 35 minutes. Even more clearly the unphysical oscillation of over 100 °C can be seen in the gas space temperature in Figure 35.

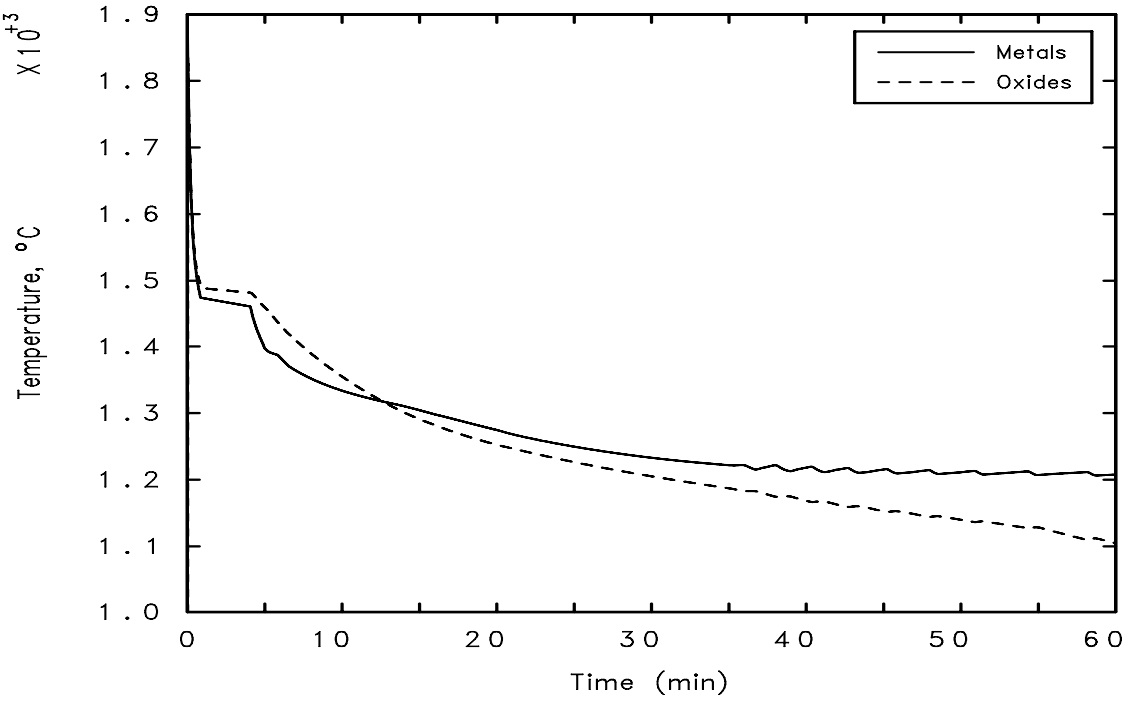

Figure 34. Temperatures of the metal and oxide layers in the stratified melt calculation of IND2 case.

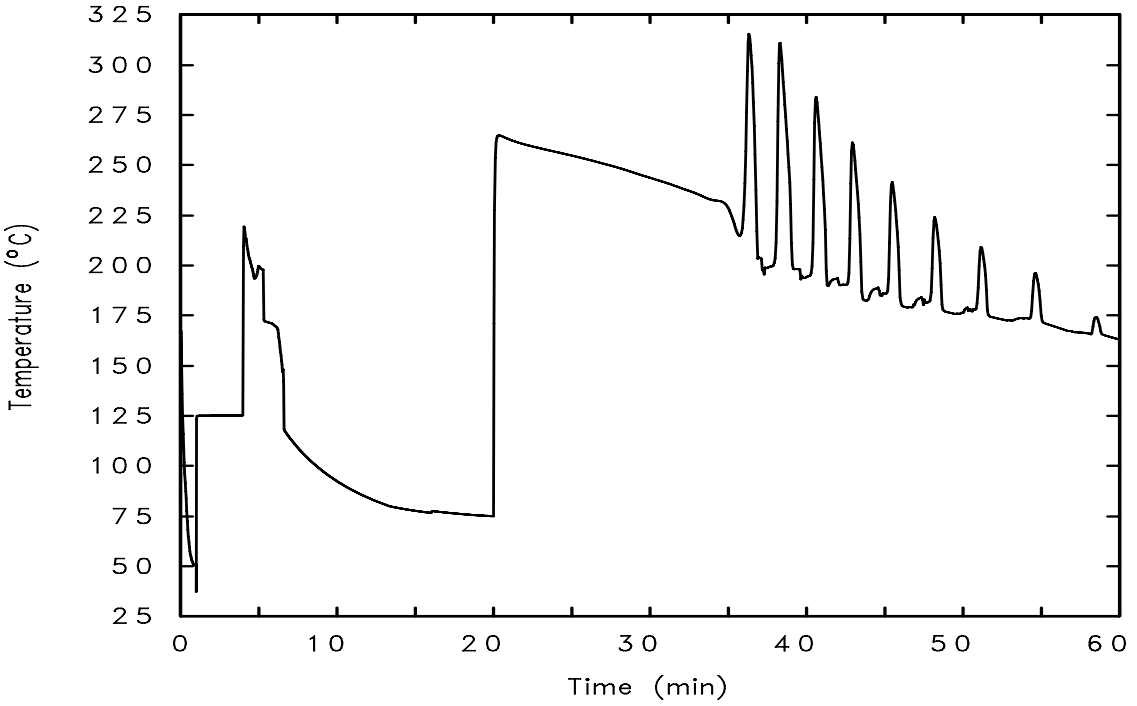

Figure 35. Temperature of the gas above the melt in the stratified melt calculation of IND2 case.

5.3.2 Conservative Estimates

To assure that complex computer programs give sensible results, simulations should always be checked by simple analytic calculations. In section 3.4, energy balance and simple geometric considerations were used to derive equation (18), which can be used to calculate the maximum possible ablation depth $d_{\mathrm{abl,\,max}}$. All the designed experimental cases have been calculated by this equation, and the parameters and the results are presented in Table 11. The melt densities and enthalpies are based on MELCOR material properties, but they have been checked against tabular data from various references to ensure that there are no major flaws in the data. The concrete decomposition enthalpies ($\Delta H_{\mathrm{actual}}$) have been taken from the calculations in section 3.2.4 at the ablation temperatures predicted by GEMINI2 calculations (Kekki 2005; Kekki et al. 2005), and the evaporable water contents and the energies needed to heat the released gases to the melt temperature have been taken into account. For the cases with chromium but no zirconium in the melt (IND2 and TH2), the chemical reaction heat of the oxidation of Cr has been taken into account by modifying ΔH as in equation (14). For the cases with Zr in the melt, the initial melt enthalpy h_{init} has been increased by the energy that is produced in the oxidation of all the Zr. Oxidation of Fe is endothermic, and in these conservative calculations it has been omitted.

The results of the conservative analytic calculations in Table 11 can be compared with the MELCOR results in Table 9. The calculated maximum ablation depths are by a factor of 1.3 to 2.1 larger than the results of the MELCOR calculations. Hence, it is very probable that there are no major errors in the MELCOR results. On the other hand, the maximum ablation depths are reasonable, so that they can be used in the design of the facility to decide the needed thickness of the concrete. However, if spalling or non-uniform ablation occurs, the actual ablation depth may exceed even these conservative maximum values.

Table 11. Parameters for the conservative analytic calculations, and the maximum ablation depths calculated with equation (18).

Case	ρ_{conc} (kg/m^3)	ρ_{melt} (kg/m^3)	ΔH (MJ/kg)	$h_{init} - h_{ablT}$ (MJ/kg)	$d_{abl,\,max}$ (cm)
IND1	2540	7142	1.49	0.81	6.0
IND2	2540	6955	1.11	0.84	7.7
IND3	2540	6660	1.49	2.04	11.3
IND4	2540	6354	1.49	3.41	15.4
IND5	2300	6354	1.79	3.35	14.5
TH1	2540	4813	1.49	1.09	6.4
TH2	2540	4752	1.11	1.11	8.1
TH3	2540	4754	1.49	2.02	10.0
TH4	2540	4738	1.49	3.08	13.3
TH5	2300	4738	1.79	2.96	12.3

6. Conclusions

An interaction between concrete and molten core of a nuclear reactor (corium) may take place in the very unlikely case of a severe accident in a nuclear power plant. In the European Pressurized water Reactor (EPR), the interaction is a part of the accident management strategy, while in other types of power plants it must be avoided. The interaction would involve melting of the concrete in the containment building, and release of water vapor and carbon dioxide from the decomposing concrete. The released gases would react chemically with the metals in the melt and produce hydrogen and carbon monoxide. The gas bubbles would enhance significantly the heat transfer from the melt to the concrete walls.

Because of the complexity of the interaction, it cannot be simulated accurately. Some heat transfer correlations from simulant material experiments do exist, but they cannot be validated because of the scarcity of experiments with real materials and large uncertainties in the measurements and the physical properties of the materials at high temperatures. In this work, physical properties of concrete and corium–concrete mixtures have been estimated on the basis of public literature and some calculations. A simple equation based on the conservation of energy was derived, which allows calculation of the maximum possible ablation depth of concrete.

A review of previous experiments revealed that the behavior of metallic melt is quite different from that of oxidic melts. In metallic melt experiments, no clear correlation between the heat transfer rate to concrete and the steady state melt temperature can be seen. The metal temperature rapidly decreases to the solidification temperature, probably because of the good thermal conductivity of the metals. However, there is a clear correlation between the heating power of the melt and the steady state heat transfer rate. This is probably caused by changes in the thickness of the crust around the melt.

In contrast to the metallic melt experiments, the tests with oxidic melts suggest that some kind of correlation between the temperature and the heat transfer rate seems to exist. However, the low number of experiments and uncertainties in the measurements and the physical properties of the materials do not allow validation of any heat transfer correlations. The difference to the metallic experiments can be explained by the large gap between the solidus and the liquidus temperatures in the oxidic melts. The steady-state temperatures of the experiments were in this “mushy” zone, where a small decrease in temperature causes a large increase in viscosity and a decrease in the heat transfer rate.

Despite the uncertainties in the heat transfer rates, the maximum possible ablation depth can be calculated by assuming that all the heat from the melt goes to the melting of the

concrete. However, this method fails if spalling, or cracking of the concrete surface, takes place. Spalling has been observed in fire tests of concrete, when the water in the concrete pores evaporates rapidly, increasing the pressure inside the concrete and generating stresses that exceed the strength of the concrete. Spalling of concrete under the pouring of molten material has not been studied systematically. In this work, an experimental facility to examine this phenomenon has been designed.

The designed facility includes a cylindrical cavity with diameter of about 30 cm, in which the bottom and the sidewalls are made of concrete. When about 70 kg of molten metal at a temperature of about 1900 °C is poured to the cavity, the concrete begins to melt. The ablation velocity will be measured by tens of thermocouples cast into the concrete. The melt temperature will be measured by high temperature thermocouples in protection tubes, and by an optical pyrometer. If the heat loss from the melt at some time interval is less than the heat needed to melt the concrete at the measured rate, it can be concluded that spalling has occurred. The experiments will be transient, i.e. no heating after the pour will be applied. To prevent hydrogen burns, the generated hydrogen must be diluted by nitrogen cover gas flow into the facility.

The melt can be generated either by induction heating or by the strongly exothermic chemical thermite reaction. The decision between these techniques has been postponed until more data on their costs is available. A preliminary experiment matrix with five experiments has been designed for both the induction and the thermite techniques. The program will be started with pure iron melt, and chromium and zirconium will be added in the subsequent experiments to generate chemical reaction heat. The concrete will be as close to the EPR sacrificial concrete as possible, except in the last experiment, where normal siliceous concrete will be used.

Simulations with the MELCOR 1.8.5 accident analysis program have been conducted to predict the results of the experiments. The simulations suggest that the final ablation depths will range from 3.5 cm with pure iron melt to over 8 cm with the largest amount of zirconium in the melt. The duration of the interaction will be 39–109 minutes. In sensitivity analysis of the MELCOR model, it was found that the predicted ablation depths are quite sensitive to the choice of the concrete ablation temperature. This parameter is not known accurately, and it is very difficult to measure. The sensibility of the MELCOR results was checked with conservative analytic calculations, which gave maximum ablation depth of 15.4 cm in the designed experiments, unless spalling takes place.

References

Albrecht, G., Huber, F., Jenes, E., Kaiser, A. & Schütz, W. 2005. KAJET Experiments on Pressure-Driven Melt Jets and their Interaction with Concrete. Karlsruhe: Forschungszentrum Karlsruhe. 50 p. (FZKA 7002.) ISSN 0947-8620. http://bibliothek.fzk.de/zb/berichte/FZKA7002.pdf

Alsmeyer, H. 1987. BETA Experiments in Verification of the WECHSL Code: Experimental Results on the Melt–Concrete Interaction. Nuclear Engineering and Design, Vol. 103, no. 1, pp. 115–125. ISSN 0029-5493.

Alsmeyer, H., Adelhelm, C., Dillmann, H.-G., Heinle, M., Ratajczak, W., Schumacher, G., Schöck, W., Skokan, A. & Tromm, W. 1992. BETA Experiments on Zirconium Oxidation and Aerosol Release during Melt–Concrete Interaction. In: Alsmayer, H. (ed.). Proceedings of the Second OECD (NEA) CSNI Specialist Meeting on Molten Core Debris–Concrete Interactions. Karlruhe, Germany, 1–3 April, 1992. Karlsruhe: Forschungszentrum Karlsruhe. Pp. 67–82. (KfK 5108, NEA/CSNI/R(92)10.) ISSN 0303-4003. http://www.nea.fr/html/nsd/docs/1992/csni-r1992-10.pdf

Alsmeyer, H., Adelhelm, C., Dillmann, H.-G., Foit, J.J., Heinle, M., Ratajczak, W., Schneider, H., Schumacher, G., Skokan, A., Stiefel, S. & Tromm, W. 1995. BETA Experiments on Melt–Concrete Interaction: The Role of Zirconium and the Potential Sump Water Contact During Core Melt-down Accidents. Nuclear Engineering and Design, Vol. 154, no. 1, pp. 61–68. ISSN 0029-5493.

Asmolov, V.G., Zagryazkin, V.N., Astakhova, E.V., Vishnevskii, V.Yu., D'yakov, E.K., Kotov, A.Yu. & Repnikov, V.M. 2003. The Density of UO_2–ZrO_2 Alloys. High Temperature, Vol. 41, no. 5, pp. 627–632. ISSN 0018-151X.

Barthelmy, D. 2004. Mineralogy Database. http://webmineral.com/

Bažant, Z.P. & Kaplan, M.F. 1996. Concrete at High Temperatures: Material Properties and Mathematical Models. Essex: Longman Group. 412 p. ISBN 0-582-08626-4.

Blose, R.E., Powers, D.A., Copus, E.R., Brockmann, J.E., Simpson, R.B. & Lucero, D.A. 1993. Core–Concrete Interactions with Overlying Water Pools: The WETCOR-1 Test. Albuquerque, NM: Sandia National Laboratories. 178 p. (NUREG/CR-5907, SAND92-1563.) http://infoserve.sandia.gov/sand_doc/1992/921563.pdf

Bradley, D.R., Gardner, D.R., Brockmann, J.E. & Griffith, R.O. 1993. CORCON-MOD3: An Integrated Computer Model for Analysis of Molten Core-Concrete Interactions. User's Manual. Albuquerque, NM: Sandia National Laboratories. 278 p. (NUREG/CR-5843, SAND92-0167.)
http://infoserve.sandia.gov/sand_doc/1992/920167.pdf

Cadwallader, L.C. & Herring, J.S. 1999. Safety Issues with Hydrogen as a Vehicle Fuel. Idaho Falls: Idaho National Engineering and Environmental Laboratory. 78 p. (INEEL/EXT-99-00522.)
http://www.inl.gov/hydrogenfuels/projects/docs/h2safetyreport.pdf

Chase, M.W. 1998. NIST-JANAF Thermochemical Tables. 4th edition. Journal of Physical and Chemical Reference Data, Monograph No. 9, Parts I and II. 1952 p. ISBN 1-56396-831-2.

Chung, J.H. & Consolazio, G.R. 2005. Numerical Modeling of Transport Phenomena in Reinforced Concrete Exposed to Elevated Temperatures. Cement and Concrete Research, Vol. 35, no. 3, pp. 597–608. ISSN 0008-8846.

Copus, E.R., Blose, R.E., Brockmann, J.E., Gomez, R.D. & Lucero, D.A. 1989. Core–Concrete Interactions Using Molten Steel with Zirconium on a Basaltic Basemat: The SURC-4 Experiment. Albuquerque, NM: Sandia National Laboratories. 326 p. (NUREG/CR-4994, SAND87-2008.)
http://infoserve.sandia.gov/sand_doc/1987/872008.pdf

Copus, E.R., Blose, R.E., Brockmann, J.E., Simpson, R.B. & Lucero, D.A. 1992a. Core–Concrete Interactions Using Molten Urania with Zirconium on a Limestone Concrete Basemat: The SURC-1 Experiment. Albuquerque, NM: Sandia National Laboratories. 277 p. (NUREG/CR-5443, SAND90-0087.)
http://infoserve.sandia.gov/sand_doc/1990/900087.pdf

Copus, E.R., Blose, R.E., Brockmann, J.E., Simpson, R.B. & Lucero, D.A. 1992b. Core–Concrete Interactions Using Molten UO_2 with Zirconium on a Basaltic Basemat: The SURC-2 Experiment. Albuquerque, NM: Sandia National Laboratories. 293 p. (NUREG/CR-5564, SAND90-1022.)
http://infoserve.sandia.gov/sand_doc/1990/901022.pdf

Corradini, M. & Reineke, H.H. 1989. A Review of the BETA Experimental Results and Code Comparison Calculations. Nuclear Science and Engineering, Vol. 102, no. 3, pp. 260–282. ISSN 0029-5639.

Eppinger, B., Fellmoser, F., Fieg, G., Massier, H. & Stern, G. 2000. Experiments on Concrete Erosion by a Corium Melt in the EPR Reactor Cavity: KAPOOL 6–8. Karlsruhe: Forschungszentrum Karlsruhe. 32 p. (FZKA 6453.)
http://www.ubka.uni-karlsruhe.de/vvv/fzk/6453/6453.pdf

Epstein, M. 1998. Thermal Hydraulics of Molten Core–Concrete Interactions: A Review and Comparison of Heat Transfer Models with Data, Interpretation of Rheologigal Data, and a Theory for the Onset of Concrete Spallation. Palo Alto: Electric Power Research Institute. (ACEX-TR-21.)

Farmer, M.T., Lomperski, S. & Basu, S. 2004. Results of Reactor Materials Experiments Investigating 2-D Core–Concrete Interaction and Debris Coolability. Proceedings of the 2004 International Congress on Advances in Nuclear Power Plants, ICAPP ’04, Pittsburgh, PA, USA, June 13–17, 2004. Paper 4102, pp. 1193–1199.

Farmer, M.T., Lomperski, S. & Basu, S. 2005. Status of the Melt Coolability and Concrete Interaction (MCCI) Program at Argonne National Laboratory. Proceedings of the 2005 International Congress on Advances in Nuclear Power Plants, ICAPP ’05, Seoul, Korea, May 15–19, 2005. Paper 5644. 13 p.

Fellmoser, F., Engel, G., Fieg, G., Massier, H. & Werle, H. 1999. Simulationsexperimente zum Verhalten von Kernschmelzen in der Reaktorgrube des EPR: KAPOOL 1–5. Karlsruhe: Forschungszentrum Karlsruhe. 59 p. (FZKA 6212.)
http://www.ubka.uni-karlsruhe.de/vvv/fzk/6212/6212.pdf

Firnhaber, M. & Alsmeyer, H. 1992. ISP-30. International Standard Problem No. 30. BETA V5.1 Experiment on Melt–Concrete Interaction. Comparison Report. OECD/NEA. 142 p. (NEA/CSNI/R(92)9.)
http://www.nea.fr/html/nsd/docs/1992/csni-r1992-9.pdf

Fischer, M. 2004. The Severe Accident Mitigation Concept and the Design Measures for Core Melt Retention of the European Pressurized Reactor (EPR). Nuclear Engineering and Design, Vol. 230, no. 1–3, pp. 169–180. ISSN 0029-5493.

Gauntt, R.O., Cole, R.K., Erickson, C.M., Gido, R.G., Gasser, R.D., Rodriguez, S.B. & Young, M.F. 2000a. MELCOR Computer Code Manuals, Vol. 2: Reference Manual, Version 1.8.5 May 2000. Material Properties (MP) Package Reference Manual. Rev 2. Albuquerque, NM: Sandia National Laboratories. 74 p. (NUREG/CR-6119, SAND2000-2417/2.)

Gauntt, R.O., Cole, R.K., Erickson, C.M., Gido, R.G., Gasser, R.D., Rodriguez, S.B. & Young, M.F. 2000b. MELCOR Computer Code Manuals, Vol. 2: Reference Manual, Version 1.8.5 May 2000. Cavity (CAV) Package Reference Manual. Rev 2. Albuquerque, NM: Sandia National Laboratories. 28 p. (NUREG/CR-6119, SAND2000-2417/2.)

Greene, G.A. 1991. Heat, Mass, and Momentum Transfer in a Multifluid Bubbling Pool. Advances in Heat Transfer, Vol. 21, pp. 277–346. ISSN 0065-2717. ISBN 0-12-020021-X.

Gronager, J.E., Suo-Anttila, A.J. & Brockmann, J.E. 1986. TURC2 and 3: Large Scale $UO_2/ZrO_2/Zr$ Melt–Concrete Interaction Experiments and Analysis. Albuquerque, NM: Sandia National Laboratories. 174 p. (NUREG/CR-4521, SAND86-0318.) http://infoserve.sandia.gov/sand_doc/1986/860318.pdf

Harmathy, T.Z. 1970. Thermal Properties of Concrete at Elevated Temperatures. Journal of Materials, Vol. 5, no. 1, pp. 47–74. ISSN 0022-2453.

Harmathy, T.Z. & Allen, L.W. 1973. Thermal Properties of Selected Masonry Unit Concretes. Journal of the American Concrete Institute, Vol. 70, no. 2, pp. 132–142. ISSN 0002-8061.

IAEA. 1996. Defense in Depth in Nuclear Safety. A report by the International Nuclear Safety Advisory Group. Vienna: International Atomic Energy Agency. 48 p. (INSAG-10.) ISSN 1025-2169.
http://www-pub.iaea.org/MTCD/publications/PDF/Pub1013e_web.pdf

Incropera, F.P. & DeWitt, D.P. 2002. Fundamentals of Heat and Mass Transfer. 5th edition. Hoboken, NJ: John Wiley & Sons. 981 p. ISBN 0-471-38650-2.

International Nuclear Safety Center. 1996a. Thermal Conductivity and Diffusivity of Liquid UO_2. Version 0 for peer review. INSC Material Properties Database. http://www.insc.anl.gov/matprop/uo2/cond/liquid/wkliqm.php

International Nuclear Safety Center. 1996b. Surface Tension and Surface Energy of Uranium Dioxide. Version 0 for peer review. INSC Material Properties Database. http://www.insc.anl.gov/matprop/uo2/surft/wsurf.php

International Nuclear Safety Center. 1998. Solidus/Liquidus of UO_2-ZrO_2-Concrete Mixtures. Version 0 for peer review. INSC Material Properties Database. 10 p. http://www.insc.anl.gov/matprop/concrete/soliuzrc.pdf

International Nuclear Safety Center. 1999a. Enthalpy and Heat Capacity of Solid Uranium Dioxide. Version 1 for peer review. INSC Material Properties Database. 28 p. http://www.insc.anl.gov/matprop/uo2/ent_hc/solid/hcpsuo2.pdf

International Nuclear Safety Center. 1999b. Enthalpy and Heat Capacity of Liquid UO_2. Version 1 for peer review. INSC Material Properties Database. 28 p. http://www.insc.anl.gov/matprop/uo2/ent_hc/liquid/hcpluo2.pdf

Kalifa, P., Menneteau, F.-D. & Quenard, D. 2000. Spalling and Pore Pressure in HPC at High Temperatures. Cement and Concrete Research, Vol. 30, no. 12, pp. 1915–1927. ISSN 0008-8846.

Kekki, T. 2005. Private communication. Espoo: VTT Processes.

Kekki, T., Zilliacus, R. & Lindholm, I. 2005. Implementation of NUCLEA Database for in and Ex-vessel Nuclear Applications. Espoo: VTT Processes. 17 p. (PRO1/P7018/04.)

Kymäläinen, O., Tuomisto, H. & Theofanous, T.G. 1997. In-vessel Retention of Corium at the Loviisa Plant. Nuclear Engineering and Design, Vol. 169, no. 1–3, pp. 109-130. ISSN 0029-5493.

Mølgaard, J. & Smeltzer, W.W. 1971. Thermal Conductivity of Magnetite and Hematite. Journal of Applied Physics, Vol. 42, no. 9, pp. 3644–3647. ISSN 0021-8979.

Nie, M. 2004. TR 107: Sacrificial Concrete Layer Thickness in the Core Catcher. Technical report, revision A. Framatome ANP. 43 p. 19 Nov. 2004.

Outokumpu Research Oy. 2002. HSC Chemistry 5.11. Chemical reaction and equilibrium software with extensive thermochemical database.

Peehs, M., Skokan, A. & Reimann, M. 1979. The Behavior of Concrete in Contact with Molten Corium in the Case of a Hypothetical Core Melt Accident. Nuclear Technology, Vol. 46, no. 2, pp. 192–198. ISSN 0029-5450.

Seiler, J.M. & Ganzhorn, J. 1997. Viscosities of Corium–Concrete Mixtures. Nuclear Engineering and Design, Vol. 178, no. 3, pp. 259–268. ISSN 0029-5493.

STUK. 2005. Statement Issued by the Radiation and Nuclear Safety Authority Concerning the Construction of the Olkiluoto Nuclear Power Plant Unit 3, Annex 1: Safety Assessment of the Olkiluoto 3 Nuclear Power Plant Unit for the Issuance of Construction License. 102 p. 21 Jan. 2005.
http://www.stuk.fi/ydinturvallisuus/ydinvoimalaitokset/viides/fi_FI/rakentamislupa/_files/73199248312178210/default/olkiluoto3_rakentamisluvan_turvallisuusarvio.pdf

Sullivan, P.J.E. 2004. A Probabilistic Method of Testing for the Assessment of Deterioration and Explosive Spalling of High Strength Concrete Beams in Flexure at High Temperature. Cement & Concrete Composites, Vol. 26, no. 2, pp. 155–162. ISSN 0958-9465.

Swedish, M.J., Epstein, M., Linehan, J.H., Lambert, G.A., Hauser, G.M. & Stachyra, L.J. 1979. Surface Ablation in the Impingement Region of a Liquid Jet. AIChE Journal, Vol. 25, no. 4, pp. 630–638. ISSN 0001-1541.

Thompson, D.H., Farmer, M.T., Fink, J.K., Armstrong, D.R. & Spencer, B.W. 1997. Compilation, Analysis and Interpretation of ACE Phase C and MACE Experimental Data: Volume I – MCCI Thermalhydraulics Results. Argonne National Laboratory. (ACEX TR-C-14.)

Published by

Series title, number and
report code of publication

VTT Research Notes 2311
VTT–TIED–2311

Author(s)
Sevón, Tuomo

Title

Molten Core – Concrete Interactions in Nuclear Accidents
Theory and Design of an Experimental Facility

Abstract

In a hypothetical severe accident in a nuclear power plant, the molten core of the reactor may flow onto the concrete floor of containment building. This would cause a molten core – concrete interaction (MCCI), in which the heat transfer from the hot melt to the concrete would cause melting of the concrete. In assessing the safety of nuclear reactors, it is important to know the consequences of such an interaction.

As background to the subject, this publication includes a description of the core melt stabilization concept of the European Pressurized water Reactor (EPR), which is being built in Olkiluoto in Finland. The publication includes a description of the basic theory of the interaction and the process of spalling or cracking of concrete when it is heated rapidly. A literature survey and some calculations of the physical properties of concrete and corium–concrete mixtures at high temperatures have been conducted. In addition, an equation is derived for conservative calculation of the maximum possible concrete ablation depth. The publication also includes a literature survey of experimental research on the subject of the MCCI and discussion of the results and deficiencies of the experiments.

The main result of this work is the general design of an experimental facility to examine the interaction of molten metals and concrete. The main objective of the experiments is to assess the probability of spalling, or cracking, of concrete under pouring of molten material. A program of five experiments has been designed, and pre-test calculations of the experiments have been conducted with MELCOR 1.8.5 accident analysis program and conservative analytic calculations.

Keywords
nuclear power plants, nuclear safety, reactor core, meltdown, concrete structures, containment buildings, spalling, cracking, simulation, MELCOR

Activity unit
VTT Processes, Lämpömiehenkuja 3 A, P.O.Box 1604, FI–02044 VTT, Finland

ISBN			Project number
951–38–6743–9 (soft back ed.) 951–38–6744–7 (URL: http://www.vtt.fi/inf/pdf/)			12S-SAN1MMCE
Date November 2005	Language English, Finnish abstr.	Pages 83 p.	Price B
Name of project Severe Accidents and Containment Integrity		Commissioned by Ministry of Trade and Industry	
Series title and ISSN VTT Tiedotteita – Research Notes 1235–0605 (soft back edition) 1455–0865 (URL: http://www.vtt.fi/inf/pdf/)		Sold by VTT Information Service P.O.Box 2000, FI–02044 VTT, Finland Phone internat. +358 20 722 4404 Fax +358 20 722 4374	

Julkaisija

Julkaisun sarja, numero ja raporttikoodi

VTT Tiedotteita 2311
VTT–TIED–2311

Tekijä(t)
Sevón, Tuomo

Nimeke

Sydänsulan ja betonin vuorovaikutukset ydinvoimalaonnettomuuksissa
Teoriaa ja koelaitteiston suunnittelu

Tiivistelmä

Vakavassa ydinvoimalaitosonnettomuudessa reaktorin sulanut sydän voi valua suojarakennuksen betonilattialle. Tästä voi seurata sydänsula–betoni-vuorovaikutus, jossa lämpöä siirtyy kuumasta sulasta betoniin, mikä aiheuttaa betonin sulamisen. Arvioitaessa ydinvoimaloiden turvallisuutta on tärkeää tuntea tällaisen vuorovaikutuksen seuraukset.

Tässä tutkimuksessa aiheen taustaksi kuvataan Olkiluotoon rakennettavan EPR-painevesireaktorin sydämen sulamisonnettomuuden hallintakonsepti. Tutkimuksessa kerrotaan sydänsula–betoni-vuorovaikutuksen perusteista sekä betonin nopean lämmittämisen aiheuttamasta spalling-ilmiöstä eli lohkeilusta. Betonin ja corium–betoni-seosten fysikaalisia ominaisuuksia korkeissa lämpötiloissa selvitetään kirjallisuuden ja laskujen avulla. Lisäksi johdetaan yhtälö betonin suurimman mahdollisen sulamissyvyyden laskemiseksi. Julkaisu sisältää myös kirjallisuusselvityksen sydänsula–betoni-vuorovaikutusten kokeellisesta tutkimuksesta sekä pohdintaa kokeiden tuloksista ja puutteista.

Tutkimuksen tärkein tulos on yleissuunnitelma koelaitteistolle, jolla voidaan tutkia sulan metallin ja betonin vuorovaikutusta. Kokeiden tärkein tavoite on selvittää spalling-ilmiön todennäköisyyttä, kun sulaa materiaalia kaadetaan betoniastiaan. Tutkimuksessa suunnitellaan viiden kokeen ohjelma ja kokeista on tehty laskelmia MELCOR 1.8.5 -onnettomuusanalyysiohjelmalla sekä konservatiivisilla käsinlaskuilla.

Avainsanat
nuclear power plants, nuclear safety, reactor core, meltdown, concrete structures, containment buildings, spalling, cracking, simulation, MELCOR

Toimintayksikkö
VTT Prosessit, Lämpömiehenkuja 3 A, PL 1604, 02044 VTT

ISBN			Projektinumero
951–38–6743–9 (nid.) 951–38–6744–7 (URL: http://www.vtt.fi/inf/pdf/)			12S-SAN1MMCE
Julkaisuaika Marraskuu 2005	Kieli Englanti, suom. tiiv.	Sivuja 83 s.	Hinta B
Projektin nimi Severe Accidents and Containment Integrity		Toimeksiantaja(t) kauppa- ja teollisuusministeriö	
Avainnimeke ja ISSN VTT Tiedotteita – Research Notes 1235–0605 (nid.) 1455–0865 (URL: http://www.vtt.fi/inf/pdf/)		Myynti: VTT Tietopalvelu PL 2000, 02044 VTT Puh. 020 722 4404 Faksi 020 722 4374	

In a hypothetical severe accident in a nuclear power plant, the molten core of the reactor may flow onto the concrete floor of containment building. This would cause a molten core – concrete interaction (MCCI), in which the heat transfer from the hot melt to the concrete would cause melting of the concrete. In assessing the safety of nuclear reactors, it is important to know the consequences of such an interaction.

This publication includes a description of the basic theory of molten core – concrete interactions. A literature survey and some calculations of the physical properties of concrete and corium–concrete mixtures at high temperatures have been conducted. In addition, an equation is derived for conservative calculation of the maximum possible concrete ablation depth. The publication also includes a literature survey of experimental research on the subject of the MCCI and discussion of the results and deficiencies of the experiments. The main result of this work is the general design of an experimental facility to examine the interaction of molten metals and concrete.

Tätä julkaisua myy
VTT TIETOPALVELU
PL 2000
02044 VTT
Puh. 020 722 4404
Faksi 020 722 4374

Denna publikation säljs av
VTT INFORMATIONSTJÄNST
PB 2000
02044 VTT
Tel. 020 722 4404
Fax 020 722 4374

This publication is available from
VTT INFORMATION SERVICE
P.O.Box 2000
FI–02044 VTT, Finland
Phone internat. + 358 20 722 4404
Fax + 358 20 7226 4374

ISBN 951–38–6743–9 (soft back ed.)
ISSN 1235–0605 (soft back ed.)

ISBN 951–38–6744–7 (URL: http://www.vtt.fi/inf/pdf/)
ISSN 1455–0865 (URL: http://www.vtt.fi/inf/pdf/)